DEVELOPMENT OF AN ATMOSPHERIC SCENE SIMULATION MODEL

Ryan B. Turkington
Maureen E. Cianciolo
Mark E. Raffensberger

TASC
55 Walkers Brook Drive
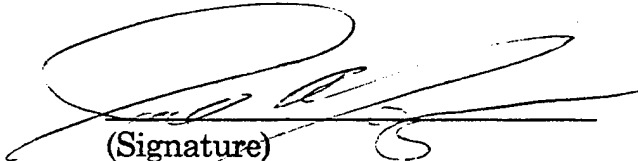Reading, MA 01867

19990719 024

14 May 1998

Final Report

Best Available Copy

DTIC QUALITY INSPECTED 4

Preceding Page Blank
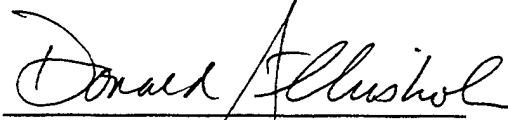
" This technical report has been reviewed and is approved for publication"

(Signature)
Dr Joel Mozer
Contract Manager

(Signature)
Mr Donald Chisholm
Branch Chief

This report has been reviewed by the ESC Public Affairs Office (PA) and is releasable to the National Technical Information Service (NTIS).

Qualified requestors may obtain additional copies from the Defense Technical Information Center (DTIC). All others should apply to the National Technical Information Service (NTIS).

If your address has changed, if you wish to be removed from the mailing list, or if the addressee is no longer employed by your organization, please notify AFRL/VSOS-IM, 29 Randolph Road, Hanscom AFB, MA 01731-3010. This will assist us in maintaining a current mailing list.

Do not return copies of this report unless contractual obligations or notices on a specific document require that it be returned.

REPORT DOCUMENTATION PAGE

Form Approved
OMB No. 0704-0188

1. AGENCY USE ONLY (Leave blank)	2. REPORT DATE 14 May 1998	3. REPORT TYPE AND DATES COVERED Final

4. TITLE AND SUBTITLE
Development of an Atmospheric Scene Simulation Model

5. FUNDING NUMBERS
PE 62601F
PR 6670　TA GS　WU BB

Contract F19628-96-C-0113

6. AUTHOR(S)　Ryan B. Turkington
Maureen E. Cianciolo
Mark E. Raffensberger

7. PERFORMING ORGANIZATION NAME(S) AND ADDRESS(ES)

TASC
55 Walkers Brook Drive
Reading, MA 01867

8. PERFORMING ORGANIZATION REPORT NUMBER

9. SPONSORING/MONITORING AGENCY NAME(S) AND ADDRESS(ES)

Air Force Research Laboratory
29 Randolph Road
Hanscom AFB, MA 01731-3010

Contract Manager: Joel Mozer/VSBE

10. SPONSORING/MONITORING AGENCY REPORT NUMBER

AFRL-VS-HA-TR-98-0051

11. SUPPLEMENTARY NOTES

12a. DISTRIBUTION/AVAILABILITY STATEMENT

Approved for public release;
distribution unlimited

12b. DISTRIBUTION CODE

13. ABSTRACT (Maximum 200 words)

The Cloud Scene Simulation Model (CSSM) was developed to generate high-resolution synthetic cloud backgrounds for a variety of DoD simulation systems. This report describes recent efforts to enhance that model and presents plans for future areas of development.

Recent efforts were focused in two areas: cirrus model development and software support. Cirrus model development began with a detailed survey of the technical literature to identify models and data from which we could derive cirrus statistics and characteristics for use in the model. We then decided to implement two cirrus types within the model: precipitating and non-precipitating types.

Cirrus databases were identified in the literature survey and several were chosen for analysis. These data were used to tune models within the current non-precipitating model. The CSSM was then tuned through comparison to the cirrus observations and statistically tested against the observations.

Our future development plans were focused on the implementation of an enhanced cirrus uncinus model and a climatological preprocessor for the CSSM. The cirrus uncinus model design simulates the vertically-developed particle distributions observed in nature. The climatological preprocessor will use climatological cloud and meteorological databases along with statistical information to build "typical" weather conditions for a user-specified location/date/time.

14. SUBJECT TERMS
Cloud model, modeling and simulation, distributed interactive simulation, visualization, water content, atmospheric model, scene generation, SUCCESS, cirrus, cirrostratus, fractal, climatology, Tshebycheff.

15. NUMBER OF PAGES
182

16. PRICE CODE

17. SECURITY CLASSIFICATION OF REPORT Unclassified	18. SECURITY CLASSIFICATION OF THIS PAGE Unclassified	19. SECURITY CLASSIFICATION OF ABSTRACT Unclassified	20. LIMITATION OF ABSTRACT SAR

NSN 7540-01-280-5500

STANDARD FORM 298 (Rev. 2-89)
Prescribed by ANSI Std 239-18
298-102

MI009
1-22-92

TABLE OF CONTENTS

LIST OF FIGURES

iv

LIST OF TABLES

PREFACE

The Cloud Scene Simulation Model (CSSM) was developed to generate high-resolution synthetic cloud backgrounds for a variety of DoD simulation systems. This report describes recent efforts to enhance that model and presents plans for future areas of development.

Recent efforts were focused in two areas: cirrus model development and software support. Cirrus model development began with a detailed survey of the technical literature to identify models and data from which we could derive cirrus statistics and characteristics for use in the model. We decided that to capture the most general cirriform types we would implement two cirrus types within the model: precipitating and non-precipitating types. The non-precipitating cirrus cloud type would be based on the current CSSM methodology (updated to include the most accurate cloud statistics) and the precipitating type would require a new methodology (an outline of the new methodology is presented in this report).

Cirrus databases were identified in the literature survey and several were chosen for analysis. These data were used to tune models within the current non-precipitating model. In particular, we used the data to tune the internal water content perturbation model parameters by comparing data from the CSSM to cirrus observations. We then tested the "tuned" model against other cirrus data observations using standard statistical hypothesis tests. Results from the analysis, tuning, and testing processes are described in this report.

Our future development plans were focused on the implementation of an enhanced cirrus uncinus model and a climatological preprocessor for the CSSM. The cirrus uncinus model design contains both parametric and dynamic components to simulate the vertically-developed particle distributions observed in nature. The climatological preprocessor will use climatological cloud and meteorological databases along with statistical information to build "typical" weather conditions for a user-specified location/date/time. The resulting weather conditions will be formatted in terms of the standard CSSM input fields.

In addition to the tasks listed above, we have provided continuing software support to users of the CSSM. A list of support tasks is included in this report along with a brief overview of the model itself.

1. INTRODUCTION

Weather in general, and atmospheric moisture in particular, can significantly impact commercial and military sensors and operations. Sophisticated simulation systems have been developed to support high-fidelity simulation of such sensors and operations. These simulation systems are generally limited in their ability to provide a high-fidelity weather environment to fully quantify its effects.

Atmospheric moisture can impact the operation of military and commercial electro-optical sensors through absorption, scattering, and emission of radiation. Examples of these effects include: variations within moisture fields (e.g., near cloud edges) introducing background clutter that can severely degrade sensor performance; the presence of water vapor attenuating electro-optical signals, thus reducing visibility and transmission; and the presence of rain regions which are completely opaque to most common sensor wavelengths.

Many of the raw weather datasets that are readily available (including temperature, moisture, pressure, wind, cloud layer information, rain rates, etc.) come from national or global networks of numerical weather prediction models, surface observations, and upper air balloon measurements. The resolution of these data sources is very coarse (on the order of tens of kilometers or more), which although useful to characterize the general state of the atmosphere on a regional scale, does not capture the higher-resolution features within local regions and therefore does not satisfy the fidelity requirements of many simulators.

The Cloud Scene Simulation Model (CSSM) was developed to satisfy the need for higher-resolution atmospheric moisture fields for use in high-fidelity simulators such as those mentioned above. It simulates cloud water (liquid and ice water content) and rain rate values for stratiform, cirriform, and fair weather cumulus cloud types. The CSSM was originally built as a part of the Smart Weapons Operability Enhancement (SWOE) Program (Cianciolo and Rasmussen, 1991) and has evolved significantly since then. This document describes recent technical progress toward an enhanced CSSM with emphasis on an improved cirrus model.

1

This report describes work performed in fulfillment of contract number F19628-96-0113. The work was conducted from 30 August 1996 through 15 May 1998. The original contract was to have extended through 29 November 1999, but funding limitations at the Air Force Research Laboratory (AFRL) Battlespace Environment Division forced us to reduce the project's scope and period of performance.

1.1 CSSM OVERVIEW

The CSSM was developed to satisfy the needs of a wide range of users within the DoD community. It generates high-resolution cloud scenes for use in a variety of simulation applications including mission rehearsal, sensor test and evaluation, and scene visualization.

The CSSM builds four-dimensional (space and time) multi-layer cloud scenes containing stratiform, cirriform, and cumulus cloud types. Output scenes are consistent with user-supplied coarse-resolution cloud and meteorological input fields. The primary output variable of the model is water content (g/m^3) at every gridpoint in a user-defined simulation domain. Typical scenes, with output resolutions of 10-100 meters and domain sizes of 10x10x3 kilometers, take only seconds to build on a standard workstation.

The CSSM is a parametric model that relies on stochastic field generation algorithms (e.g., the Rescale and Add (RSA) fractal algorithm, [Saupe, 1989]) to build external cloud structures and their internal water density perturbation fields. For stratiform and cirriform cloud types, the resulting perturbation fields are converted to absolute water content using computed field statistics and a mean liquid water content (LWC) profile given by the Feddes model (Feddes, 1974). A simple convection model is also employed when simulating cumulus cloud structures and water content values. (Note: the model does not attempt to model the exact cloud structures present at a given date/time/location, rather, it generates cloud fields that are statistically consistent with the observed cloud conditions.)

CSSM output files contain water content (and rain rates when applicable) at every cloud-filled gridpoint. These gridded cloud fields can be used as input to radiative transfer calculations, visualization programs, line-of-site analyses, ground mobility calculations, etc.

1.2 PURPOSE OF THE PROJECT

The objectives of the Atmospheric Scene Simulation Model project are to enhance the CSSM and to facilitate its usage within the DoD simulation community. These objectives have three complementary aspects: model development, improvement, and integration. Three tasks were funded to contribute to these objectives:

- ***Develop cirrus model*** — Research and design a new cirrus model capable of capturing the unique structures observed in "precipitating" cirrus clouds (e.g., cirrus uncinus). Tune parameters within the existing cirrus models to better replicate the water content observed in nature.
- ***Plan climatological preprocessor*** — Design a preprocessor application to provide climatological inputs (meteorological data and cloud layer specifications) to the CSSM.
- ***Provide software support*** — Train users in the correct usage of the CSSM, test/debug software, distribute input files, test the model in a variety of computational environments, and build/maintain a baseline version of the CSSM.

More detailed descriptions of the specific project tasks that were performed to meet the project objective along with results from this research effort are described in the following sections.

1.3 OVERVIEW OF PROJECT TASKS

This effort consists of three primary tasks. A brief description of each task is included below. Each of the tasks is described in more detail in the technical proposal "Development of an Atmospheric Scene Simulation Model" (1996).

Task 1 — Develop Cirrus Model

A primary focus of this research effort is improving the cirriform model within the CSSM. This effort complements previous development of the CSSM's stratiform and cumuliform models (Cianciolo et al., 1991; Cianciolo and Rasmussen, 1992; Cianciolo et al., 1996). Although the CSSM contained a cirriform cloud model from the beginning, that model had never been evaluated in any quantitative manner. One of the objectives of the current modeling effort was to improve the CSSM's ability to simulate cirrus cloud fields. This effort consisted of two primary tasks: first, to evaluate the overall CSSM cloud generation methodology and identify areas for improvement, as

necessary, to better replicate the structure of cirrus clouds; and second, to analyze cirrus observations for model parameter estimation and verification purposes.

Several steps were required to achieve our objective. A brief description of each of these steps is included below. A complete discussion of the cirrus model development and analysis results is contained in Section 2 of this report.

Steps to develop cirrus model:

- **_Survey literature for models_** — Review the scientific literature to identify models and/or data that best characterize cirrus cloud structures at high resolutions. Identify the most suitable cirrus model from those developed at national laboratories, universities, or other scientific communities. Select a model which uses the meteorological variables available in the CSSM to build cirrus cloud fields. The model will simulate horizontal and vertical variations in microphysical parameters as well as overall cloud structures.

- **_Design/adapt model for CSSM architecture_** — Adapt the model selected in the previous sub-task to the CSSM architecture. This may involve developing new algorithms in the model, building a time dependency into the model, mapping the independent input variables to those already supplied to the CSSM, ensuring interoperability, reproducibility, etc. Design software changes to the CSSM to accommodate the new cirrus model.

- **_Outline data sources for analysis_** — Survey literature and interview members of various experimental programs to identify the most suitable cirrus observations for our model development. Observations may include some of the following data types: lidar, radar, satellite, aircraft, radiometric, and camera (or imager) data.

- **_Identify/obtain cirrus observations_** — Identify/obtain the most suitable observations to use in our model-data comparisons. Develop (or download, as available) software to extract, study, and process the various data types.

- **_Analyze observations_** — Process the cirrus observations to extract statistical information concerning cloud structures, and physical parameters (specifically, ice water content). Horizontal and vertical paths through observed cirrus clouds will be extracted as available. Acquire empirical datasets for use in model testing and tuning. Test and tune the cirrus model by comparing empirical data with CSSM output.

Task 2 — Plan Climatological Preprocessor

The CSSM is typically initialized with data derived from either a single meteorological profile or gridded numerical weather prediction or analysis model. Often such data are not readily available to the user and thus initializing the CSSM can be burdensome. (Recall that the CSSM requires both meteorological data and cloud layer information for initialization.) In such cases, the user may be

satisfied with using "typical" weather data for the region and time of interest. For example, consider a mission planning simulation in which the players wish to build cloud environments that are typical for a winter night in Bosnia. Or taking it one step further, players may wish to run their planning simulations using a range of conditions that may be experienced for a given region and time of interest. Such applications could be initialized with data sets drawn out of the climatological preprocessor.

The climatological preprocessor will function as a stand-alone preprocessor for the CSSM. The user will specify geographic location, date and time of day. The preprocessor will then access data from a climatological database or build data using climatological inputs. The resulting cloud and meteorological data will be formatted directly into the necessary CSSM input files.

This current task tackles the planning and design aspects of the climatological preprocessor. Future efforts will involve the implementation of the design and corresponding software development.

Several steps were required to develop a plan for the preprocessor. A brief description of each of these steps is included below. A complete discussion of the climatological preprocessor planning task is contained in Section 3 of this report.

Steps to plan climatological preprocessor:

- *Identify suitable climatological databases* — Perform survey of databases maintained at national laboratories, universities, scientific communities, and military facilities. Suitable databases must include climatological cloud (e.g., amount, base, top, and type), temperature, humidity, and wind information. This information should include some description of the frequency distribution for each of the parameters as well as some measure of cross-parameter correlation.

- *Develop algorithms to infer input variables* — Develop the algorithms necessary to derive CSSM input variables (e.g., temperature and wind profiles, cloud fraction, cloud height) from the information available in the selected climatological databases. These algorithms may use statistical information in the databases (e.g., frequency of occurrence, mean, and standard deviation) to derive a self-consistent set of meteorological and cloud information for use in initializing the CSSM.

- *Develop plan* — Gather all results and develop plan for the preprocessor. Present findings and preliminary algorithms to CSSM users at the AFRL Battlespace Environment Division.

Task 3 — Provide Software Support

This task encompasses all the software support required to maintain and develop the CSSM. (Documentation — including memos, reports, user's guides, etc. — also falls under this task, but is not discussed in this technical report.) Specific software support tasks have been performed as needed to satisfy the research and analysis needs of CSSM developers as well as those of the various CSSM users at the AFRL Battlespace Environment Division and elsewhere. Such needs evolved from demonstration requirements, changing system specifications, continued testing, user training, etc.

Software support and integration consisted of many varied tasks. A brief description of some of these tasks is included below. Unlike Tasks 1 (develop cirrus model) and 2 (plan climatological preprocessor), no further discussion of this task is contained in this report.

A partial list of software support tasks:

- *Train CSSM users in the proper specification of input data* — Usually the most difficult aspect of running the CSSM is gathering and correctly specifying the four types of input data required to run the model: meteorological data, cloud layer definitions, terrain elevation, and user-specified input parameters. We provided guidance and examples to users in this area with corresponding output files for verification purposes.

- *Debug the CSSM to identify and resolve software problems* — As a part of an ongoing process, we attempt to resolve any bugs that may remain in the code by stressing the model in new ways, usage by new users, and integration with various applications. We fixed several errors over the course of this research effort including an intermittent, but relatively significant memory error.

- *Review modifications made to the code by the client* — Personnel at AFRL reviewed the CSSM carefully and suggested several code changes to increase speed. We reviewed these suggestions and implemented only those changes which did not detrimentally affect the model physics and inner algorithms. We thoroughly tested and documented these changes.

- *Install a new baseline version of the CSSM* — Working with personnel at AFRL Battlespace Environment Division, we defined a baseline version of the CSSM to be maintained at the PL site and documented all updates to this version from the previous model version.

- ***Develop/expand a variety of pre- and post-processor programs*** — We built an array of analysis programs that display and analyze CSSM output fields, for example: IDL programs to display X-Y, X-Z, and Y-Z slices, histograms, time series paths, basic statistical characteristics, and 3-D renderings of the CSSM water content and rain rate fields, C programs to compute the fractal dimension of water content paths using two independent algorithms (Higuchi, 1988; Keller et al., 1989), a C program which displays ASCII cloud type maps to the screen for immediate verification of output data, and a C program which displays gridded meteorological, cloud, and terrain input data fields, etc.

- ***Test model with new input meteorological and cloud datasets*** — Throughout this research effort, we tested the CSSM with a wide variety of input data and corresponding weather conditions. For example, we identified a series of new soundings to initialize the cumulus convection model and verified its ability to correctly simulate approximate cloud top heights.

2.   CIRRUS MODEL DEVELOPMENT

This section describes the various tasks associated with ongoing improvements to the CSSM's cirrus model. The primary tasks are as follows: first, survey literature to identify models/data of high-resolution cirrus structures and internal properties (e.g., water content, particle size distributions); second, incorporate any findings from the survey task into the design for an improved cirrus model; third, obtain and analyze cirrus data for model parameter estimation and testing. Each of these tasks is covered in this section of the report.

2.1   LITERATURE SURVEY

To aid in the cirrus model development and data analysis tasks, we reviewed the meteorological journals for relevant sources of information and data. We performed on-line library searches to identify the most recent and promising model development and cloud observation efforts. We studied older technical reports to extract measurement information on cirrus characteristics. We searched the World Wide Web for models and data. And we consulted personnel at the Air Force Research Laboratory and elsewhere for guidance in special projects concerning cirrus clouds. All of these sources were reviewed in the context of the CSSM cirrus model improvement and testing. In particular, we were looking for sources of high-resolution cirrus observations, parametric models of microphysical properties, vertical and horizontal fine structure, simple dynamic models, large-scale structure characteristics (e.g., correlation distances, distance between cloud bands, length of bands), particle size distributions, etc.

The results of our survey are compiled in an annotated bibliography which is included in Appendix A. Each reference consists of citation, abstract, and summary of pertinent information for our model development process.

Note: many of the references reviewed as part of this task contain information useful in the Fast-Map modeling effort (a separate task not discussed in this report). However, we are not explicitly extracting information regarding the optical and radiative properties of cirrus as a part of this effort and therefore we did not identify those references at this time.

2.2   CONCEPTUAL MODEL DESIGN

The CSSM baseline cirrus model was developed under a previous effort (Cianciolo et al., 1991). It was implemented then as a complement to the stratiform model and uses many of the same algorithms. Parameters within the model were originally selected based on a limited qualitative comparison with satellite cloud imagery and photographs. The baseline model creates visibly realistic simple cloud structures, but lacks the ability to simulate more dynamic cloud features. For example, it simulates thin cirrus layers with realistic horizontal bands, but does not simulate the vertical falling streaks seen in some ice clouds.

Analysis of cirrostratus and cirrus observations (presented later in this report) along with results from the literature survey, led us to develop a plan to build an improved CSSM cirrus model. The survey did not find a single specific model which was well matched to the geometries, resolutions, and simulation requirements of the CSSM. Nonetheless, we did extract a large amount of useful information concerning the average ice water contents, vertical structure, and general characteristics of a variety of cirrus cloud types.

No one model can capture the nearly infinite variety in cirriform cloud types and structures. However, for our modeling purposes, we have simplified the possibilities into two primary cloud categories: non-precipitating and precipitating types. *Non-precipitating* cloud types (cirrus, cirrostratus, cirrocumulus in our model) include those types in which the horizontal scale dominates the vertical scale and ice precipitation is relatively limited. Conversely, the *precipitating* cloud type (cirrus uncinus in our model) is that in which the vertical scale dominates and vertical motion is non-negligible.

We built our model development plan based on those two cloud categories. The plan consists of two parts: first, to improve the existing cirriform cloud model within the CSSM (including improved model parameters), and second, to build a new vertically-developed cirrus cloud model. The cirrus model development plan is outlined in the following two sections. Due to funding constraints we did not implement the plan at this time, with the exception of tuning model parameters. We will use this plan to guide future development efforts.

9

2.2.1 Non-precipitating Cloud Types (cirrus, cirrostratus, cirrocumulus)

The new non-precipitating cloud model will retain the three current cirrus models (ci, cs, cc) and much of the underlying methodology, but includes the following improvements:

- *Tune internal IWC model parameters* — Fine-tune model parameters based on results of parameter estimation task. This effort was recently completed for cirrus and cirrostratus cloud types and results are documented in depth in the next section of this report. We analyzed ice water content data taken during the SUCCESS experiment to estimate fractal dimension, spatial correlation, and basic statistical measures. By comparing these observed values to those computed from model cloud fields, we were able to "tune" the related model parameters. These parameters control the internal four-dimensional ice water content perturbation field that is added to the mean water content predicted by the Feddes model. Results are limited to cirrus and cirrostratus cloud types. We will tune the cirrocumulus model in a future effort.

- *Update horizontal spatial characteristics* — The RSA fractal algorithm controls the external shape and spatial distribution of the simulated cloud fields. Using observed data (e.g., satellite imagery, LIDAR) and results from the literature survey (Heymsfield, 1977; Sassen et al., 1989), update the relevant parameters that control the spatial characteristics of the cloud fields. For example, update the lattice resolution and Hurst parameters that control the length, width, and distance between cloud bands; revise the maximum deviation angle of the cloud bands with respect to the large-scale wind features; modify the maximum amount of "meander" in the cirrus field. Modify these parameters only as necessary.

- *Modify CSSM to accept vertical velocity as an input variable* — Vertical velocity and temperature information can be used to infer mean ice water content throughout the cirriform cloud layer (Heymsfield, 1977; Heymsfield and Donner, 1990; Heymsfield and Platt, 1991). Modify the input routines to accept vertical velocity when available (e.g., output from a numerical weather prediction model). Provide the ability to generate vertical velocity fields based on climatological values when necessary. Obtain climatological values through a literature survey of meteorological journals and databases. Use the vertical velocity field as described in the following bullet.

- *Modify the vertical IWC distribution* — Update the predicted mean ice water content to account for ice production, growth, and sublimation regions (this may involve modification to or removal of the Feddes model (Feddes, 1974) which currently controls the vertical distribution of ice water content). The RSA algorithm is an efficient and flexible tool for generating stochastic fields. We have found that it is an excellent way to simulate the complex shapes seen in some cirrus cloud types. Based on data analysis presented later in this report, it appears to provide a good foundation structure defining the overall shape of a cirrus cloud layer. However, as several researchers point out, the vertical structure of cirrus clouds is anything but "random" (e.g., see the discussion of generating cells in Heymsfield (1975a and 1975b). To date, we have employed the Feddes model to describe the vertical variations in mean ice water content through all cloud types (with the exception of cumulus). The Feddes model does not differentiate for varying levels within cirrus types. It assumes a constant mean water content throughout, with only coarse changes associated with changing temperature. In light of recent research, the Feddes model appears insufficient to describe the vertical structure throughout the layer. Therefore the vertical structure model within the thin cirrus (non-precipitating) clouds is one of the first things we will change in an improved cirrus cloud model. We will employ parameterizations presented in Heymsfield (1977), Heymsfield and Donner (1990), and Heymsfield and Platt (1991) which rely on temperature and vertical velocity to infer vertical distributions of IWC (see bullet above).

- *Introduce concept of cellular generating head* — Generating cells provide a source for ice crystals in cirriform clouds. They are usually defined by pockets of higher water content values ranging in horizontal size from 800-2000 meters and vertical size from 300-1400 meters (Heymsfield, 1975a) located at or near the cloud top. Modify the internal RSA algorithm to simulate such cellular structures by generating high frequency localized cells within the larger cloud layers. Likewise, modify the procedures used to generate the external structure of the cirrocumulus cloud layer to introduce the more cellular structure produced by generating regions within the cloud layer.

2.2.2 Precipitating Cloud Type (cirrus uncinus)

We will add a fourth cirrus cloud type, cirrus uncinus (cn), that contains the characteristic cirrus precipitation trails consisting of generating head and particle fallout regions. The new precipitating cloud model will combine fractal field generation and trajectory dynamics to simulate cirrus uncinus cloud types. (Recall that a similar combination of fractals and dynamics was employed to simulate cumulus cloud types.) Typical dimensions, average ice water contents, and variations of microphysical properties with temperature and altitude will be taken primarily from papers by Heymsfield and Sassen (see references in bullets below). Model development will entail the following:

11

- *Define horizontal distribution of generating head elements* — Use the RSA algorithm to build the initial field of generating elements across the horizontal domain. Select fractal parameters (including lattice resolution, Hurst parameter, and maximum number of frequency terms to use in the RSA algorithm) to replicate the typical shapes, sizes, spacing, and overall distribution of cloud elements as found in the literature survey (Heymsfield, 1975a and 1975b).

- *Simulate generating head internal structure* — Model ice crystal generating head with upshear and downshear regions and "holes" separating the two regions where ice concentrations are at a minimum. Typical characteristics for the size and overall structure of a generating head are presented in Heymsfield, (1975a and 1975b) and Sassen et al. (1989).

- *Estimate ice crystal terminal velocity* — Estimate terminal velocities of single bullet and rosette crystals created in generating head. Use information presented in Heymsfield (1972) to aid in this calculation.

- *Calculate ice crystal trajectories* — Build a trajectory model based on work presented in Heymsfield (1975c) and Heymsfield and Coen (1996). Simulate ice crystal precipitation with this trajectory model assuming that ice particles fall out of the generating head in downshear regions and are advected by local scale winds. Use input wind conditions to drive advection. Build a simplified trajectory model from parametric fits to Heymsfield's work if necessary. Capture the ice crystal positions at any time in "snapshot" form to construct a CSSM output cloud scene. This component of the cirrus uncinus model simply determines where the cloud is. The next bullet describes how to calculate the ice water content everywhere within the cloud field.

- *Estimate vertical IWC profiles* — Model temperature dependence of ice water content for vertically extended cirrus precipitation trails. Modify the CSSM as mentioned above for non-precipitating cirrus cases to accept vertical velocity on input. Use the parameterizations outlined in Heymsfield and Donner (1990) and Heymsfield and Platt (1991) which rely on both vertical velocity and temperature to infer mean ice water content throughout the cloud layer. Superimpose the water content perturbation field on the mean values to produce the final output field in a similar fashion to the method used for all other CSSM cloud types (except cumulus).

- *Compare model and observed cloud fields* — Acquire cirrus uncinus cloud observations and extract any quantitative information on cirrus uncinus characteristics from literature sources. Verify the CSSM cirrus uncinus cloud model by comparing simulated cloud fields to the sample observations and literature-based data sources. Employ the same methods used for testing the cirrus and cirrostratus models described later in this report when possible. Tune model parameters and algorithms as guided by this analysis.

2.3 DATA ANALYSIS / MODEL PARAMETER ESTIMATION

This section describes the data analysis and model parameter estimation tasks. The goal of these tasks was to gather and analyze high-resolution cirrus cloud observations to extract statistical information concerning cloud structure and physical parameters (specifically ice water content). This statistical information formed the basis for tuning several CSSM parameters.

The general approach used in this effort was similar to that described in Cianciolo et al. (1996) for estimating cumulus model parameters. However, the statistical analysis employed in this effort has been expanded. The process consists of the following steps:

- Collect and process high-resolution aircraft observations of cirrus cloud ice water content
- Collect and process coincident standard meteorological observations
- Identify individual path segments from aircraft data for later comparisons to model paths
- Obtain statistical information on each of the observed cloud paths
- Run the CSSM with appropriate input conditions (meteorological conditions, cloud layer specification, resolution, etc.) for each corresponding aircraft path
- Extract path segments from CSSM output grids
- Compare aircraft and CSSM data paths
- Estimate improved CSSM parameters based on comparison
- Re-run CSSM and compare again
- Iterate as necessary until CSSM output paths best match the aircraft data paths.

This section of the report describes all of these data analysis steps. We begin in Section 2.3.1 by describing the aircraft data and corresponding meteorological conditions. Section 2.3.2 provides a description of the CSSM parameters that we selected for tuning. Section 2.3.3 outlines the actual parameter estimation process. Lastly, Section 2.4, discusses the results from the statistical comparisons of the aircraft and model water content data paths.

2.3.1 Aircraft Data

We examined datasets from many aircraft-based experiments (see Tables 1 and 2) that measured the water content of cirriform clouds. Several types of water content (wc) probes were used in these experiments; the most commonly used being the Particle Measuring Systems' (PMS) 2D-C, PMS Forward Scattering Spectrometer Probe (FSSP), and the King Probe. None of the PMS instruments

measure ice water content directly. The FSSP is a droplet sizing instrument and the 2D-C is a particle imaging instrument; ice water content is derived from their output. The King Probe is designed to measure liquid water content only and therefore is not applicable for cirriform cloud sampling.

Although the FSSP and PMS 2D-C have been used in most experiments which measure ice water content, these instruments are not ideal for this purpose. Many assumptions are made when converting the data from these sensors to ice water content, leading to possible large errors in the results. To reduce the error, the data output is typically averaged to 5 seconds. For CSSM validation and parameter estimation, this is insufficient, since desirable sampling rates are approximately 1 Hz.

Recently, newer instruments have become more commonly used for microphysical cloud sampling; the Counterflow Virtual Impactor (CVI) and the Gerber Scientific PVM-100A. Both of these instruments accurately sample water content at a substantially higher rate than their older Particle Measuring Systems (PMS) probe counterparts (at least 1Hz vs. 5Hz). Therefore, data sampled from the CVI and PVM-100A probes are more appropriate for our analysis since we wanted to test the high resolution cirrus structure generated by the CSSM. The sampling rates of these two probes correspond to approximately 100-200 meters (assuming an aircraft speed of 100-200 m/s). This resolution gives a lower limit for the validity of our derived parameter estimates and model verification.

Aircraft-based data were analyzed from five of the experiments listed in Table 1. These included CEPEX, TOGA-COARE, FIRE I and II, and SUCCESS. These experiments all used one or both of the PMS probes in their cirriform cloud data sampling. Additional microphysical cloud measuring instruments were used during the SUCCESS experiment, including the CVI and the PVM-100A. Since SUCCESS was the only experiment which used these high-resolution instruments for sampling cirriform clouds, we chose to use data solely from this experiment.

Table 1 Internet Locations of Available Data Sets

PROGRAM NAME	LOCATION	DATE	WEB ADDRESS
CEPEX	Equatorial Pacific	Mar-Apr '93	http://www.aoml.noaa.gov/hrd/CEPEX.html
CLARET I	Erie, Colorado	Sep-Oct '89	NA
CLARET II	Erie, Colorado	Feb-Mar '91	NA
FIRE I Cirrus	Central Wisconsin	Oct '86	http://asd-www.larc.nasa.gov/fire/fire1.html
FIRE II Cirrus	Coffeyville, Kansas	Nov-Dec '91	http://asd-www.larc.nasa.gov/fire/fire2.html
FIRE III Cirrus	Arctic and Tropics	1994-1997	http://asd-www.larc.nasa.gov/fire/fire3.html
JACCS	Western Pacific	1991-2000	http://www.mri-jma.go.jp/Proj/JACCS/jaccs.html
SUCCESS	Western U.S.	Apr-May '96	http://cloud1.arc.nasa.gov/espo/success/
TOGA-COARE	Equatorial Pacific	Nov '92-Feb '93	http://daac.gsfc.nasa.gov/CAMPAIGN_DOCS/TOGA/nasa_coare.html
WISP	Midwestern U.S.	Feb-Mar '94	http://www-das.uwyo.edu/atsc/research/wisp.html

Table 2 Internet Locations of Water Content Data Sets

PROGRAM NAME	DATA SET LOCATION
CEPEX	http://www-c4.ucsd.edu:80/~cids/DLOAD/cids_transfer.cgi/CEPEX http://www.joss.ucar.edu/cgi-bin/codiac/projs/CEPEX
FIRE I Cirrus FIRE II Cirrus	Telnet: eosdis.larc.nasa.gov Login: ims Password: larcims
SUCCESS	Telnet: cloud1.arc.nasa.gov Login and password available via the SUCCESS homepage (see Table 1)
TOGA-COARE	http://www.ncdc.noaa.gov/coare/

2.3.1.1 Description of SUCCESS Data

Data used for the parameter estimation came from the Subsonic aircraft: Contrail and Cloud Effects Special Study (SUCCESS) project based at Salina, Kansas, during April and May of 1996. We selected the SUCCESS experiment for its excellent spatial resolution, availability, and range of experimental locations. The primary purpose of the SUCCESS mission was to analyze the microphysical structure of aircraft contrails and compare it to the microphysical structure of cirriform clouds. Water content values were measured by three separate instruments; the CVI, PVM-100A, and the PMS 2D-C. These instruments were mounted on the exterior of a DC-8 aircraft.

The PMS 2D-C instrument performance precluded our usage of its data (see previous subsection). Thus, we compared the specific features of the PVM-100A and the CVI. One differing aspect between the two instruments is the range of particle sizes that it processes. We selected the CVI water content dataset for use in our parameter estimation task, since it covered the greatest range of particle

15

sizes in addition to having a high sampling rate (1 Hz). The particle size distribution for the PVM-100A probe is more limited. The CVI instrument performance is outlined in Table 3.

Table 3 CVI Instrument Performance

TYPE	PERFORMANCE
Linear Range	Number: 0.04 to 4000 cm^3 Condensed Water Content: 1 to 500 mg/m^3
Response Time	1 second with 3-5 second delay in instrument
Detection Limits	Particle Size: > 3-4 microns radius Number: 0.04 cm^3 Condensed Water Content: 1 mg/m^3
Accuracy	Number: 20% Condensed Water Content: 10%
Precision	Number: 0.002 cm^3 Condensed Water Content: 0.1 mg/m^3

Several other instruments and observations were used to support SUCCESS. For example, the NASA ER-2 aircraft flew in relative unison with the DC-8 to measure cloud heights with the Cloud Lidar System (CLS). However, the two aircraft's flight paths were not always coincident, causing possible errors in the cloud height calculations. The DC-8 in-cloud observations were derived from a combination of aircraft logs and GOES 8 and 9 satellite imagery. We used both cloud height estimates in our analysis as we describe later in this report. The DC-8 flight paths were overlaid onto the associated satellite image, thereby aiding our analysis. Sample images from each experiment day are presented in Figures 1 through 5. Meteorological data were gathered from standard National Weather Service upper air stations across the United States, Canada, and Mexico at 000000 GMT and 120000 GMT on each day of the experiment.
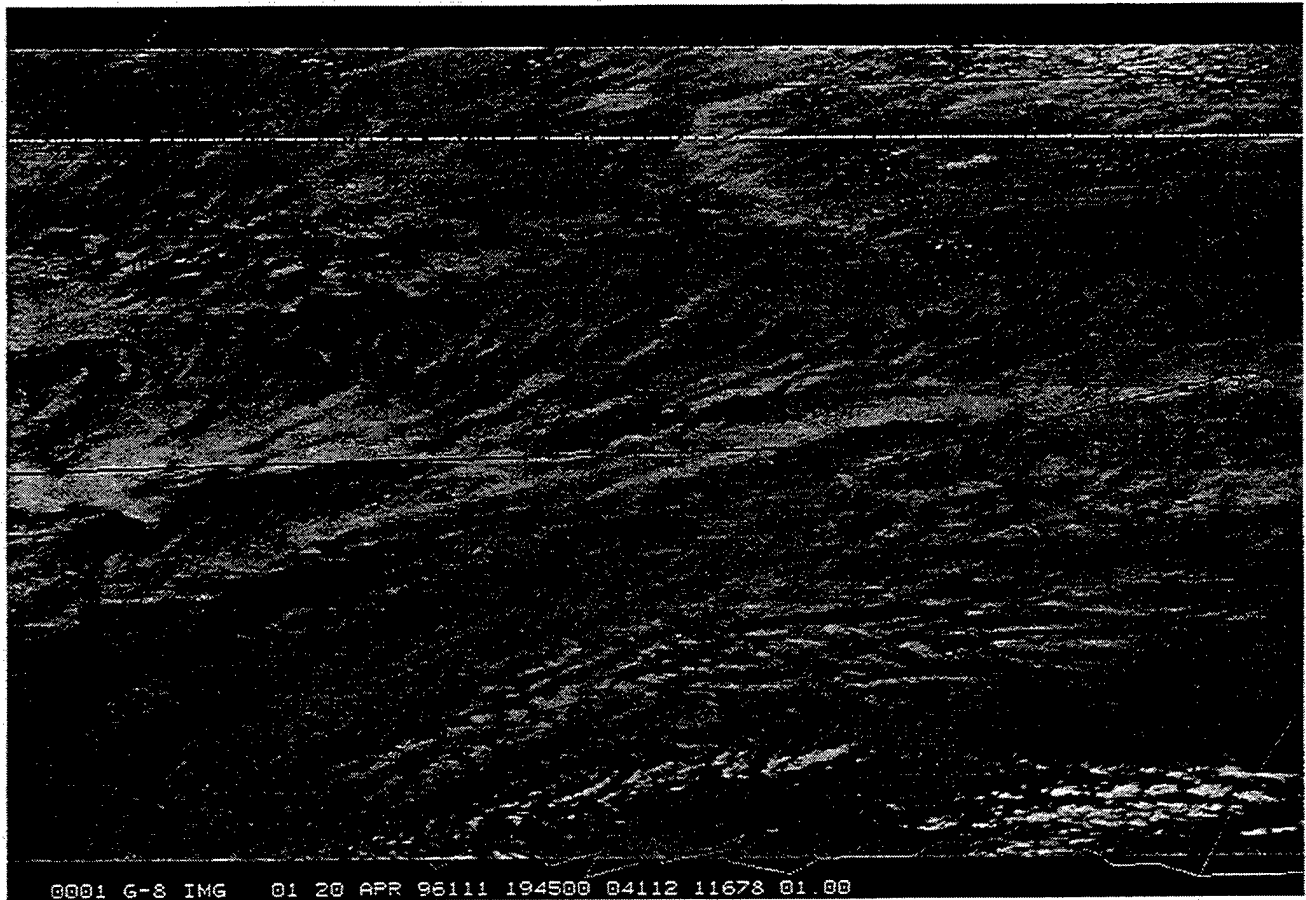
**Figure 1 GOES-8 Satellite Image Over Oklahoma 4/20/96: 194500 GMT with
DC-8 Path Overlaid: 192436 — 200448 GMT**

17
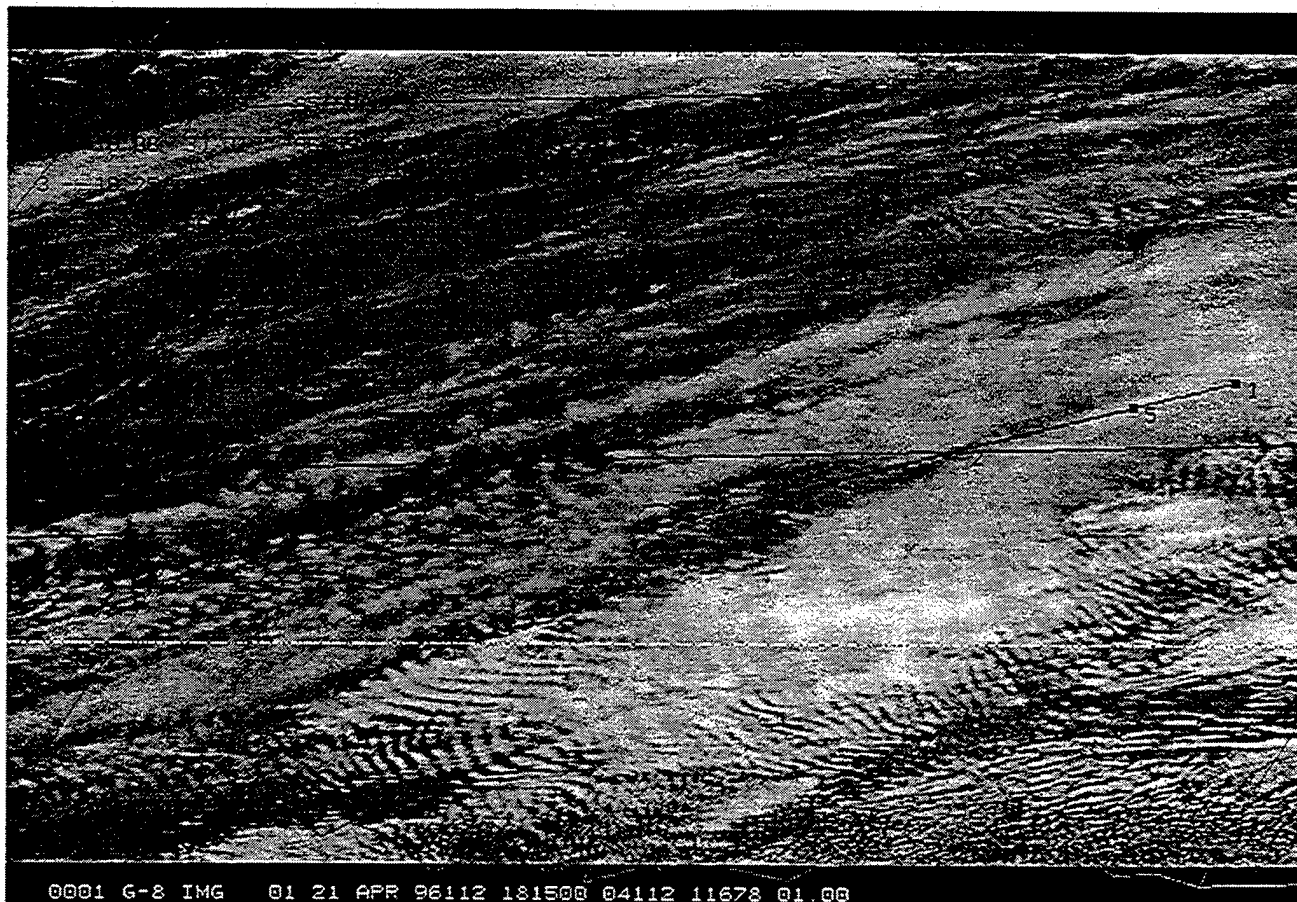
Figure 2 GOES-8 Satellite Image Over Kansas 4/21/96: 181500 GMT with DC-8 Path Overlaid: 175436 — 183448 GMT
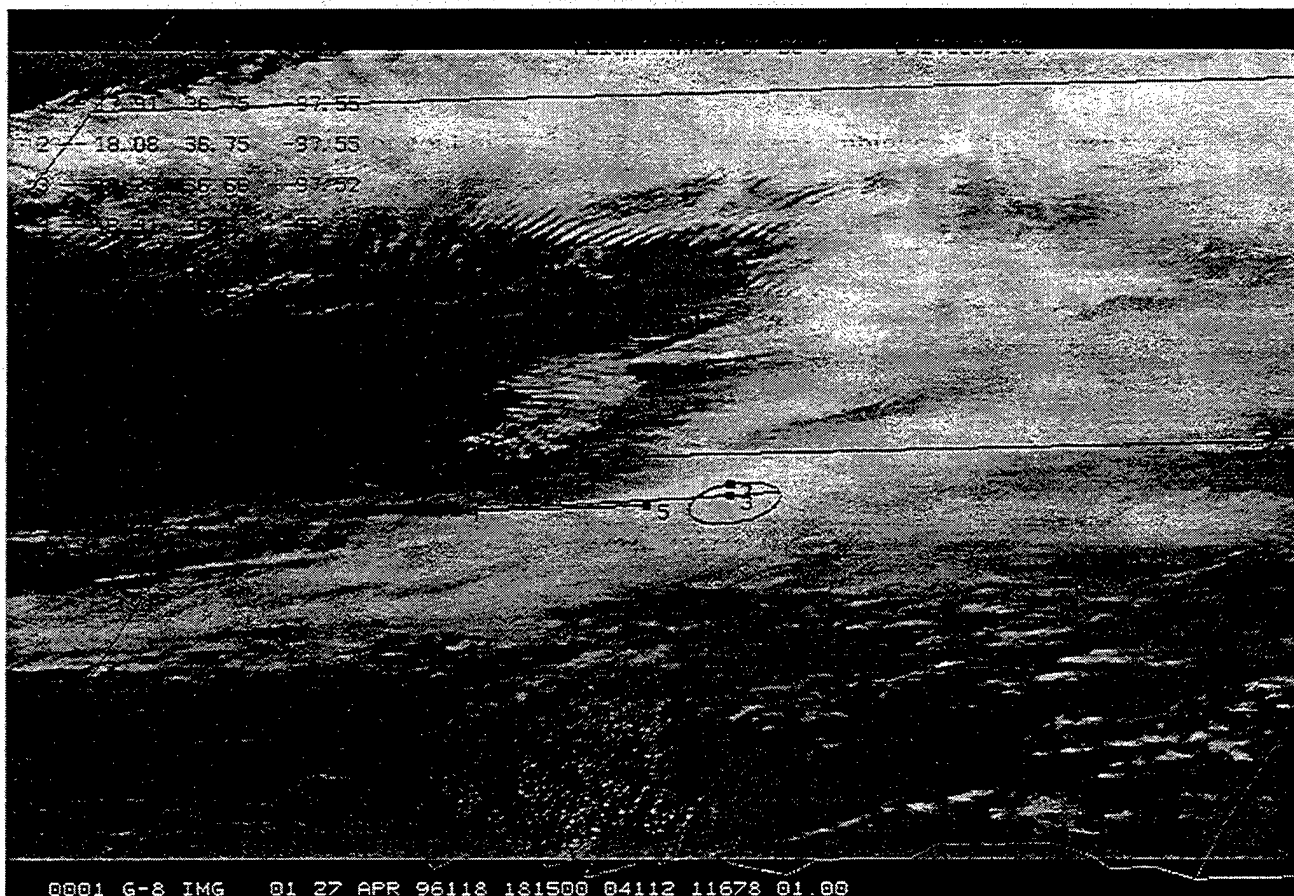
**Figure 3 GOES-8 Satellite Image Over Oklahoma 4/27/96: 181500 GMT with
DC-8 Path Overlaid: 175436 — 183448 GMT**
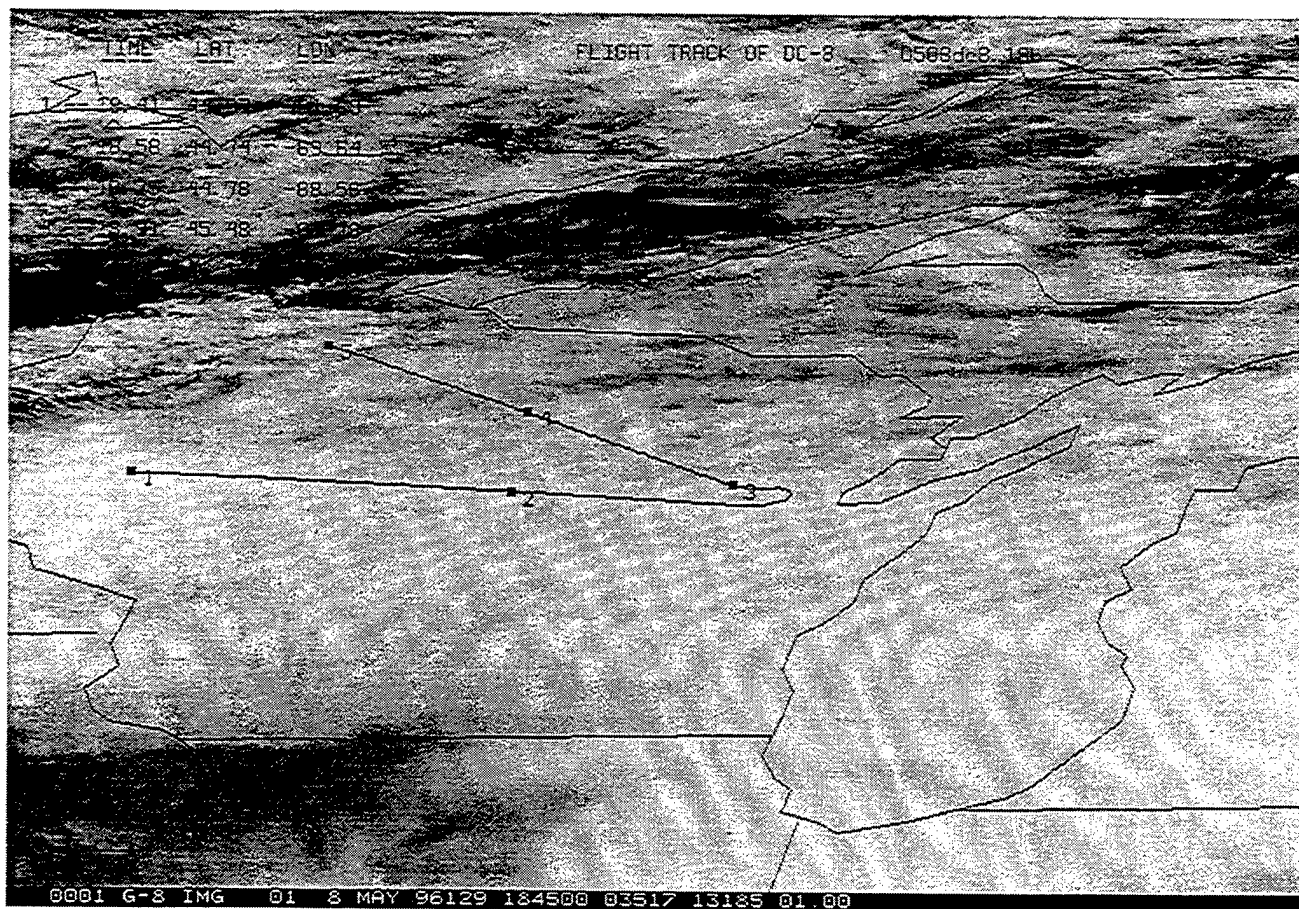
Figure 4 GOES-8 Satellite Image Over Wisconsin 5/08/96: 184500 GMT with DC-8 Path Overlaid: 182436 — 190448 GMT
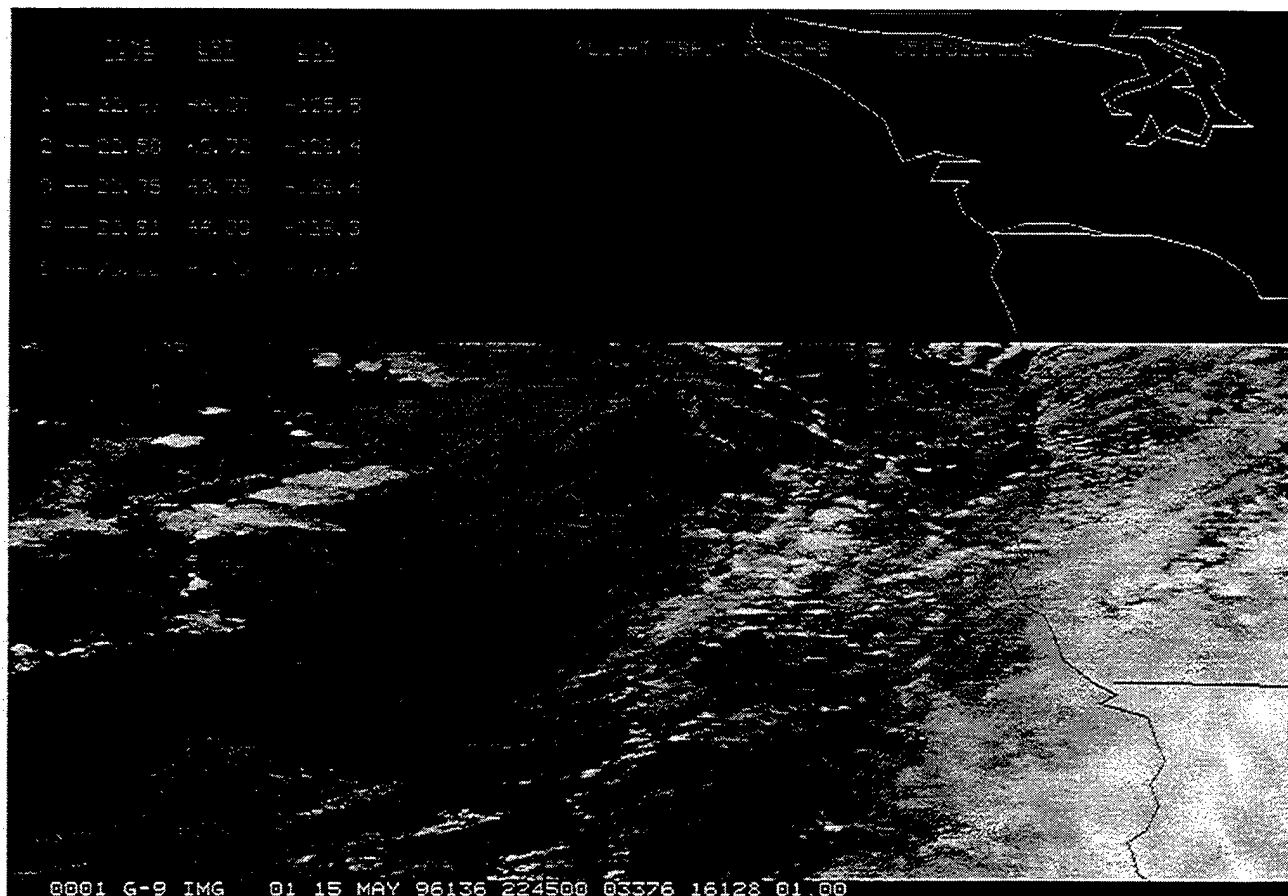
Figure 5 GOES-9 Satellite Image Over Oregon 5/15/96: 224500 GMT with
DC-8 Path Overlaid: 222436 — 230448 GMT

Our preliminary analysis of the SUCCESS data found at least 20 aircraft paths through cirriform clouds that could be used for parameter estimation. Further analysis of the aircraft observations led to the extraction of 29 path segments from the aircraft data, sampled across five days (several of these paths were generated by breaking longer paths into consecutive smaller path segments). Of these five sampling days, three were in geographically unique locations; Oklahoma/Kansas, Wisconsin, and Coastal Oregon (see Table 4). Of the 29 paths selected, 25 traversed through cirrus clouds and four through cirrostratus. Cirrocumulus clouds were not present in any of the 29 aircraft paths and were not sampled during the SUCCESS experiment. Therefore, we are unable at this time to estimate parameters for the cirrocumulus model. We will test the cirrocumulus model in a future effort.

Since the purpose of the SUCCESS experiment was to compare the microphysical properties of cirriform cloud types with aircraft contrails, only those paths through cirriform clouds could be used in

21

our analysis. This limited the overall number of paths available to us. In addition, aircraft logs taken during the experiment were not detailed, leading to some ambiguity about whether the aircraft were measuring cirriform clouds or contrails. Those paths that were ambiguous were discarded, leading to an additional reduction in the number of possible water content paths. A list of all 29 paths selected for analysis is included in Table 4. These paths are listed by date/time for each cloud type.

Table 4 Path Information

PATH NUMBERS	DATE (MM/DD/YY)	TIME (GMT) (HHMMSS)	LOCATION	CLOUD TYPE
2-1	04/21/96	182753 – 183006	Southwest Kansas	Cirrostratus
2-2	04/21/96	183006 – 183247	Southwest Kansas	Cirrostratus
3	04/21/96	184434 – 184712	Southwest Kansas	Cirrostratus
1	04/27/96	181917 – 182330	Northern Oklahoma	Cirrostratus
4-1	04/20/96	175031 – 175315	Northwest Oklahoma	Cirrus
4-2	04/20/96	175316 – 175612	Northwest Oklahoma	Cirrus
5-1	04/20/96	181741 – 181931	Northwest Oklahoma	Cirrus
5-2	04/20/96	181932 – 182247	Northwest Oklahoma	Cirrus
5-3	04/20/96	182248 – 182418	Northwest Oklahoma	Cirrus
5-4	04/20/96	182502 – 182720	Northwest Oklahoma	Cirrus
5-5	04/20/96	182722 – 182923	Northwest Oklahoma	Cirrus
7	04/20/96	184057 – 184221	Northern Oklahoma	Cirrus
8	04/20/96	184252 – 184407	Northern Oklahoma	Cirrus
9	04/20/96	184456 – 184615	Northern Oklahoma	Cirrus
10	04/20/96	184659 – 184818	Northern Oklahoma	Cirrus
11	04/20/96	190358 – 190619	Northern Oklahoma	Cirrus
12-1	04/20/96	192706 – 192944	Southwest Kansas	Cirrus
12-2	04/20/96	192945 – 193301	Southern Kansas	Cirrus
12-3	04/20/96	193302 – 193522	Northern Oklahoma	Cirrus
1	04/21/96	182113 – 182439	Northern Oklahoma	Cirrus
1-1	05/08/96	182915 – 183141	Central Wisconsin	Cirrus
1-2	05/08/96	183142 – 183503	Central Wisconsin	Cirrus
1-3	05/08/96	183504 – 183643	Central Wisconsin	Cirrus
1-4	05/08/96	183644 – 184058	Eastern Wisconsin	Cirrus
2-1	05/08/96	184437 – 184915	Eastern Wisconsin	Cirrus
2-2	05/08/96	184916 – 185323	Northern Wisconsin	Cirrus
2-3	05/08/96	185326 – 185732	Northwest Wisconsin	Cirrus
1-1	05/15/96	224817 – 224944	Coast of Oregon	Cirrus
3-1	05/15/96	230656 – 230945	Coast of Oregon	Cirrus

2.3.1.2 Selection Criteria

We used several criteria to select aircraft paths suitable for model parameter estimation. The basic tenet of our criteria is that the aircraft paths would be compared in a meaningful and consistent manner with paths extracted from the simulated cloud fields. The selection criteria were:

- Paths must be entirely within a cloud layer (i.e., no zero water content values)
- Paths must be straight
- Paths must be at constant altitude
- Aircraft speed must be relatively constant.

The rationale behind these selection criteria is driven by the nature of CSSM simulated paths. For proper comparison of the aircraft data to the model data, the conditions in which each path were extracted must be approximately the same. Simulated water content paths are extracted along a fixed horizontal (x, y) grid of water content values at a constant height. The paths are along a straight line from one end of a CSSM cloud boundary to the other, thus yielding a constant distance between data points along the path.

Determination of suitable aircraft paths was facilitated by visual inspections of the latitude, longitude, and height variables of recorded with each path. A summary of the path data is included in the next section.

2.3.1.3 Sample Data

Appendix B includes data summaries for each of the 29 water content paths that we selected for analysis. Each summary shows water content distributions along the path, the autocorrelation function, log-log plots of the fractal dimension (discussed in Section 2.3.2), and a histogram of the water content along the path. Each path is identified from the aircraft title.

2.3.2 Cirrus Model Parameters

This section describes the parameters that control the non-precipitating cirrus model of the CSSM. As described in Cianciolo et al. (1996), the CSSM employs the RSA algorithm to simulate the water content perturbation field in four dimensions inside the cirriform cloud boundaries. The CSSM then applies the perturbation field to the mean water content values predicted by the Feddes model (Feddes, 1974) and scales the result to achieve a given distributional form. A review of the primary

parameters used in the modeling process is included in the next subsection. These are the parameters which were tuned in the parameter estimation task.

2.3.2.1 Fractal Parameters

The character of the underlying RSA field is controlled by five key parameters: The Hurst parameter, lacunarity parameter, lattice resolution, and the upper and lower summation limits. A brief description of each parameter is included below. Following that, we include several figures which illustrate the effects of altering these parameters The RSA model was introduced in Saupe (1989). Its adaptation to the CSSM is described fully in Cianciolo et al. (1996). Here we assume some working knowledge of the algorithm.

- *Hurst Parameter (H)* — The Hurst parameter controls the amplitude of each term in the RSA sum. Higher values of H cause the amplitude to decrease more rapidly, with increasing frequency index, k, while lower values tend to decrease the amplitude more slowly. The qualitative effects of changing the Hurst parameter are illustrated in Figure 6.

- *Lacunarity Parameter (r)* — The lacunarity parameter alters the RSA sum in a similar manner to that of the Hurst parameter. However, the visual effects of altering this parameter are more difficult to detect. Small values of r lead to a smooth field with limited small scale structure while larger values of r roughen the field and yield greater small-scale detail. Figure 7 summarizes the effects of varying the lacunarity parameter.

- *Lattice Resolution (R)* — The lattice resolution relates the physical output grid to the random lattice. It specifies the number of output gridpoints per lattice point. By varying the resolution, the spatial distribution of field values is altered. Higher values of R yield a visually smoother field. Figure 8 illustrates the effects of varying R.

- *Summation Limits (k_0 and k_{max})* — The summation limits k_0 and k_{max} in the RSA formula are chosen to represent all spatial scales of the desired output field. The lower limit, k_0, represents the largest spatial scale in the output field and the upper limit k_{max} represents the smallest scale. Each successive frequency term in the RSA sum represents higher frequency variations within the water content perturbation field. Within the CSSM, the lower limit was set to 0, since negative values revealed negligible variations in the final field. The upper limit enables us to differentiate grid points separated by small distances for a given lacunarity parameter and lattice resolution. Figure 9 contains images of five individual frequency terms: $k = 0, 1, 2, 3, 4$ and an image containing the summation of those five frequencies. Notice that the higher the k index, the smaller the fine-scale structures are within the field.

24
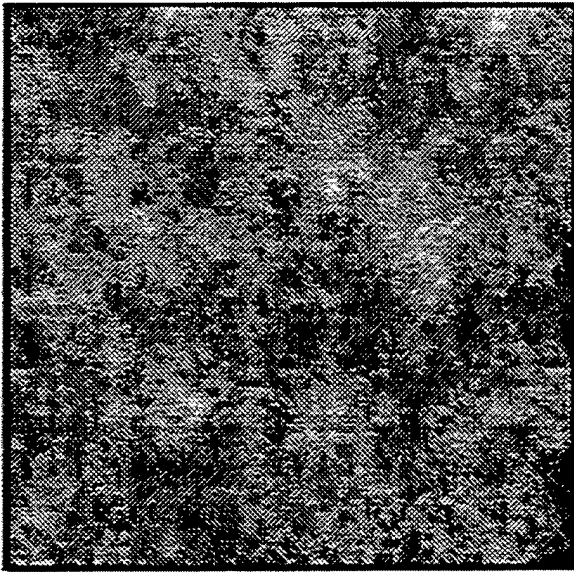
H = 0.2   **H = 0.4**
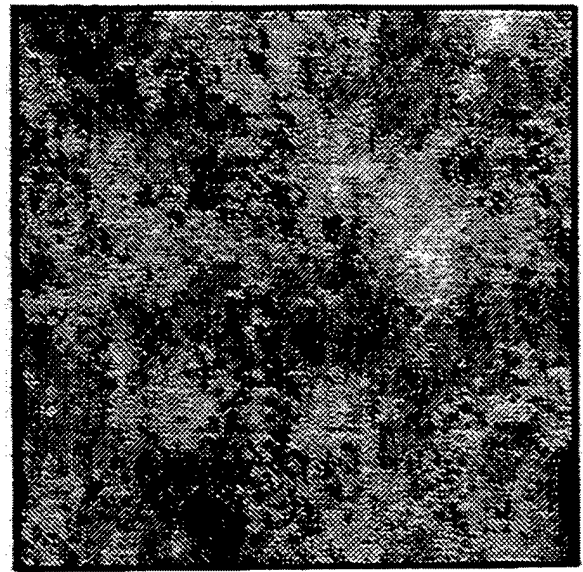
H = 0.6   **H = 0.8**

**Figure 6 Sequence of Grey-Scale Images Generated with the RSA Model
with Various Values for the Hurst Parameter**

r = 2   r = 3

r = 4   r = 5
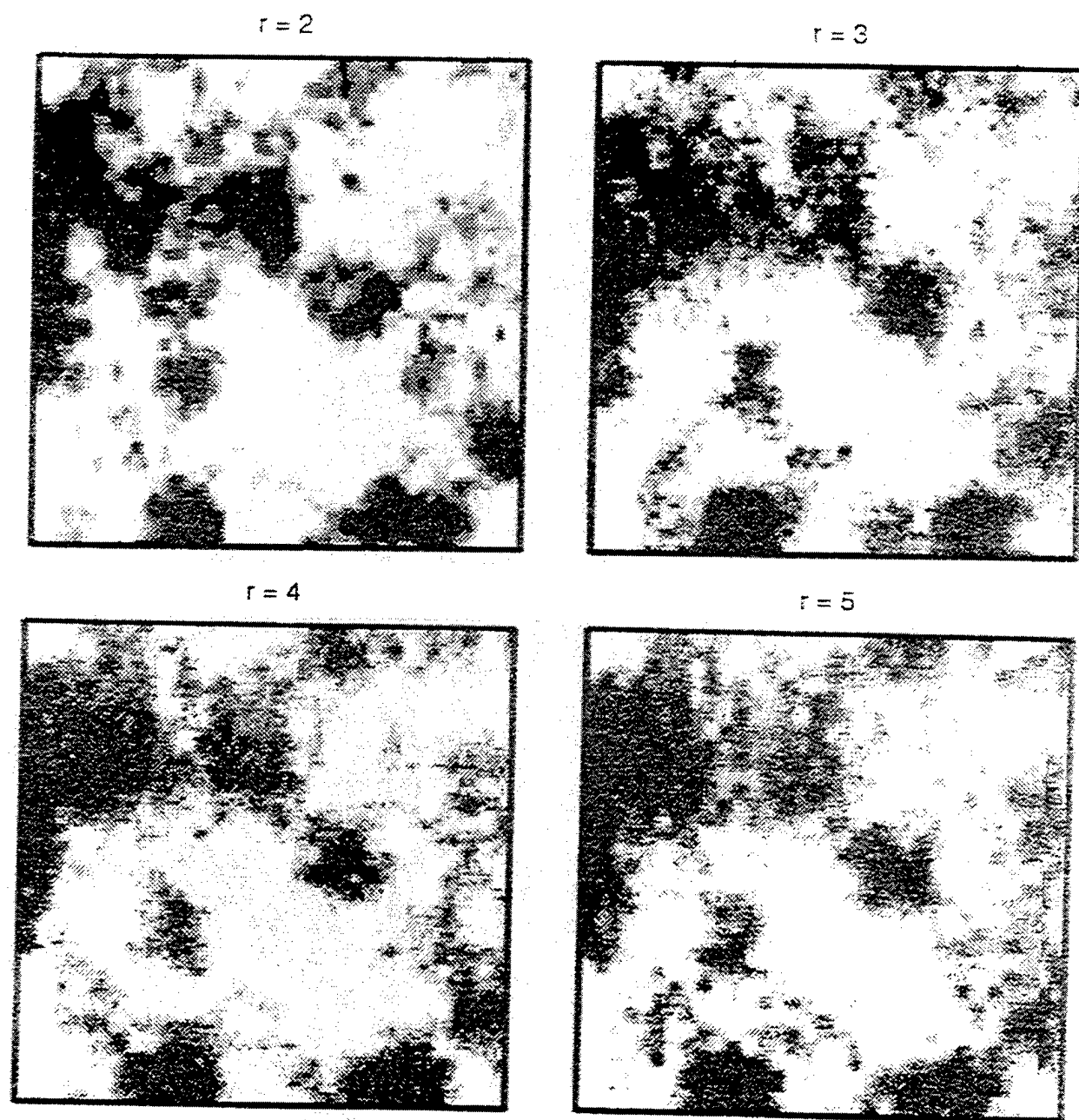
**Figure 7 Sequence of Grey-Scale Images Generated with the RSA Model
with Various Values for the Lacunarity Parameter**

Resolution = 10
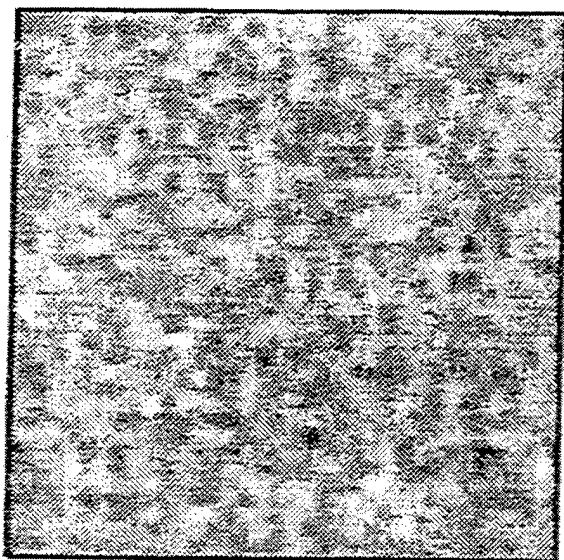
Resolution = 25

Resolution = 50
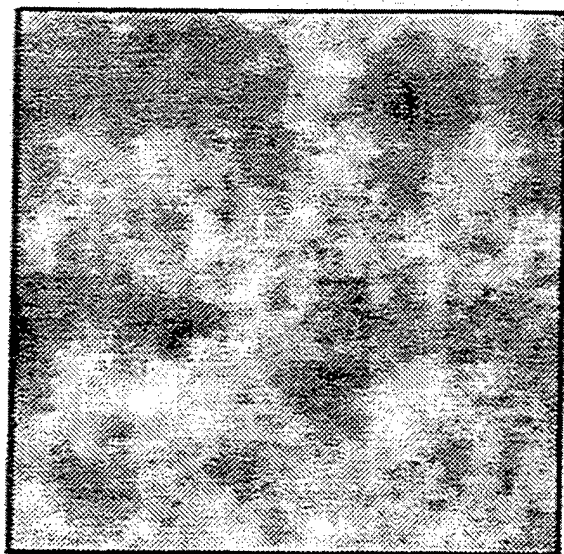
Resolution = 100
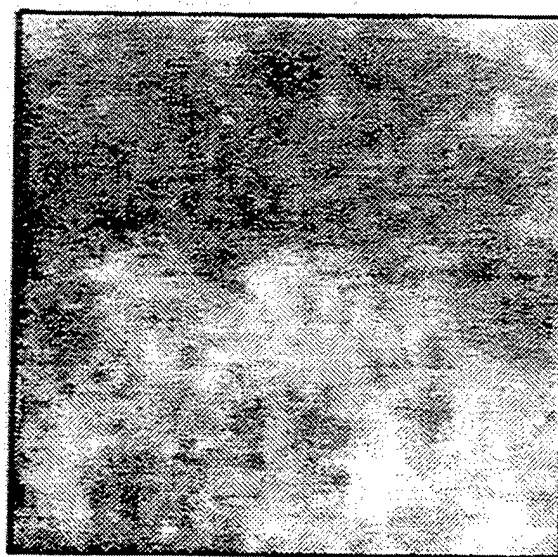
**Figure 8 Sequence of Grey-Scale Images Showing the Effects of Varying
the Lattice Resolution in the RSA Model**
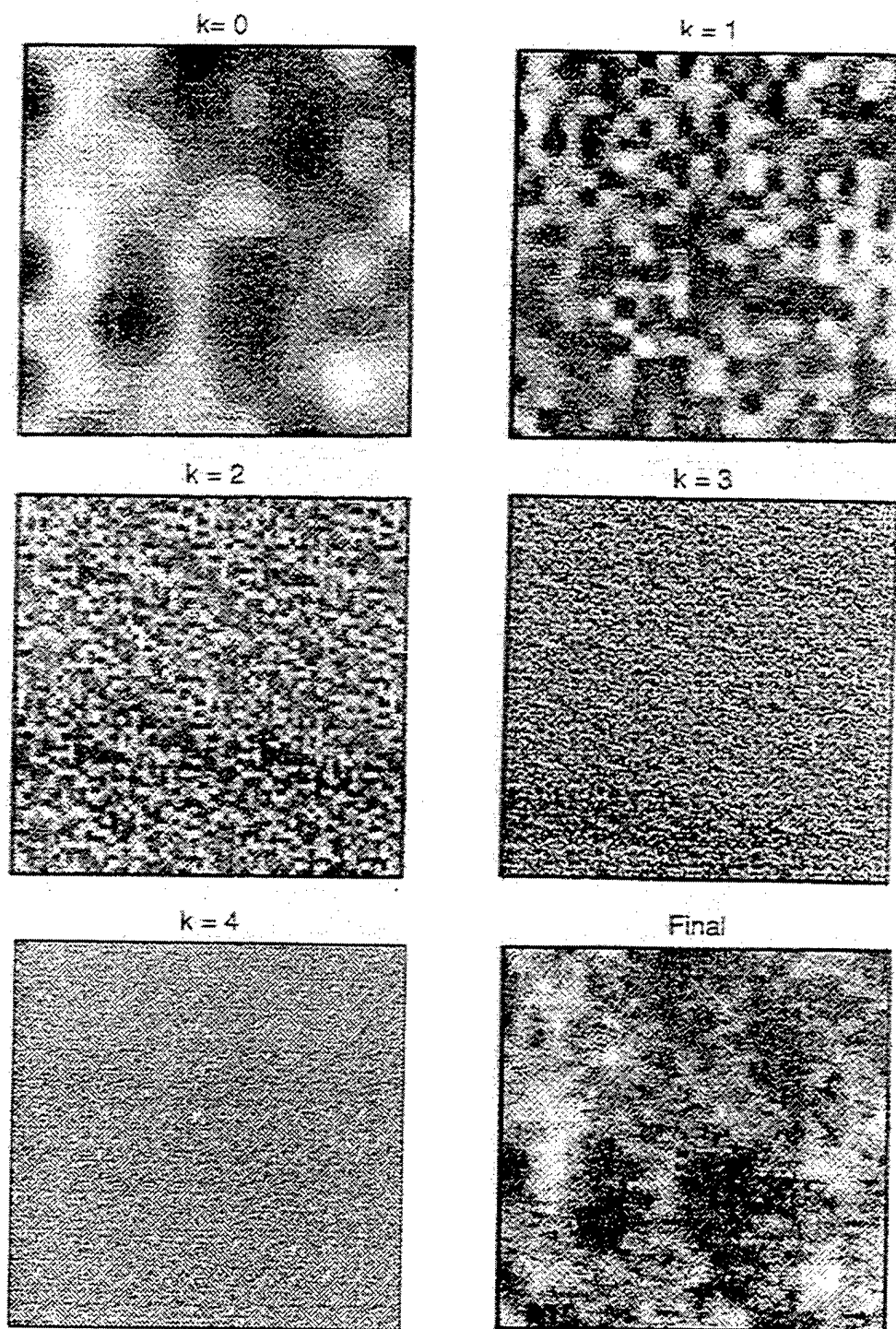
Figure 9 Sequence of Grey Scale Images Showing Five Frequency Terms and the Resulting RSA Field Generated by Summing the Terms

28

2.3.2.2 Internal Water Content Parameters

The CSSM uses the internal RSA algorithm to build the water content perturbation field at each gridpoint within a previously determined cloud "shell" (as defined by local base and top heights). (See Cianciolo et al., 1996 for details). The water content inside the cloud boundaries is then calculated by

$$wc = wc_{avg} + wc_{perturbation} \qquad (2\text{-}1)$$

where

- wc is the water content at the current gridpoint
- wc_{avg} is the average water content
- $wc_{perturbation}$ is a small perturbation generated with the four-dimensional RSA model.

The average water content (wc_{avg}) is calculated following Feddes (1974). The Feddes relationship provides average water content as a function of cloud type, cloud temperature, and vertical position in the cloud layer. The perturbation water content ($wc_{perturbation}$) field is calculated by scaling the RSA field values by the ratio of the standard deviations of the RSA field and an assumed standard deviation of the water content. The parameter of interest here is the standard deviation of the water content field. It is defined as follows:

$$sdev_{wc} = sdev_{ratio} * wc_{avg} \qquad (2\text{-}2)$$

Where $sdev_{ratio}$ is a parameter within the model which is estimated based on analysis of cloud water observations. (It is one of the parameters which we tuned as a part of this parameter estimation process.) The transformation from RSA field value to water content perturbation value is then simply

$$wc_{perturbation} = rsa * sdev_{wc} / sdev_{rsa} \qquad (2\text{-}3)$$

where $sdev_{wc}$ and $sdev_{rsa}$ are the standard deviations of the water content and rsa fields, respectively.

2.3.3 Parameter Estimation Process

The CSSM is very sensitive to the model parameters that control the water content output. We used an iterative approach to estimate model parameters which produce simulated water content paths

with characteristics similar to the observations described above. This process consisted of the following several steps:

- *Initialize CSSM* — We initialized the model with single-point meteorological profiles taken from radiosonde observations coincident with the selected observed paths. The radiosonde stations used were selected based on their proximity in time and space to the aircraft paths. The CSSM was initialized with coincident cloud information taken from the NASA ER-2. Terrain information was extracted from the radiosonde reports.

- *Run the baseline model* — We ran the baseline model ten times each for four different aircraft path observations (two cirrus, two cirrostratus). The model was initialized with differing random number seeds for each of the ten simulations to ensure a unique solution for each run.

- *Extract data paths from CSSM output fields* — Simulated water content paths were extracted from each simulation in each ensemble. These paths were extracted using an automated path extraction program which selected paths based on several criteria:

    Paths must match length of matching aircraft path.

    Angle of path must match angle of mean wind direction.

- *Compare aircraft and simulated paths* — The simulated water content paths were compared to the aircraft paths qualitatively (by comparing fractal dimensions, water content means, standard deviations, and autocorrelation functions).

- *Derive new CSSM parameters* — Based on the comparison between the aircraft and model water content paths and the statistical parameters calculated from the observations, a new set of model parameters was derived, keeping in mind how each parameter controls the character of the output field.

- *Repeat process* — This process was repeated until the simulated paths' characteristics agreed (within statistical limitations) with the observed paths' characteristics.

- *Run remaining cases* — After we developed an acceptable set of parameters, we ran the CSSM ten times each for each of the 25 remaining aircraft paths for final tuning and hypothesis testing. The final tuning procedure is outlined in Section 2.4.

Figures 10 through 12 outline the analysis and tuning process for two of the simulated model paths (one cirrus, one cirrostratus). These sample plots follow the same format as the one-page aircraft path summaries presented in Figure 6. The first figure (Figure 10) shows the results of the baseline model, the second (Figure 11) shows the results of the third tuning iteration, and the third (Figure 12) shows the results of the fully tuned model.

Model Path 11: 4/20/96 Run Number 1
Cloud Type: Cirrus

Path Height: 6700 m
Resolution: .169 km

Cloud Base: 5925 m
Cloud Top: 8910 m

Mean Water Content: 0.045 g/m³
Standard Deviation: 0.010 g/m³

Model Path 2-2: 4/21/96 Run Number 1
Cloud Type: Cirrostratus

Path Height: 7300 m
Resolution: .169 km

Cloud Base: 6870 m
Cloud Top: 10065 m

Mean Water Content: 0.061 g/m³
Standard Deviation: 0.012 g/m³
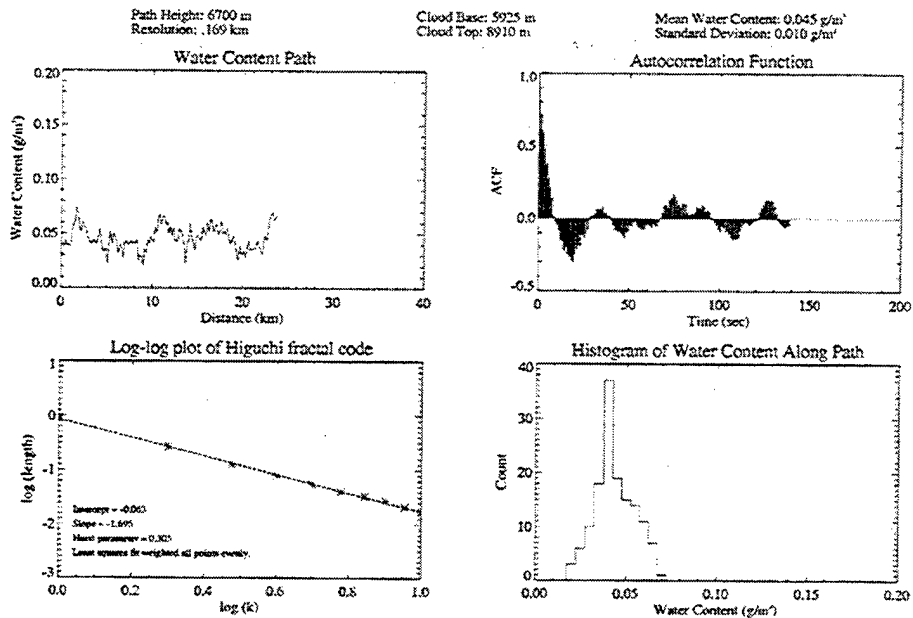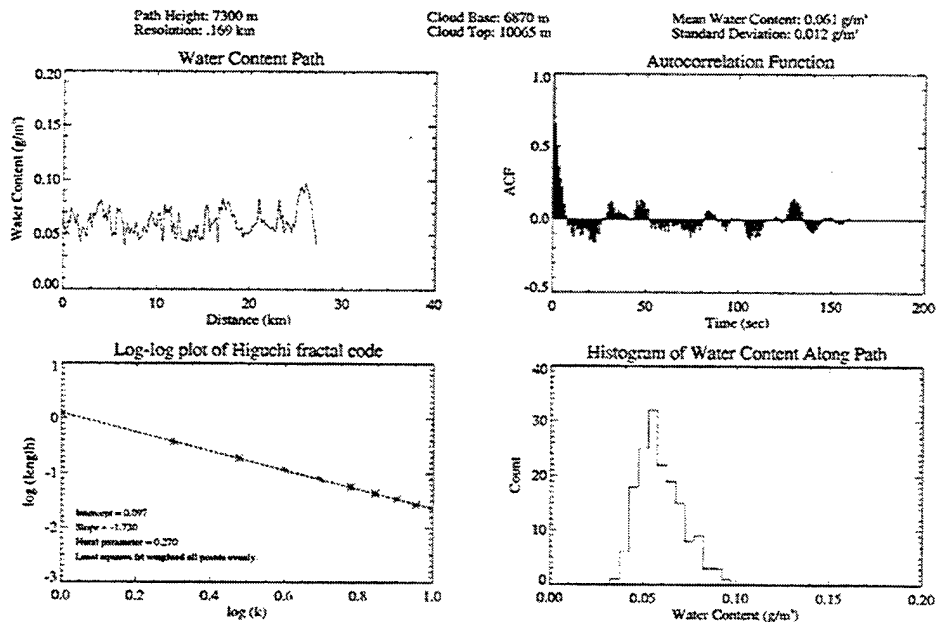
Figure 10 Baseline Model One-Page Summary for Path 11 (4/20/96) and Path 2-2 (4/21/96)

3rd Updated Model Path 11: 4/20/96 Run Number 1
Cloud Type: Cirrus

Path Height: 6700 m
Resolution: .169 km

Cloud Base: 5925 m
Cloud Top: 8910 m

Mean Water Content: 0.062 g/m³
Standard Deviation: 0.017 g/m³

3rd Updated Model Path 2-2: 4/21/96 Run Number 1
Cloud Type: Cirrostratus

Path Height: 7300 m
Resolution: .169 km

Cloud Base: 6870 m
Cloud Top: 10065 m

Mean Water Content: 0.069 g/m³
Standard Deviation: 0.008 g/m³
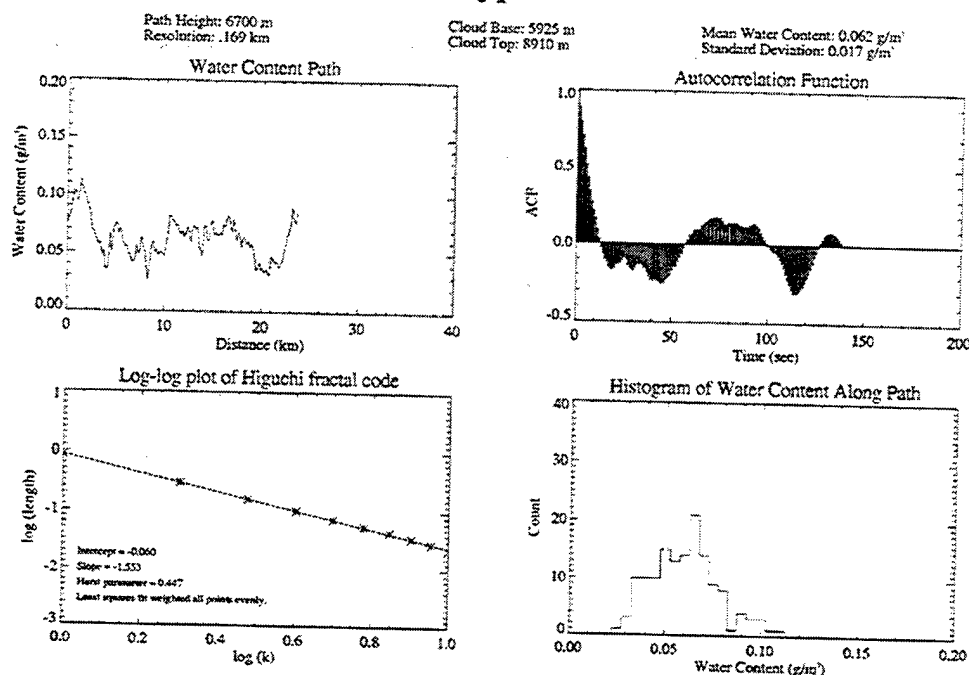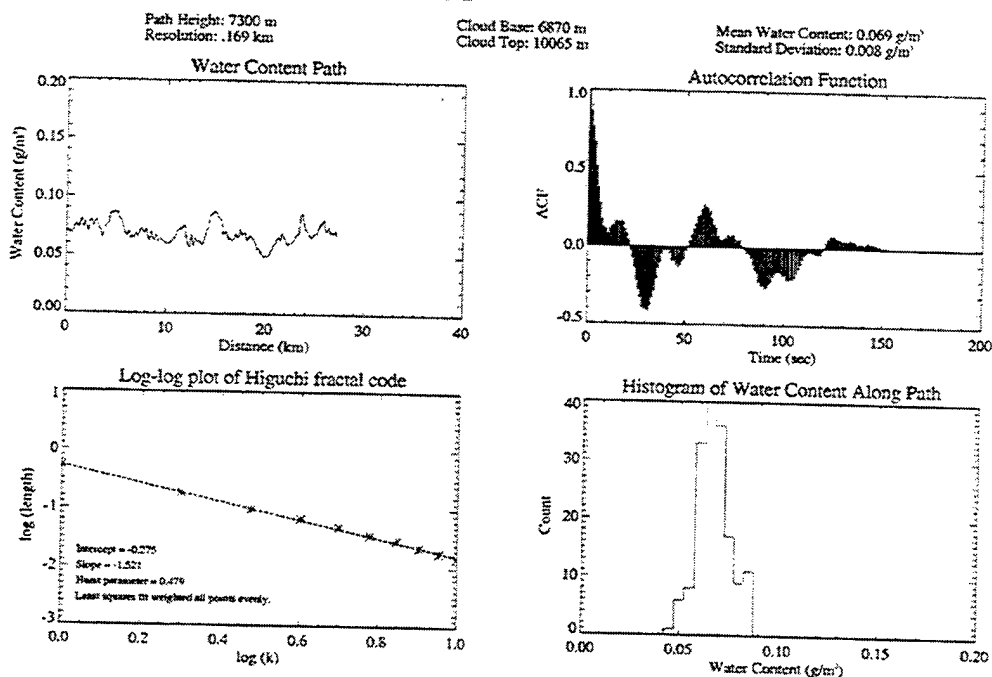
Figure 11 Third Model Tuning One-Page Summary for Path 11 (4/20/96) and Path 2-2 (4/21/96)

32

6th Updated Model Path 11: 4/20/96 Run Number 1
Cloud Type: Cirrus

Path Height: 6700 m
Resolution: .169 km

Cloud Base: 5925 m
Cloud Top: 8910 m

Mean Water Content: 0.059 g/m³
Standard Deviation: 0.022 g/m³

6th Updated Model Path 2-2: 4/21/96 Run Number 1
Cloud Type: Cirrostratus

Path Height: 7300 m
Resolution: .169 km

Cloud Base: 6870 m
Cloud Top: 10065 m

Mean Water Content: 0.094 g/m³
Standard Deviation: 0.029 g/m³
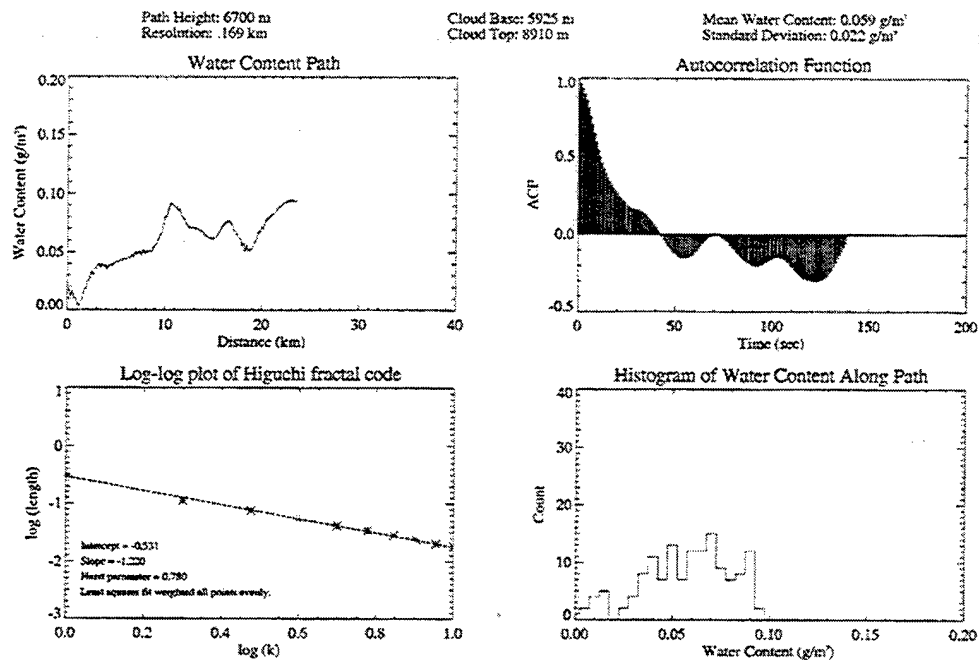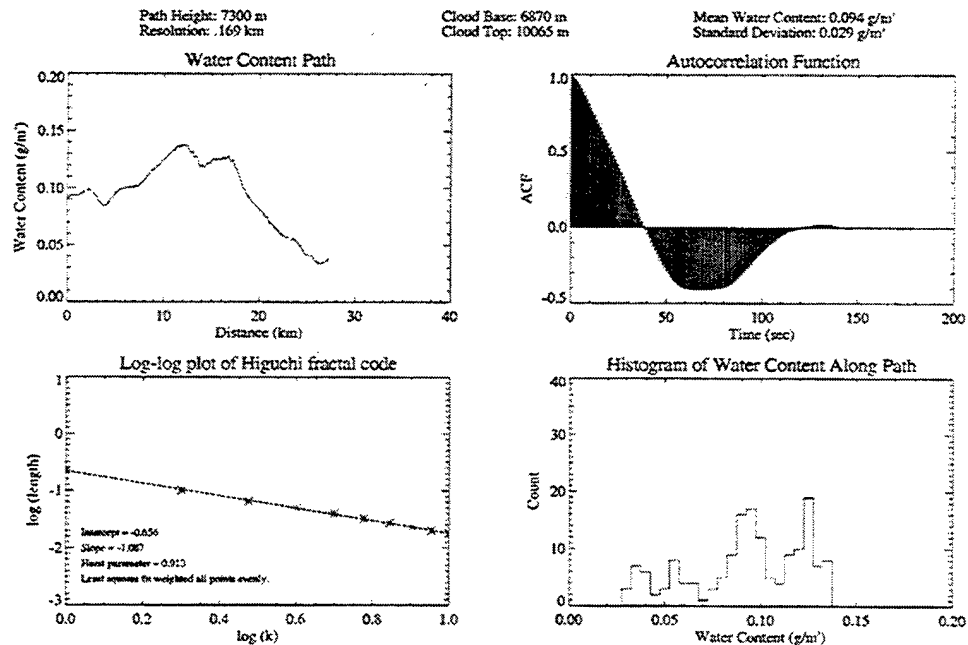
Figure 12 Fully Tuned Model One-Page Summary for Path 11 (4/20/96) and Path 2-2 (4/21/96)

33

Note that in several of these final 25 cases, we were unable to automatically extract complete water content paths due to the geometry of the path itself. In those cases, the DC-8 aircraft sampled water content near the extreme top of the cloud layer. This had the effect of creating water content sparse regions in the CSSM generated cloud fields at those observed heights. These water content sparse regions created problems, since we desired simulated water content paths that were within the cloud boundaries (like the aircraft water content paths). For those situations where this was a concern, we identified three possible solutions to the problem (applied separately or in combination):

1. Run the model with the same cloud input conditions and increase the domain size. This would increase the probability of suitable simulated path length extraction (i.e., with no zero values).

2. Run the model with an extended cloud top height. This would create a larger cloud and indirectly move the relative simulated path height within the layer, thereby increasing the probability of suitable simulated path length extraction.

3. Run the model with the same cloud input conditions and decrease the simulated path height. This would directly move the path height and increase the probability of suitable simulated path length extraction.

Given that we desired to replicate the observed conditions as best as possible, we opted for the first option whenever possible. Modifying the cloud domain size has no discernable effect on the distribution of the water content. However, this required that we run the CSSM with domain sizes on the order of 200 square kilometers in some cases, thereby greatly increasing the computation time. In those cases where extracted path lengths were still not long enough, we opted to use option 2. Increasing the size of the cloud does not alter the vertical distribution of water content since the Feddes model predicts a constant maximum condensed moisture everywhere throughout the vertical cloud layer for cirrus and cirrostratus cloud types. Option 3 was not used, since this would have caused the most deviation from the observations. We preferred to keep the simulated locations the same as the observed locations. In the end, we successfully extracted one complete path from each of the 290 CSSM runs.

The parameter estimation process documented here resulted in the modification of four parameters in the cirrus model: the standard deviation ratio, Hurst parameter, lattice resolution, and k_{max}. The entire set of baseline and tuned model parameters are listed at the beginning of Section 2.4.

2.4   TUNED MODEL RESULTS AND STATISTICAL ANALYSIS

2.4.1   Results

When the initial cirrus model in the CSSM was created, the goal was to produce realistic visualizations of cirriform clouds. Suitable cirrus data was not available to properly estimate the parameters. Thus, model parameters were estimated through a combination of visual inspection and literature research. For visualization purposes, this parameterization was sufficient. However, if other parameters were to be estimated from the water content data, such as radiometric information, a more rigorous approach was required.

When we initially compared the baseline model to the SUCCESS aircraft data, it became evident that it was necessary to change the parameters. The baseline model parameters were visually too "bumpy." Through analysis and extrapolation of basic statistics and fractal dimensions from the aforementioned SUCCESS data, we estimated new parameters for the cirriform clouds via the parameter estimation process outlined in Section 2.3.3.

Of those model parameters listed in Section 2.3.2 which are tunable, four were changed for cirrus and cirrostratus clouds. Due to the lack of sampled cirrocumulus water content data from SUCCESS, we did not change any parameters for this cloud type. The modified parameters include the Hurst parameter, standard deviation ratio, k_{max}, and lattice resolution. Table 5 outlines the baseline model parameters and Table 6 outlines the newly tuned model parameters.

Table 5 Baseline Cirriform Model Parameters

	CIRRUS	CIRROSTRATUS
Hurst Parameter (internal)	0.3	0.3
Hurst Parameter (external)	0.3	0.3
standard deviation ratio	50%	50%
k_{max}	4	4
lattice resolution	2, 10	2, 15

Table 6 Tuned Cirriform Model Parameters

	CIRRUS	CIRROSTRATUS
Hurst Parameter (internal)	0.5	0.4
Hurst Parameter (external)	0.6	0.5
standard deviation ratio	120%	50%
k_{max}	2	2
lattice resolution	6, 18	10, 15

The net effect of modifying these four variables was a smoother water content field (further explanation of each model parameter and its effects can be found in Section 2.3.2). The modification of these model parameters yielded model water content data which was in better agreement to the SUCCESS water content data. However, these new parameters were estimated based on only four water content paths. Thus, for verification of the newly estimated parameters, the model was run for the remaining 25 aircraft paths. Analysis of the new parameters was achieved through statistical comparisons and hypothesis testing, as described in the following subsections.

2.4.2 Statistical Comparison of Aircraft and Model Parameters

Having tuned the model parameters to better replicate the statistical characteristics observed in just four of the aircraft paths, we then ran the tuned CSSM for the remaining 25 aircraft paths and analyzed the output water content fields. The purpose of the analysis was to answer the following basic question:

Does the CSSM generate realistic cirriform water content fields?

One way in which to answer that question is to draw upon the field of statistical hypothesis testing. We can begin by rewording our basic question into a null hypothesis statement which we will test throughout the analysis. The null hypothesis is that the data simulated by the CSSM are similar to those observed in nature, or more specifically:

*Aircraft-based measurements and CSSM simulations of water content
data are drawn from the same distribution function.*

As with all hypothesis testing, we can disprove the null hypothesis if the distributions of the two data sets are shown to be different (at some confidence level). However, failing to *disprove* the hypothesis is not the same as *proving* it (that would require an infinite amount of data and resources). Failing to

36

disprove the hypothesis simply allows us to state that the two data sets under consideration are *consistent* with a single distribution.

The best test of the null hypothesis requires vast amounts of "ground truth" data. Ideally, cloud data from a wide range of locations, dates, times, altitudes, temperatures, probes, etc. would be used. However, as discussed previously, the data set used to support this analysis is quite limited. In fact, of the 29 paths selected for analysis, only some of them are independent. Many of the sampled paths were taken from successive tracks through a continuous cloud field and are therefore highly correlated. All data paths selected were sampled on constant altitude flight paths and all data paths were taken as part of the SUCCESS experiment. These factors in combination with the limited number of paths reduce the universality of our conclusions. Future efforts could expand the analysis to include other experimental data sets, other flight path configurations, etc.

The types of statistical tools which are available for use in hypothesis testing vary depending on the type of data one is analyzing. In our case, data were highly correlated (time series). As can be seen in the series of histograms presented in the right-hand lower corner of the one-page aircraft summaries (Appendix B) our data are not necessarily normally distributed, although most distributions show some central tendency. These features of the data limit the analysis tools at our disposal and limit the conclusions that can be drawn from our analysis.

After a fair amount of research, we decided upon the following analysis steps (each of these steps is discussed in turn in the following sections):

- Qualitative visual inspection of IWC data paths
- Qualitative visual inspection of basic statistics via scatterplots
- Quantitative comparison of basic statistics and sigma distance measures
- Application of the Tshebycheff inequality measure.

The analysis process consisted of generating ten CSSM runs for each of the aircraft paths. The ten CSSM runs were identical in all aspects except for the initial random number seed, thus providing a range of paths sampled from one underlying water content distribution. We computed the following variables for all ten CSSM paths and the associated aircraft path: mean IWC, standard deviation of IWC, measured Hurst parameter, and time at which the autocorrelation function reaches zero.

The next several subsections describe the results of the data analysis task. Throughout the following discussion, we refer to both the parameter estimation and model verification processes as we used identical techniques for the two.

Visual inspection

The first step in the analysis process was to simply look at the IWC data series and determine whether the model paths agreed qualitatively with their aircraft counterparts. (It is very important to remind the reader at this time that the CSSM does not replicate the exact water content observed at a given date/time/altitude, rather it simulates data fields with the same "character" as those observed in nature.)

We relied on visual inspection of water content paths (discussed in this subsection) along with analysis of means, variances, and autocorrelation functions (see next subsection) to initially tune several CSSM parameters. We generated graphs of IWC data paths for each iteration in the tuning process and observed the changing character of the data paths with each change in parameters. We settled on updated parameters based on four test cases and later, as part of the verification process, verified the model for the remaining 25 cases.

As expected, our initial visual comparisons between baseline model data and aircraft data showed significant discrepancies between model and observed data. Recall that the parameters used in the CSSM were simple placeholders until improved values were identified. It was clear from the beginning that the baseline CSSM cirrostratus and cirrus models produced ice water content paths that were too "bumpy" when compared to the SUCCESS data. That is, the model produced cloud fields in which the IWC spatial correlations were too short, and the variances were too high. Initial changes in the internal Hurst parameter (used to control the cloud interior IWC field) and the standard deviation ratio used within the CSSM corrected many of the qualitative discrepancies. Continued analysis led us to modify the k_{max} parameter, lattice resolution, and the external Hurst parameter (used to control the external cloud shapes). The final combination of parameters and the associated initial values were presented in Tables 7 and 8.

38

Iterative visual inspection was critical for estimating improved values of the Hurst parameter (H), k_{max}, and the lattice resolution since for each of these parameters there exists no direct relationship between a measured output parameter and the associated input parameter. For example, the fractal dimension (and associated H value) that is estimated from the IWC data series using the Higuchi algorithm (Higuchi, 1988) appears to be a complicated function of H, k_{max}, and the lattice resolution. In an ideal world, we may have built a large experiment consisting of hundreds of model runs to sample the entire parameter space to identify the functional relationships between all of the input and output parameters. However, with limited resources, we instead performed a limited trial and error experiment, in which we attempted to quickly achieve reasonable cloud fields with a minimal number of parameter changes.

Figures 13 and 14 show side-by-side observed and simulated IWC paths for all four initial test cases. The graphs in Figure 13 correspond to two cirrostratus paths, and those in Figure 14 correspond to cirrus cloud paths. The left plot in each series corresponds to the aircraft data, the middle plot corresponds to the baseline model (with untuned parameters), and the right plot shows the new model (with tuned parameters). The model runs shown in these figures were selected at random from the 10 possible runs generated for each of the aircraft cases.

It is easy to see that for the cases shown, the new model parameters produce a more realistic IWC distribution. The overall amount of variability, the bumpiness, and the intervals between IWC peaks agree favorably with the tuned model. Keep in mind however, that only four cases are shown and only one model run is used for comparison. As we will show in Appendix C, there is a fair amount of variability between individual model runs with widely varying means, variances, and autocorrelation lengths. However, as we know, there is also a vast range in observed cirrus cloud variables. For example, note the very high maximum IWC in Path 11 presented in the top row of Figure 14.
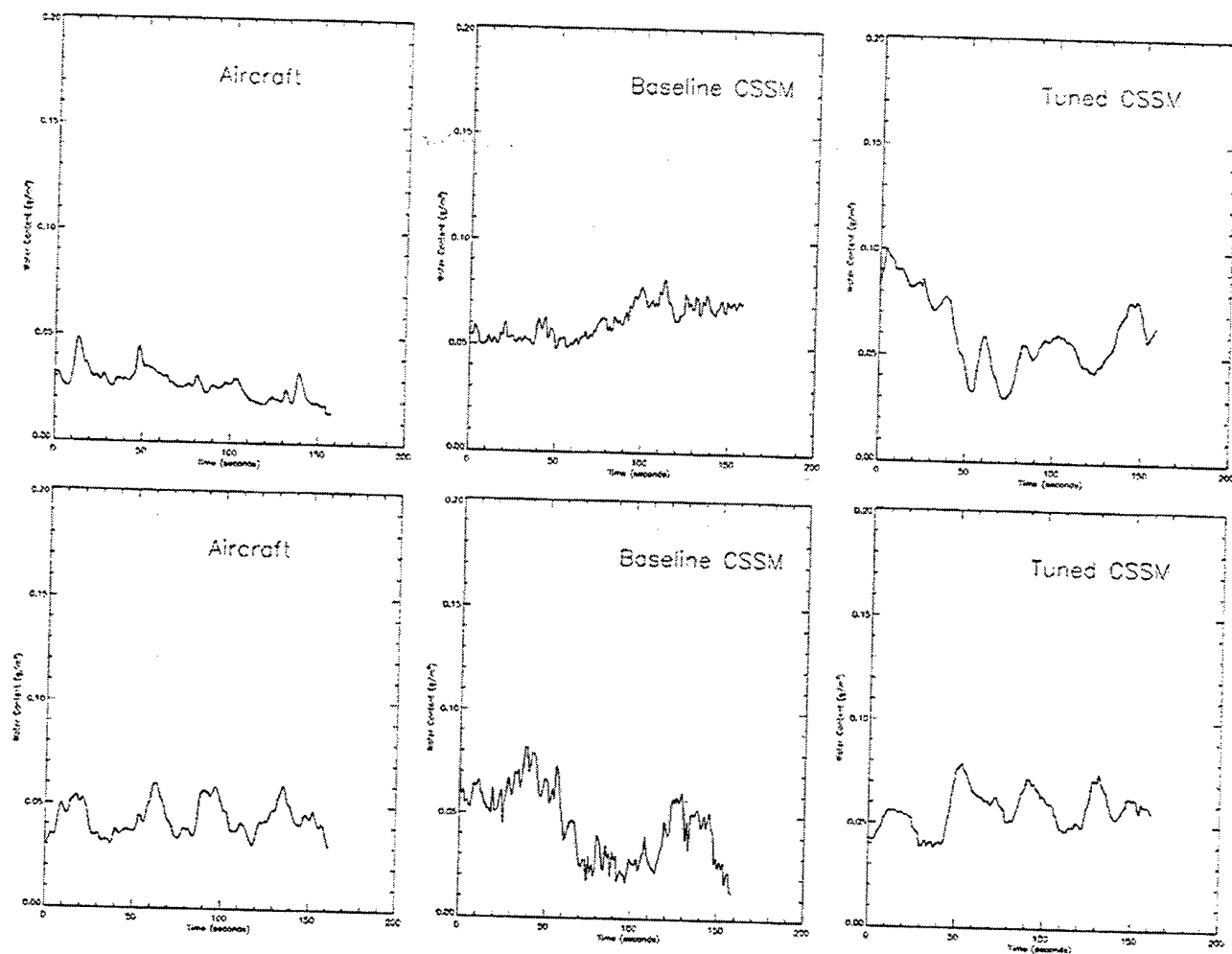
Figure 13 Cirrostratus Path 3 (top row) and Path 2-2 (bottom row) — IWC sampled along horizontal paths showing the qualitative agreement between observed and simulated clouds (left — aircraft observations; middle — baseline CSSM; right — tuned CSSM)

40
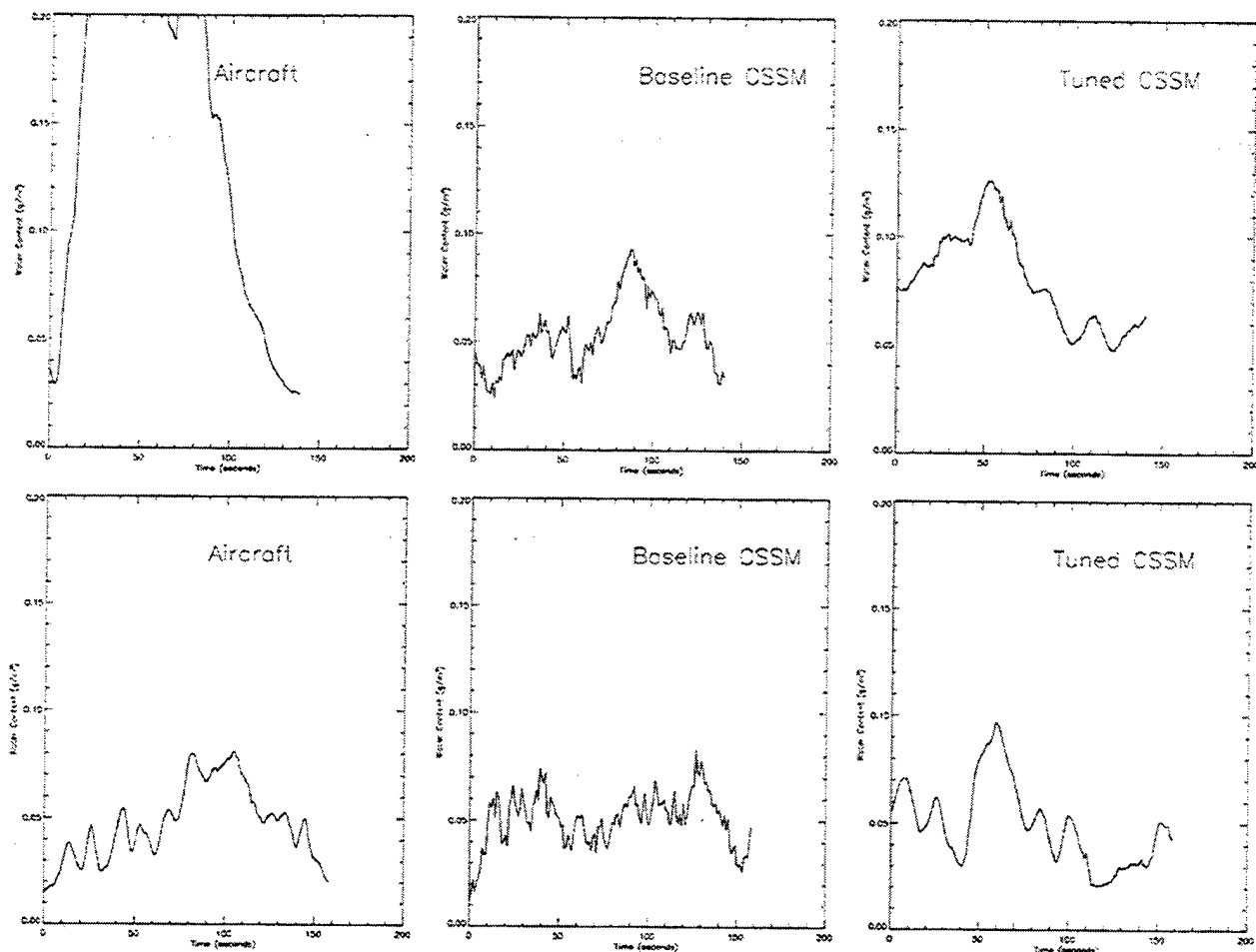
Figure 14　Cirrus Path 11 (top row) and Path 12-1 (bottom row) — IWC sampled along horizontal paths showing the qualitative agreement between observed and simulated clouds (left — aircraft observations; middle — baseline CSSM; right — tuned CSSM)

Scatterplots

Another useful visual tool in our analysis is the scatter plot. It offers a quick view of the parameter space associated with the selected data. We used scatterplots to visually summarize both observed and simulated IWC data both during parameter estimation and model verification. We computed basic statistical characteristics of each of the 29 observed and 290 simulated IWC data paths. These statistics include:

- mean IWC
- standard deviation of IWC
- measured Hurst parameter using Higuchi code ($H_{measured}$)
- time at which autocorrelation function reaches zero ($ACF_{zero\ crossing}$).

41

The statistics derived from the "tuned" model are presented in their entirety in table format in the next subsection. They are presented here in the scatterplots shown in Figure 15 and 16, for cirrostratus and cirrus data paths, respectively. To generate these plots, we overlaid parameters from all 29 aircraft paths and the corresponding 290 CSSM-produced paths. Figure 15 contains only those four observed and 40 simulated cases containing cirrostratus cloud data. Figure 16 contains the remaining 25 observed and 250 simulated cirrus cases.

Table 7 Qualitative agreement between observed and simulated water content paths

	CIRROSTRATUS	CIRRUS
Mean IWC	fair[5]	poor[6,7]
Standard Deviation	good[5]	fair[8]
Hurst Parameter	poor[3,4]	good[2]
$ACF_{zero\ crossing}$	good[1]	good[1]

A summary of the qualitative findings from the series of scatterplots is presented in Table 7. Several general comments can be made concerning these findings:

The scatterplots show the *overall ranges* of each output parameter. It does not provide comparisons of the *individual* path parameters. (See the next subsection for parameter comparisons on a path-by-path basis.) However, in keeping with the primary goal of the CSSM, the scatterplots are quite useful since it provides evidence of whether the CSSM simulates typical cloud data with realistic water content distributions.

The number of observed data paths (especially in the case of cirrostratus) is limited. Consequently, the ranges presented in the scatterplots are incomplete. One should expect a wider range of parameter values as the number of data paths increases. In addition, we might expect to see a central tendency to emerge as the number of data paths increases.

Some data paths are highly correlated since they were sampled along successive tracks through the same cloud fields. This further reduces the variability in parameter ranges.

These scatterplots show the range of values for each of the four measured statistical parameters. It is important to remember that the IWC data series are not necessarily sampled from a normal distribution and thus the standard statistical metrics are not necessarily appropriate. However, most of the

42

IWC distributions are at least centrally peaked and therefore a mean and deviation are useful none-theless. (Distribution functions for each of the *aircraft* paths are presented in Appendix B). Distribution functions for select *simulated* paths were presented in Figures 10 through 12.

Several specific comments follow concerning individual parameters presented in Figure 15 and 16. These numbered comments correspond to the numbered notes in Table 7.

1. *ACF$_{zero\ crossing}$* values compare well between observed and simulated data paths for both cirrostratus and cirrus cloud types. Qualitatively, this implies that the horizontal correlation distances modeled by the CSSM are realistic.

2. Hurst parameters compare well between observed and simulated data for *cirrus* cloud paths. Qualitatively, this implies that the data paths have similar fractal dimension.

3. Hurst parameters compare poorly between observed and simulated data for cirrostratus cloud paths. Qualitatively, this implies that the CSSM produces data paths with unrealistic fractal dimensions for the cirrostratus cloud type. However, this may be partly due to the limited number of data paths and the fact that three of the four paths are sampled from the same cloud. Thus, the observed data are not covering the range of fractal dimensions expected.

4. Attempts to decrease the internal H parameter used in the CSSM to achieve closer measured fractal dimensions on output produced qualitatively unrealistic cirrostratus IWC paths. Specifically, lower values of H produced higher frequency "bumps" in the data not visible in the observed IWC series. This is a good example of the non-linearity and non-independence of the various parameters used within the model. We tried to select the best combination of parameters to achieve our most important goal — realistic IWC fields. Thus, we thought it best to refrain from decreasing the H value beyond its current "tuned" value.

5. Mean IWC values for cirrostratus data paths compare well. The three observed values grouped about 0.05 g/m³ are all taken from the same cloud field. There is more variability present in the simulated paths because there are more paths and all are sampled from completely independent cloud fields. Same comments apply for the associated standard deviation.

6. Mean IWC values for cirrus data paths compare poorly. The CSSM appears to over predict water content. However, deeper investigation shows that the majority of the means clustered just around 0.005 g/m³ (seven out of eight paths) were sampled from the same cloud field on 8 May 1996. Analysis of satellite imagery from that date/time indicate that the cirrus cloud layer is very optically thin (See Figure 4). The mean water contents simulated in the CSSM using the Feddes model (Feddes, 1974) do not include optically thin cloud layers and thus do not compare well. We may need to develop a "thin cirrus" cloud type in future versions of the CSSM.

7. Going beyond the thin cirrus cases, the CSSM also tends to over predict IWC for the optically thick cirrus clouds sampled in SUCCESS. The Feddes model (Feddes, 1974) is used to specify the mean IWC within the CSSM. During our literature search we identified several sources containing mean IWC values measured from a variety of experiments (Heymsfield and Knollenberg, 1972; Kosarev and Mazin, 1991; Quante et al., 1990). The means varied widely depending on the experiment, the measurement technique, the individual cloud fields, the position within the cloud layers, the synoptic conditions, and the age of the cloud, among other variables. The means predicted by the Feddes model fit within the range of measurements presented in those references. Therefore, we have not modified the Feddes model at this time and we accept its differences with the SUCCESS data used in our analysis.

8. Many of the same comments apply for the associated standard deviation. The CSSM does not simulate the low standard deviations seen in the optically thin cirrus cases. However, it does produce values in the range shown in Figures 15 and 16 for the thicker cloud layers and presented in various literature sources (e.g., Heymsfield and Knollenberg, 1972). As we will discuss in the next subsection, the ratio of standard deviation to mean (*sdev_ratio*) used within the model compares fairly well even on a case by case basis (including the thin cirrus case).
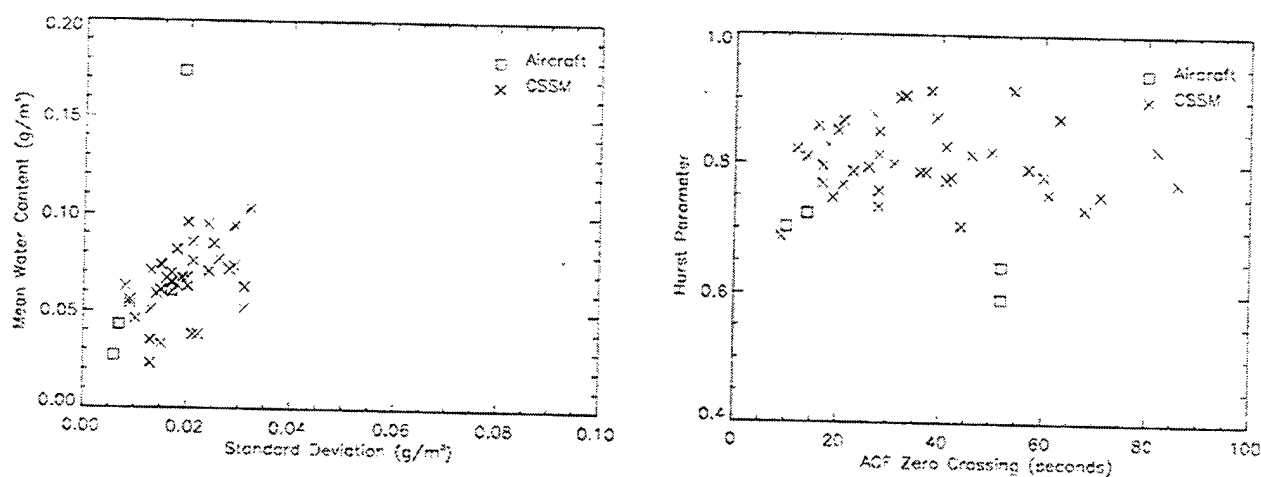
Figure 15   **Cirrostratus — scatterplot of IWC statistics estimated from aircraft and model data paths**

44
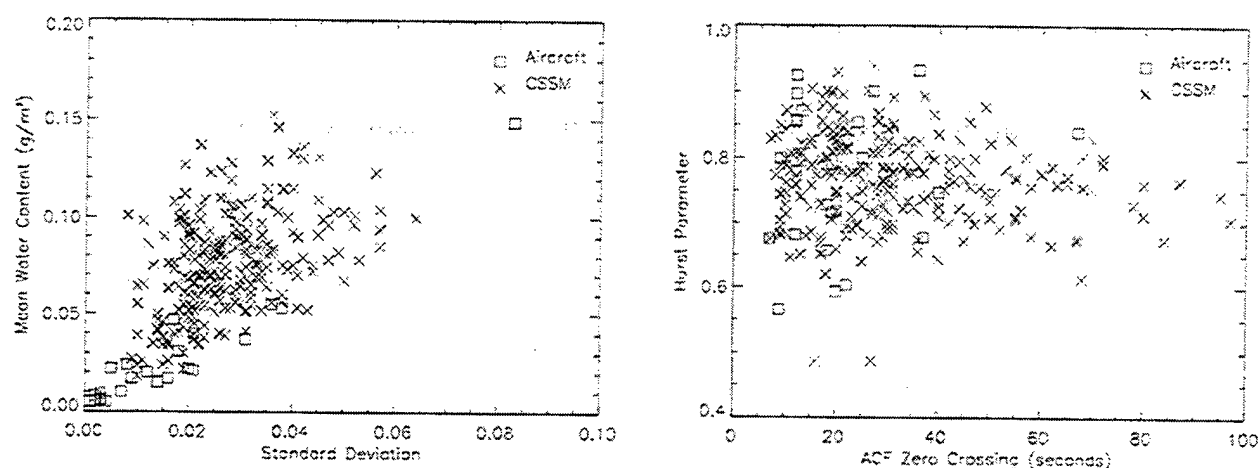
Figure 16   Cirrus — scatterplot of IWC statistics estimated from aircraft and model data paths

Comparison of average statistics

In the previous subsection, we displayed several basic statistical parameters that characterized each of the 29 IWC data cases (including aircraft and simulated data). Parameters from those paths were grouped by cloud type and displayed to show the range of measured values. In this section we show the same parameter values for each *individual* data path. As before, we are interested in the following statistical variables which include one additional parameter ($sdev_{ratio}$):

- mean IWC
- standard deviation of IWC ($sdev$)
- standard deviation ratio ($sdev_{ratio} = sdev$ / mean)
- measured Hurst parameter using Higuchi code ($H_{measured}$)
- time at which autocorrelation function reaches zero ($ACF_{zero\ crossing}$).

These statistical parameters were computed for each of the 29 observed and 290 simulated IWC data paths. They were computed during each stage of the parameter estimation process and compared to observed values. The statistics derived from the final "tuned" model are presented in their entirety in Table 8.

45

Table 8 List of statistical parameters derived for each IWC path (aircraft and 10 CSSM runs), average values calculated from the 10 model runs for each parameter, and distance (measured in units of sigma) between aircraft parameter value and average value. Parameters include the mean ice water content (g/m^3), standard deviation of IWC (g/m^3), standard deviation ratio (sdev/mean), measured Hurst parameter, and time (in seconds) that ACF goes to zero.

DATE	PATH	MEAN	SDEV	SDEV RATIO	H	ACF
21-Apr	2-1 (cirrostratus)	0.061	0.017	0.279	0.723	14.00
	cssm1	0.063	0.02	0.317	0.857	16.00
	cssm2	0.033	0.015	0.455	0.769	17.00
	cssm3	0.072	0.028	0.389	0.828	18.00
	cssm4	0.063	0.031	0.492	0.734	28.00
	cssm5	0.035	0.013	0.371	0.787	23.00
	cssm6	0.103	0.032	0.311	0.902	32.00
	cssm7	0.023	0.013	0.565	0.686	9.00
	cssm8	0.038	0.021	0.553	0.871	39.00
	cssm9	0.038	0.022	0.579	0.779	42.00
	cssm10	0.052	0.031	0.596	0.705	44.00
	Mean	0.052	0.0226	0.463	0.7918	26.80
	Sdev	0.024	0.008	0.110	0.072	12.14
	Distance	0.377	0.744	1.674	0.955	1.05
21-Apr	2-2 (cirrostratus)	0.043	0.007	0.163	0.702	10.00
	cssm1	0.094	0.029	0.309	0.913	38.00
	cssm2	0.063	0.008	0.127	0.809	14.00
	cssm3	0.046	0.01	0.217	0.865	21.00
	cssm4	0.059	0.014	0.237	0.814	46.00
	cssm5	0.065	0.017	0.262	0.905	33.00
	cssm6	0.067	0.019	0.284	0.793	57.00
	cssm7	0.054	0.009	0.167	0.796	17.00
	cssm8	0.056	0.009	0.161	0.821	12.00
	cssm9	0.071	0.013	0.183	0.782	60.00
	cssm10	0.076	0.021	0.276	0.915	54.00
	Mean	0.0651	0.0149	0.222	0.8413	35.20
	Sdev	0.013	0.007	0.061	0.053	18.54
	Distance	1.655	1.181	0.975	2.628	1.36

Table 8 (Continued)

DATE	PATH	MEAN	SDEV	SDEV RATIO	H	ACF
21-Apr	3 (cirrostratus)	0.027	0.006	0.222	0.592	52.00
	cssm1	0.085	0.025	0.294	0.787	36.00
	cssm2	0.068	0.019	0.279	0.747	19.00
	cssm3	0.063	0.02	0.317	0.875	27.00
	cssm4	0.06	0.017	0.283	0.8	31.00
	cssm5	0.065	0.017	0.262	0.766	21.00
	cssm6	0.068	0.02	0.294	0.827	41.00
	cssm7	0.063	0.018	0.286	0.813	28.00
	cssm8	0.067	0.016	0.239	0.758	28.00
	cssm9	0.074	0.029	0.392	0.871	63.00
	cssm10	0.071	0.024	0.338	0.755	61.00
	Mean	**0.0684**	**0.0205**	**0.298**	**0.7999**	**35.50**
	Sdev	**0.007**	**0.004**	**0.043**	**0.047**	**15.36**
	Distance	**5.814**	**3.455**	**1.787**	**4.468**	**1.07**
27-Apr	1 (cirrostratus)	0.174	0.019	0.109	0.642	52.00
	cssm1	0.096	0.02	0.208	0.823	82.00
	cssm2	0.065	0.017	0.262	0.753	71.00
	cssm3	0.086	0.021	0.244	0.774	41.00
	cssm4	0.082	0.018	0.220	0.731	68.00
	cssm5	0.077	0.026	0.338	0.772	86.00
	cssm6	0.07	0.017	0.243	0.794	26.00
	cssm7	0.051	0.013	0.255	0.85	20.00
	cssm8	0.074	0.015	0.203	0.819	50.00
	cssm9	0.061	0.015	0.246	0.787	37.00
	cssm10	0.095	0.024	0.253	0.849	28.00
	Mean	**0.0757**	**0.0186**	**0.247**	**0.7952**	**50.90**
	Sdev	**0.015**	**0.004**	**0.038**	**0.040**	**24.24**
	Distance	**6.751**	**0.097**	**3.660**	**3.857**	**0.05**

Table 8 (Continued)

DATE	PATH	MEAN	SDEV	SDEV RATIO	H	ACF
20-Apr	4-1 (cirrus)	0.017	0.009	0.529	0.897	12.00
	cssm1	0.103	0.048	0.466	0.822	50.00
	cssm2	0.093	0.024	0.258	0.808	27.00
	cssm3	0.092	0.02	0.217	0.765	29.00
	cssm4	0.034	0.022	0.647	0.752	31.00
	cssm5	0.066	0.021	0.318	0.724	40.00
	cssm6	0.069	0.024	0.348	0.847	31.00
	cssm7	0.046	0.015	0.326	0.758	12.00
	cssm8	0.073	0.023	0.315	0.806	38.00
	cssm9	0.063	0.016	0.254	0.729	29.00
	cssm10	0.039	0.027	0.692	0.825	34.00
	Mean	**0.0678**	**0.024**	**0.384**	**0.7836**	**32.10**
	Sdev	**0.023**	**0.009**	**0.165**	**0.043**	**9.85**
	Distance	**2.164**	**1.632**	**0.880**	**2.622**	**2.04**
20-Apr	4-2 (cirrus)	0.015	0.014	0.933	0.857	12.00
	cssm1	0.083	0.025	0.301	0.868	28.00
	cssm2	0.052	0.021	0.404	0.717	30.00
	cssm3	0.064	0.01	0.156	0.646	11.00
	cssm4	0.044	0.023	0.523	0.839	17.00
	cssm5	0.074	0.031	0.419	0.835	20.00
	cssm6	0.075	0.033	0.440	0.748	49.00
	cssm7	0.128	0.028	0.219	0.791	72.00
	cssm8	0.083	0.036	0.434	0.724	35.00
	cssm9	0.081	0.023	0.284	0.759	63.00
	cssm10	0.045	0.021	0.467	0.741	20.00
	Mean	**0.0729**	**0.0251**	**0.365**	**0.7668**	**34.50**
	Sdev	**0.025**	**0.007**	**0.118**	**0.067**	**20.47**
	Distance	**2.355**	**1.497**	**4.815**	**1.342**	**1.10**

Table 8 (Continued)

DATE	PATH	MEAN	SDEV	SDEV RATIO	H	ACF
20-Apr	5-1 (cirrus)	0.053	0.038	0.717	0.901	27.00
	cssm1	0.115	0.038	0.330	0.894	37.00
	cssm2	0.108	0.017	0.157	0.761	12.00
	cssm3	0.042	0.014	0.333	0.694	9.00
	cssm4	0.078	0.053	0.679	0.798	39.00
	cssm5	0.034	0.015	0.441	0.807	11.00
	cssm6	0.052	0.018	0.346	0.728	10.00
	cssm7	0.104	0.022	0.212	0.64	25.00
	cssm8	0.11	0.026	0.236	0.782	21.00
	cssm9	0.127	0.019	0.150	0.698	24.00
	cssm10	0.094	0.057	0.606	0.826	36.00
	Mean	**0.0864**	**0.0279**	**0.349**	**0.7628**	**22.40**
	Sdev	**0.033**	**0.016**	**0.180**	**0.075**	**11.82**
	Distance	**1.011**	**0.636**	**2.040**	**1.854**	**0.39**
20-Apr	5-2 (cirrus)	0.02	0.012	0.600	0.855	12.00
	cssm1	0.068	0.031	0.456	0.71	40.00
	cssm2	0.099	0.046	0.465	0.822	35.00
	cssm3	0.056	0.038	0.679	0.799	39.00
	cssm4	0.069	0.034	0.493	0.786	62.00
	cssm5	0.039	0.021	0.538	0.687	15.00
	cssm6	0.089	0.022	0.247	0.768	45.00
	cssm7	0.069	0.022	0.319	0.691	52.00
	cssm8	0.087	0.023	0.264	0.789	15.00
	cssm9	0.096	0.047	0.490	0.756	46.00
	cssm10	0.066	0.021	0.318	0.709	55.00
	Mean	**0.0738**	**0.0305**	**0.427**	**0.7517**	**40.40**
	Sdev	**0.019**	**0.010**	**0.137**	**0.049**	**15.59**
	Distance	**2.852**	**1.789**	**1.265**	**2.115**	**1.82**

Table 8 (Continued)

DATE	PATH	MEAN	SDEV	SDEV RATIO	H	ACF
20-Apr	5-3 (cirrus)	0.031	0.018	0.581	0.799	9.00
	cssm1	0.088	0.026	0.295	0.762	10.00
	cssm2	0.08	0.026	0.325	0.777	24.00
	cssm3	0.103	0.05	0.485	0.85	22.00
	cssm4	0.052	0.043	0.827	0.896	21.00
	cssm5	0.104	0.018	0.173	0.812	21.00
	cssm6	0.052	0.018	0.346	0.679	9.00
	cssm7	0.152	0.036	0.237	0.714	27.00
	cssm8	0.137	0.022	0.161	0.84	22.00
	cssm9	0.068	0.02	0.294	0.871	10.00
	cssm10	0.115	0.04	0.348	0.834	23.00
	Mean	**0.0951**	**0.0299**	**0.349**	**0.8035**	**18.90**
	Sdev	**0.034**	**0.011**	**0.192**	**0.070**	**6.61**
	Distance	**1.899**	**1.035**	**1.204**	**0.065**	**1.50**
20-Apr	5-4 (cirrus)	0.017	0.016	0.941	0.780	12.00
	cssm1	0.074	0.027	0.365	0.699	47.00
	cssm2	0.102	0.027	0.265	0.696	24.00
	cssm3	0.123	0.024	0.195	0.723	33.00
	cssm4	0.067	0.05	0.746	0.776	37.00
	cssm5	0.092	0.04	0.435	0.78	34.00
	cssm6	0.072	0.025	0.347	0.758	15.00
	cssm7	0.08	0.035	0.438	0.724	29.00
	cssm8	0.069	0.024	0.348	0.67	28.00
	cssm9	0.063	0.023	0.365	0.704	9.00
	cssm10	0.129	0.035	0.271	0.743	9.00
	Mean	**0.0871**	**0.031**	**0.377**	**0.7273**	**26.50**
	Sdev	**0.024**	**0.009**	**0.150**	**0.036**	**12.42**
	Distance	**2.958**	**1.696**	**3.760**	**1.445**	**1.17**

50

Table 8 (Continued)

DATE	PATH	MEAN	SDEV	SDEV RATIO	H	ACF
20-Apr	5-5 (cirrus)	0.021	0.021	1.000	0.719	20.00
	cssm1	0.057	0.026	0.456	0.746	10.00
	cssm2	0.09	0.041	0.456	0.846	21.00
	cssm3	0.103	0.037	0.359	0.905	15.00
	cssm4	0.034	0.016	0.471	0.683	9.00
	cssm5	0.101	0.052	0.515	0.777	23.00
	cssm6	0.098	0.029	0.296	0.787	26.00
	cssm7	0.081	0.026	0.321	0.792	13.00
	cssm8	0.098	0.019	0.194	0.749	20.00
	cssm9	0.078	0.021	0.269	0.766	29.00
	cssm10	0.107	0.03	0.280	0.737	37.00
	Mean	**0.0847**	**0.0297**	**0.362**	**0.7788**	**20.30**
	Sdev	**0.023**	**0.011**	**0.107**	**0.061**	**8.88**
	Distance	**2.737**	**0.793**	**5.985**	**0.977**	**0.03**
20-Apr	7 (cirrus)	0.022	0.005	0.227	0.675	7.00
	cssm1	0.036	0.016	0.444	0.767	25.00
	cssm2	0.059	0.029	0.492	0.806	13.00
	cssm3	0.047	0.014	0.298	0.833	8.00
	cssm4	0.027	0.009	0.333	0.788	9.00
	cssm5	0.07	0.022	0.314	0.822	13.00
	cssm6	0.1	0.018	0.180	0.774	34.00
	cssm7	0.026	0.011	0.423	0.698	30.00
	cssm8	0.03	0.019	0.633	0.774	19.00
	cssm9	0.027	0.009	0.333	0.684	10.00
	cssm10	0.036	0.3	8.333	0.876	14.00
	Mean	**0.0458**	**0.0447**	**1.178**	**0.7822**	**17.50**
	Sdev	**0.024**	**0.090**	**2.517**	**0.058**	**9.18**
	Distance	**0.986**	**0.442**	**0.378**	**1.837**	**1.14**

Table 8 (Continued)

DATE	PATH	MEAN	SDEV	SDEV RATIO	H	ACF
20-Apr	8 (cirrus)	0.005	0.001	0.200	0.790	19.00
	cssm1	0.056	0.036	0.643	0.72	27.00
	cssm2	0.026	0.016	0.615	0.809	19.00
	cssm3	0.084	0.026	0.310	0.897	19.00
	cssm4	0.024	0.01	0.417	0.678	17.00
	cssm5	0.075	0.013	0.173	0.828	7.00
	cssm6	0.035	0.016	0.457	0.783	24.00
	cssm7	0.024	0.015	0.625	0.773	8.00
	cssm8	0.035	0.022	0.629	0.901	18.00
	cssm9	0.107	0.035	0.327	0.811	20.00
	cssm10	0.035	0.013	0.371	0.85	12.00
	Mean	**0.0501**	**0.0202**	**0.457**	**0.805**	**17.10**
	Sdev	**0.029**	**0.009**	**0.165**	**0.071**	**6.44**
	Distance	**1.545**	**2.068**	**1.555**	**0.212**	**0.30**
20-Apr	9 (cirrus)	0.04	0.021	0.525	0.728	18.00
	cssm1	0.06	0.021	0.350	0.782	20.00
	cssm2	0.083	0.023	0.277	0.831	19.00
	cssm3	0.066	0.026	0.394	0.84	19.00
	cssm4	0.022	0.019	0.864	0.73	17.00
	cssm5	0.018	0.01	0.556	0.714	10.00
	cssm6	0.101	0.008	0.079	0.745	9.00
	cssm7	0.041	0.014	0.341	0.712	28.00
	cssm8	0.055	0.01	0.182	0.675	7.00
	cssm9	0.05	0.014	0.280	0.486	27.00
	cssm10	0.048	0.02	0.417	0.821	15.00
	Mean	**0.0544**	**0.0165**	**0.374**	**0.7336**	**17.10**
	Sdev	**0.025**	**0.006**	**0.216**	**0.104**	**7.11**
	Distance	**0.569**	**0.732**	**0.700**	**0.054**	**0.13**

Table 8 (Continued)

DATE	PATH	MEAN	SDEV	SDEV RATIO	H	ACF
20-Apr	10 (cirrus)	0.022	0.02	0.909	0.925	12.00
	cssm1	0.065	0.011	0.169	0.652	17.00
	cssm2	0.1	0.064	0.640	0.901	26.00
	cssm3	0.039	0.01	0.256	0.709	20.00
	cssm4	0.055	0.03	0.545	0.825	30.00
	cssm5	0.04	0.021	0.525	0.856	17.00
	cssm6	0.055	0.02	0.364	0.849	9.00
	cssm7	0.076	0.017	0.224	0.747	20.00
	cssm8	0.026	0.016	0.615	0.788	10.00
	cssm9	0.043	0.019	0.442	0.771	22.00
	cssm10	0.086	0.012	0.140	0.843	10.00
	Mean	**0.0585**	**0.022**	**0.392**	**0.7941**	**18.10**
	Sdev	**0.023**	**0.016**	**0.187**	**0.076**	**7.02**
	Distance	**1.569**	**0.126**	**2.759**	**1.725**	**0.87**
20-Apr	11 (cirrus)	0.149	0.083	0.557	0.933	36.00
	cssm1	0.059	0.022	0.373	0.78	42.00
	cssm2	0.054	0.021	0.389	0.838	25.00
	cssm3	0.08	0.022	0.275	0.866	39.00
	cssm4	0.018	0.01	0.556	0.485	16.00
	cssm5	0.061	0.019	0.311	0.78	46.00
	cssm6	0.063	0.016	0.254	0.74	31.00
	cssm7	0.073	0.017	0.233	0.755	28.00
	cssm8	0.055	0.019	0.345	0.684	26.00
	cssm9	0.063	0.026	0.413	0.732	40.00
	cssm10	0.09	0.041	0.456	0.723	44.00
	Mean	**0.0616**	**0.0213**	**0.360**	**0.7383**	**33.70**
	Sdev	**0.019**	**0.008**	**0.099**	**0.104**	**9.90**
	Distance	**4.572**	**7.581**	**1.984**	**1.872**	**0.23**

Table 8 (Continued)

DATE	PATH	MEAN	SDEV	SDEV RATIO	H	ACF
20-Apr	12-1(cirrus)	0.047	0.017	0.362	0.678	37.00
	cssm1	0.051	0.031	0.608	0.878	49.00
	cssm2	0.049	0.019	0.388	0.833	28.00
	cssm3	0.062	0.027	0.435	0.844	30.00
	cssm4	0.067	0.03	0.448	0.878	17.00
	cssm5	0.076	0.016	0.211	0.801	18.00
	cssm6	0.08	0.027	0.338	0.816	22.00
	cssm7	0.076	0.017	0.224	0.815	32.00
	cssm8	0.06	0.02	0.333	0.929	20.00
	cssm9	0.052	0.02	0.385	0.807	13.00
	cssm10	0.04	0.026	0.650	0.875	19.00
	Mean	**0.0613**	**0.0233**	**0.402**	**0.8476**	**24.80**
	Sdev	**0.013**	**0.005**	**0.143**	**0.041**	**10.46**
	Distance	**1.068**	**1.146**	**0.280**	**4.109**	**1.17**
20-Apr	12-2 (cirrus)	0.055	0.036	0.655	0.748	40.00
	cssm1	0.088	0.031	0.352	0.846	18.00
	cssm2	0.065	0.021	0.323	0.718	20.00
	cssm3	0.07	0.021	0.300	0.739	23.00
	cssm4	0.108	0.035	0.324	0.827	44.00
	cssm5	0.058	0.032	0.552	0.747	51.00
	cssm6	0.076	0.033	0.434	0.765	30.00
	cssm7	0.069	0.033	0.478	0.768	42.00
	cssm8	0.064	0.03	0.469	0.813	22.00
	cssm9	0.088	0.027	0.307	0.815	28.00
	cssm10	0.081	0.036	0.444	0.761	65.00
	Mean	**0.0767**	**0.0299**	**0.398**	**0.7799**	**34.30**
	Sdev	**0.015**	**0.005**	**0.088**	**0.042**	**15.57**
	Distance	**1.453**	**1.146**	**2.912**	**0.751**	**0.37**

54

Table 8 (Continued)

DATE	PATH	MEAN	SDEV	SDEV RATIO	H	ACF
20-Apr	12-3 (cirrus)	0.01	0.007	0.700	0.871	13.00
	cssm1	0.106	0.029	0.274	0.734	50.00
	cssm2	0.061	0.025	0.410	0.847	20.00
	cssm3	0.069	0.019	0.275	0.724	15.00
	cssm4	0.067	0.025	0.373	0.69	31.00
	cssm5	0.086	0.019	0.221	0.783	25.00
	cssm6	0.053	0.041	0.774	0.821	20.00
	cssm7	0.062	0.029	0.468	0.855	28.00
	cssm8	0.104	0.057	0.548	0.782	53.00
	cssm9	0.091	0.034	0.374	0.765	43.00
	cssm10	0.09	0.029	0.322	0.786	30.00
	Mean	**0.0789**	**0.0307**	**0.404**	**0.7787**	**31.50**
	Sdev	**0.019**	**0.011**	**0.162**	**0.053**	**13.04**
	Distance	**3.653**	**2.091**	**1.825**	**1.737**	**1.42**
21-Apr	1 (cirrus)	0.037	0.031	0.838	0.854	24.00
	cssm1	0.078	0.047	0.603	0.801	68.00
	cssm2	0.079	0.042	0.532	0.855	46.00
	cssm3	0.123	0.056	0.455	0.94	27.00
	cssm4	0.085	0.025	0.294	0.777	31.00
	cssm5	0.086	0.035	0.407	0.892	31.00
	cssm6	0.086	0.026	0.302	0.761	31.00
	cssm7	0.065	0.032	0.492	0.795	44.00
	cssm8	0.064	0.035	0.547	0.672	67.00
	cssm9	0.053	0.027	0.509	0.679	58.00
	cssm10	0.075	0.04	0.533	0.613	68.00
	Mean	**0.0794**	**0.0365**	**0.467**	**0.7785**	**47.10**
	Sdev	**0.019**	**0.010**	**0.104**	**0.102**	**16.93**
	Distance	**2.255**	**0.553**	**3.576**	**0.737**	**1.36**

Table 8 (Continued)

DATE	PATH	MEAN	SDEV	SDEV RATIO	H	ACF
8-May	1-1 (cirrus)	0.008	0.002	0.250	0.682	12.00
	cssm1	0.094	0.031	0.330	0.787	20.00
	cssm2	0.089	0.03	0.337	0.752	41.00
	cssm3	0.073	0.039	0.534	0.836	40.00
	cssm4	0.136	0.042	0.309	0.759	42.00
	cssm5	0.112	0.019	0.170	0.819	14.00
	cssm6	0.066	0.021	0.318	0.796	17.00
	cssm7	0.133	0.04	0.301	0.672	45.00
	cssm8	0.054	0.032	0.593	0.743	38.00
	cssm9	0.083	0.031	0.373	0.785	33.00
	cssm10	0.038	0.015	0.395	0.706	19.00
	Mean	**0.0878**	**0.03**	**0.366**	**0.7655**	**30.90**
	Sdev	**0.032**	**0.009**	**0.121**	**0.050**	**12.02**
	Distance	**2.478**	**3.051**	**0.961**	**1.666**	**1.57**
8-May	1-2 (cirrus)	0.006	0.003	0.500	0.716	19.00
	cssm1	0.11	0.032	0.291	0.827	54.00
	cssm2	0.085	0.033	0.388	0.78	31.00
	cssm3	0.091	0.02	0.220	0.742	13.00
	cssm4	0.11	0.027	0.245	0.717	36.00
	cssm5	0.068	0.026	0.382	0.674	36.00
	cssm6	0.096	0.02	0.208	0.698	31.00
	cssm7	0.099	0.022	0.222	0.678	29.00
	cssm8	0.056	0.029	0.518	0.755	58.00
	cssm9	0.083	0.033	0.398	0.827	20.00
	cssm10	0.083	0.02	0.241	0.68	22.00
	Mean	**0.0881**	**0.0262**	**0.311**	**0.7378**	**33.00**
	Sdev	**0.017**	**0.005**	**0.104**	**0.059**	**14.13**
	Distance	**4.789**	**4.255**	**1.811**	**0.371**	**0.99**

Table 8 (Continued)

DATE	PATH	MEAN	SDEV	SDEV RATIO	H	ACF
8-May	1-3 (cirrus)	0.009	0.003	0.333	0.603	22.00
	cssm1	0.091	0.03	0.330	0.735	34.00
	cssm2	0.091	0.045	0.495	0.852	31.00
	cssm3	0.041	0.031	0.756	0.892	17.00
	cssm4	0.064	0.018	0.281	0.62	18.00
	cssm5	0.1	0.031	0.310	0.81	31.00
	cssm6	0.124	0.026	0.210	0.826	20.00
	cssm7	0.1	0.039	0.390	0.744	28.00
	cssm8	0.146	0.037	0.253	0.775	16.00
	cssm9	0.098	0.011	0.112	0.684	9.00
	cssm10	0.085	0.036	0.424	0.784	29.00
	Mean	**0.094**	**0.0304**	**0.356**	**0.7722**	**23.30**
	Sdev	**0.029**	**0.010**	**0.178**	**0.080**	**8.33**
	Distance	**2.944**	**2.721**	**0.128**	**2.102**	**0.16**
8-May	1-4 (cirrus)	0.005	0.002	0.400	0.657	18.00
	cssm1	0.061	0.032	0.525	0.72	56.00
	cssm2	0.07	0.023	0.329	0.808	12.00
	cssm3	0.072	0.03	0.417	0.712	80.00
	cssm4	0.053	0.028	0.528	0.798	18.00
	cssm5	0.094	0.029	0.309	0.705	97.00
	cssm6	0.114	0.038	0.333	0.828	70.00
	cssm7	0.075	0.038	0.507	0.776	60.00
	cssm8	0.06	0.025	0.417	0.643	40.00
	cssm9	0.06	0.038	0.633	0.705	55.00
	cssm10	0.054	0.022	0.407	0.708	50.00
	Mean	**0.0713**	**0.0303**	**0.440**	**0.7403**	**53.80**
	Sdev	**0.019**	**0.006**	**0.105**	**0.059**	**26.02**
	Distance	**3.436**	**4.617**	**0.383**	**1.417**	**1.38**

Table 8 (Continued)

DATE	PATH	MEAN	SDEV	SDEV RATIO	H	ACF
8-May	2-1 (cirrus)	0.006	0.003	0.500	0.800	25.00
	cssm1	0.077	0.033	0.429	0.787	29.00
	cssm2	0.075	0.044	0.587	0.808	28.00
	cssm3	0.072	0.034	0.472	0.676	67.00
	cssm4	0.115	0.035	0.304	0.755	68.00
	cssm5	0.08	0.025	0.313	0.749	25.00
	cssm6	0.081	0.031	0.383	0.75	70.00
	cssm7	0.096	0.052	0.542	0.8	72.00
	cssm8	0.082	0.049	0.598	0.729	78.00
	cssm9	0.13	0.042	0.323	0.764	87.00
	cssm10	0.037	0.021	0.568	0.7	42.00
	Mean	**0.0845**	**0.0366**	**0.452**	**0.7518**	**56.60**
	Sdev	**0.025**	**0.010**	**0.118**	**0.042**	**23.16**
	Distance	**3.111**	**3.348**	**0.411**	**1.149**	**1.36**
8-May	2-2 (cirrus)	0.007	0.003	0.429	0.827	22.00
	cssm1	0.07	0.024	0.343	0.754	48.00
	cssm2	0.041	0.018	0.439	0.749	30.00
	cssm3	0.09	0.02	0.222	0.693	22.00
	cssm4	0.109	0.045	0.413	0.805	34.00
	cssm5	0.097	0.034	0.351	0.799	42.00
	cssm6	0.074	0.035	0.473	0.801	57.00
	cssm7	0.097	0.034	0.351	0.767	55.00
	cssm8	0.072	0.044	0.611	0.778	37.00
	cssm9	0.052	0.031	0.596	0.71	46.00
	cssm10	0.078	0.024	0.308	0.691	30.00
	Mean	**0.078**	**0.0309**	**0.411**	**0.7547**	**40.10**
	Sdev	**0.021**	**0.009**	**0.123**	**0.044**	**11.48**
	Distance	**3.373**	**2.984**	**0.146**	**1.653**	**1.58**

Table 8 (Continued)

DATE	PATH	MEAN	SDEV	SDEV RATIO	H	ACF
8-May	2-3 (cirrus)	0.006	0.003	0.500	0.840	67.00
	cssm1	0.07	0.027	0.386	0.674	84.00
	cssm2	0.062	0.023	0.371	0.691	23.00
	cssm3	0.084	0.029	0.345	0.744	95.00
	cssm4	0.07	0.041	0.586	0.665	62.00
	cssm5	0.054	0.023	0.426	0.76	80.00
	cssm6	0.072	0.044	0.611	0.799	47.00
	cssm7	0.078	0.025	0.321	0.828	15.00
	cssm8	0.048	0.021	0.438	0.659	20.00
	cssm9	0.084	0.026	0.310	0.771	65.00
	cssm10	0.062	0.024	0.387	0.759	27.00
	Mean	**0.0684**	**0.0283**	**0.418**	**0.735**	**51.80**
	Sdev	**0.012**	**0.008**	**0.104**	**0.059**	**29.46**
	Distance	**5.187**	**3.224**	**0.792**	**1.770**	**0.52**
15-May	1-1 (cirrus)	0.024	0.008	0.333	0.565	9.00
	cssm1	0.085	0.057	0.671	0.901	19.00
	cssm2	0.119	0.028	0.235	0.781	11.00
	cssm3	0.109	0.023	0.211	0.798	10.00
	cssm4	0.099	0.018	0.182	0.739	13.00
	cssm5	0.092	0.021	0.228	0.68	14.00
	cssm6	0.097	0.018	0.186	0.651	13.00
	cssm7	0.038	0.023	0.605	0.727	25.00
	cssm8	0.106	0.028	0.264	0.67	17.00
	cssm9	0.09	0.015	0.167	0.789	15.00
	cssm10	0.08	0.019	0.238	0.801	13.00
	Mean	**0.0915**	**0.025**	**0.299**	**0.7537**	**15.00**
	Sdev	**0.022**	**0.012**	**0.182**	**0.076**	**4.40**
	Distance	**3.053**	**1.414**	**0.191**	**2.487**	**1.36**

Table 8 (Continued)

DATE	PATH	MEAN	SDEV	SDEV RATIO	H	ACF
15-May	3-1 (cirrus)	0.005	0.004	0.800	0.593	20.00
	cssm1	0.051	0.025	0.490	0.726	40.00
	cssm2	0.089	0.031	0.348	0.819	21.00
	cssm3	0.131	0.045	0.344	0.771	55.00
	cssm4	0.052	0.034	0.654	0.778	35.00
	cssm5	0.07	0.027	0.386	0.777	18.00
	cssm6	0.094	0.02	0.213	0.71	23.00
	cssm7	0.102	0.028	0.275	0.863	21.00
	cssm8	0.04	0.017	0.425	0.772	12.00
	cssm9	0.052	0.021	0.404	0.655	36.00
	cssm10	0.101	0.019	0.188	0.788	36.00
	Mean	**0.0782**	**0.0267**	**0.373**	**0.7659**	**29.70**
	Sdev	**0.030**	**0.008**	**0.136**	**0.058**	**12.91**
	Distance	**2.474**	**2.687**	**3.133**	**2.990**	**0.75**

Table 8 consists of 29 consecutive groups of numbers. A description of the table's contents follows:

- The first four groups of values correspond to the cirrostratus cases.
- The remaining 25 groups correspond to the cirrus cases.
- The first row in each group contains parameters computed from the aircraft data.
- The next 10 rows in the group contain parameters computed from each of the ten simulated cases.
- Summary statistics are presented in bold type in the next two rows of each group (summary statistics include a group mean and standard deviation computed for each statistical parameter from the ten simulated runs).
- The final row shows a "sigma distance" for each parameter. That is, the distance, as measured in number of standard deviations, that the aircraft mean is from the simulated group mean for each parameter.

One of the most useful pieces of information to gather from Table 8 is an idea of the amount of variability across CSSM runs. (Appendix C provides graphical overlays of the one aircraft and ten simulated runs for each case, thus also showing the amount of variability across CSSM runs.) The sigma distance measure can be used to test whether the aircraft path (as it is described by its mean, standard deviation, standard deviation ratio, Hurst parameter, and $ACF_{zero\ crossing}$ value) fits within the CSSM envelope described by the group mean and standard deviation. As we've stated

before, these data are not necessarily normal, but we found it useful to compare against the mean nonetheless. The sigma distance measure helps us test the null hypothesis:

Aircraft-based measurements and CSSM simulations of water content data are drawn from the same distribution function.

Sigma distance measures are presented in Table 8. Histograms of those values (built from grouping all 29 cases) are presented in Figure 17 and identified by the "aircraft" title. Five figures are included in Figure 17 corresponding to the five statistical parameters estimated from the IWC paths.

To put the sigma distance measures in perspective, we built a similar set of sigma distance measures by comparing one CSSM run to the other nine. That is, we created a pseudo aircraft path from the first CSSM run and tested it against the distribution created by grouping the other nine CSSM runs. Histograms of these "model" values (built from grouping all 29 cases) are presented along side the "aircraft" values in Figure 17.
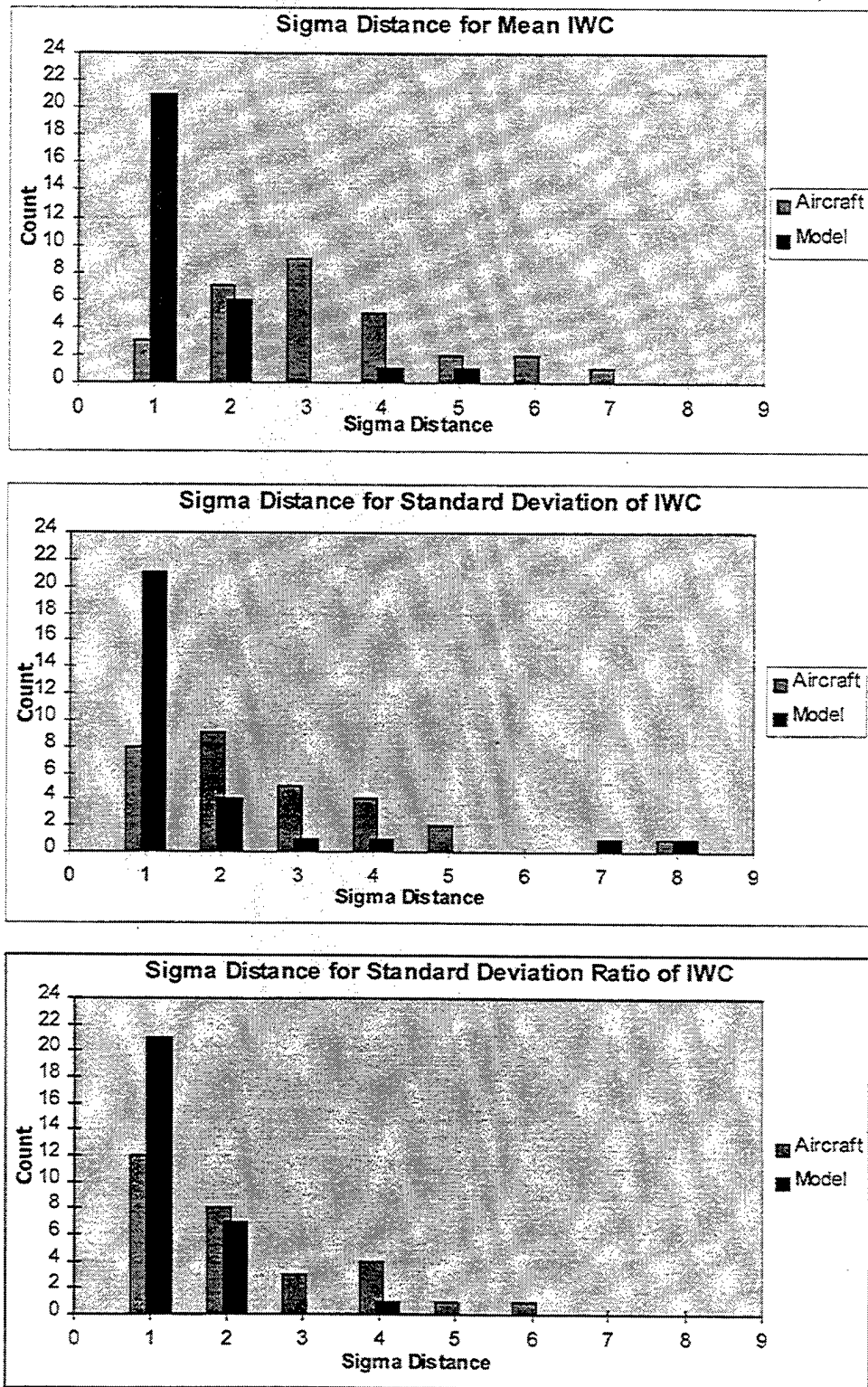
Figure 17 Histograms of sigma distance values for each of the five statistical parameters. Both aircraft-model and model-model values are presented.
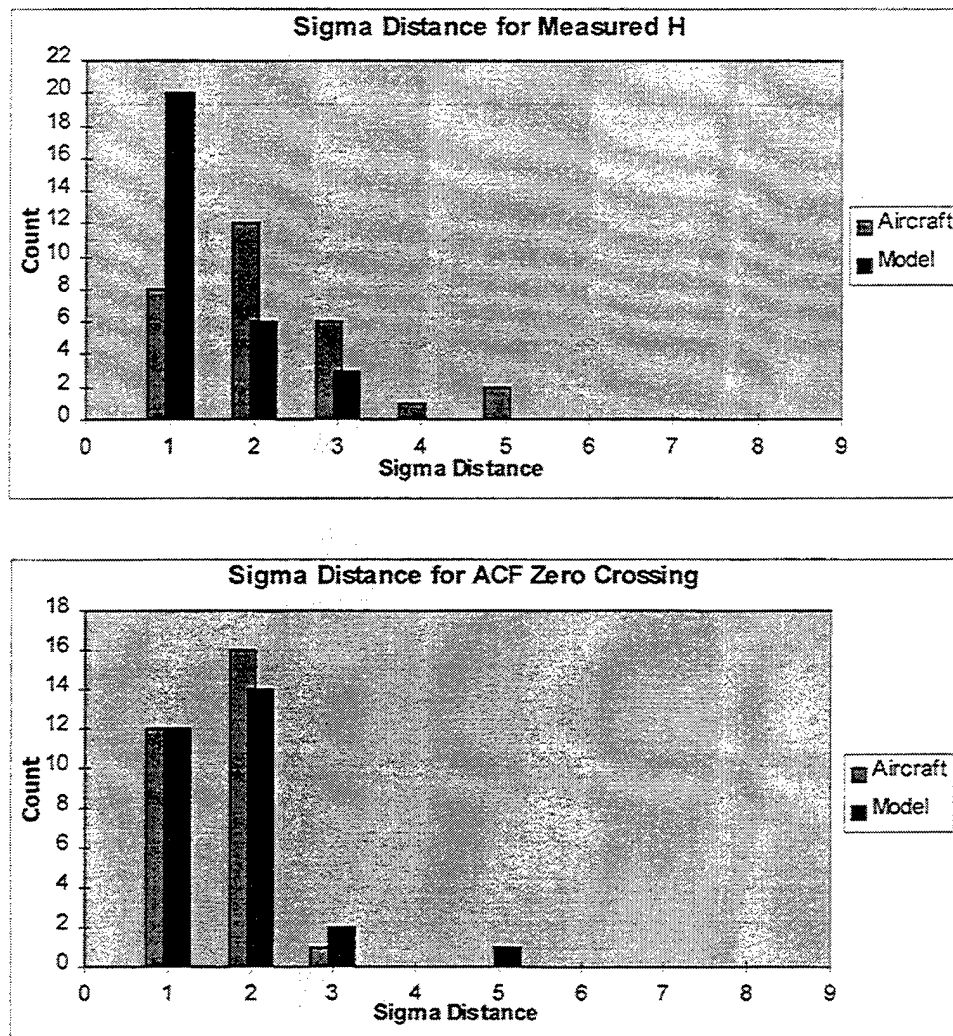
Figure 17   Histograms of sigma distance values for each of the five statistical parameters. Both aircraft-model and model-model values are presented. (Continued)

Several results can be inferred from the information presented in Table 8 and Figure 17:

- The most obvious result is that the *model-model* distributions compare better than the *aircraft-model* distributions. That is, sigma distance measures are typically lower when comparing the one model path to its nine counterparts than the one aircraft path to the ten model runs for all five parameters. This result, is of course not a surprise; we expect the model paths to share the same distributional characteristics. However, it is interesting to note that the model-model sigma distance measures in many of the 29 cases are appreciable and much greater than a standard one-sigma level. Note for example, the large percentage of cases with sigma distance values greater than one for the $ACF_{zero\ crossing}$ parameter. The remaining parameters show only approximately 30% of cases with sigma distance values greater than one (which coincidentally agrees well with the standard nor-

63

mal distribution). This analysis shows that there exists a fair amount of variability even across the ten model runs, but that the distributions appear to be samples from the same underlying distribution.

- The number of cases in which the *aircraft-model* sigma distance is greater than one is 26, 21, 17, 21, 17 for mean, *sdev*, *sdev$_{ratio}$*, H, and ACF parameters, respectively. These numbers correspond to 90%, 72%, 59%, 72%, and 59% of the total 29 cases with parameter values greater than one sigma away from the associated mean parameter value predicted by the CSSM runs. In particular, the model and aircraft mean IWC distributions do not appear to agree. That is, the model and aircraft distributions do not appear to be samples from the same underlying distribution. Recall however, that this analysis assumes normally distributed data, which IWC data paths (and in particular, observed paths) are not. Therefore, the underlying estimates for mean and sigma do not suitably explain these distributions and our results are ambiguous. Also, recall that there are several thin cirrus cases included in the aircraft data which the CSSM does not currently model.

- We could apply a battery of more quantitative tests to compare these data sets. For example, we could use the Student's t-test to measure the significance of a difference of means (assuming unequal variances) and the F-test to measure the significance of a difference of variances. These tests and many others used to compare two distributions assume that the underlying data are normally distributed. That assumption does not hold true for our IWC data sets and therefore the significance results would not be fair tests of the data. Instead, we have selected a statistical test that assumes a more general distributional form — known as the Tshebycheff inequality test. Our results are presented in the next section.

Tshebycheff inequalities

We have used a variety of tools to aid in the parameter estimation and model verification tasks with the goal of testing whether the aircraft and simulated IWC data sets came from the same underlying distributions. First, we simply viewed the IWC data paths to check for qualitative similarities. Second, we computed a number of basic statistical characteristics of the data and displayed them in a series of scatterplots to compare parameter ranges. Third, we analyzed the statistical characteristics by computing sigma distance measures showing the distance between the aircraft and model parameter means. None of these tests provided conclusive evidence to the acceptability of the CSSM IWC fields. In this section, we report on one final method to compare aircraft and simulated data. It is called the Tshebycheff inequality test (Laha and Rohatgi, 1979).

The Tshebycheff inequality test assumes a more general form for the underlying distributional form of the data; it does not assume normal distributions. It is defined in a probability statement as follows:

$$P \left(\, | x\text{-}E(x) | \geq \lambda\sigma \, \right) \leq 1/\lambda^2$$

where

- x is an individual IWC value sampled from the aircraft data
- $E(x)$ is the expected value of x (i.e., the mean IWC value predicted by the theoretical CSSM distribution)
- λ is a constant (e.g., 2,3,4,5)
- σ is the standard deviation of the theoretical distribution.

The Tshebycheff inequality states that the probability that a given value in a data set exceeds some constant, λ, times σ is less than $1/\lambda^2$. For example, we should not expect to find more than 6.25% (i.e., $1/4^2$) of aircraft IWC values data values that are more than 4σ from the mean predicted by the CSSM.

One quick way to determine what percentage of data samples exceed various sigma levels (i.e., 2σ, 3σ, 4σ, 5σ) is to plot histograms of the quantity "$|x\text{-}E(x)| / \sigma$." Then we can simply count how many of those exceed 2, 3, 4, 5, etc. We then compare that actual percentage with the maximum percentage predicted by the Tshebycheff inequality. If the actual percentage is less than the value predicted by the Tshebycheff inequality, we cannot *disprove* the null hypothesis that the aircraft and model data are sampled from the same distribution. (Of course, we cannot *prove* that the two data sets are from the same distribution either.)

To build up the histogram of Tshebycheff values, we chose to use the theoretical mean IWC predicted by the Feddes model within the CSSM for the expected value, $E(x)$. This mean is our best estimate for $E(x)$. The means predicted by the Feddes curve at temperatures present during the SUCCESS experiment are 0.06 and 0.04 g/m^3 for cirrostratus and cirrus types, respectively. We evaluated each aircraft data point (x_i) against an equivalent set of data points sampled from each of the corresponding ten CSSM runs. The reference standard deviation for each x_i was estimated from

the ten CSSM data points. The result is a histogram of Tshebycheff quantities for each of the 29 cases.

The 29 histograms are presented in Appendix C. Each row in the figure consists of the results for a single case (29 total). The leftmost plot in each row shows the ten CSSM IWC data paths and the one aircraft data path for a single case. The IWC paths are overlaid on a single axis which allows a good view of the cloud data. One can quickly understand the amount of variability within a single CSSM path as well as across the group of paths. The overall shapes and characteristics of the IWC paths are clearly seen. The middle plot of each row contains a histogram of the Tshebycheff quantities (i.e., $|x-E(x)| / \sigma$). The quantity is dimensionless. The information printed on the right-hand side of the row contains the actual and predicted percentages of data points exceeding a list of sigma levels (2-5). Those percentages are derived directly from the histogram data. The final column shows whether or not the two distributions pass the Tshebycheff inequality test (yes or no).

You'll note that there are two groups of values listed on the right. The top group (with subtitle "with means") is the default. We have also listed the results based on data in which the means were removed ("without means"). This was a side study in which we tried to test the variability of the water content paths alone without the effects of differencing group means. In that study we wished to remove the effects of the extremely low IWC values present in the 8 May 1996 data paths. By removing the means from both the aircraft and CSSM data, we effectively test only the remaining variability in the IWC values. This improves our chances of passing the Tshebycheff inequality test.

The results presented in Appendix C show that with only two exceptions, the aircraft and CSSM data distributions pass the Tshebycheff test at all sigma levels used. That is, the actual number of aircraft data points which fall outside an envelope defined by the mean IWC $\pm 2\sigma$, 3σ, 4σ, etc. is less than the Tshebycheff inequality value $1/2^2$, $1/3^2$, $1/4^2$, etc. Therefore, we can state that the aircraft and model data sets are consistent with a single distribution.

One additional factor that should be accounted for is that the water content data paths consist of *correlated* time series data rather than independent measurements. In effect, this reduces the overall number of independent data points and thus increases the efficacy of the Tshebycheff inequality test.

The fact that the aircraft-model distributions "pass" this test and "fail" the sigma distance test presented in the previous section is a testament to the looser constraints placed on the distributional form assumed in the Tshebycheff analysis. The IWC data could not satisfy the more rigorous requirement of normalcy assumed previously.

Also, note that this test only evaluates the overall difference in values from the mean. It does not evaluate whether or not the data paths have the correct variances, correlation lengths, "bumpiness," etc. To fully understand whether or not the CSSM output paths simulate the type of data seen in the observed data sets, we need to rely on a range of analysis tools such as those presented in this report — qualitative visual analysis, derivation of basic statistical parameters and comparison of those statistics using scatterplots, quantitative comparison of statistical parameters, and finally, the Tshebycheff inequality test.

3. CLIMATOLOGICAL PREPROCESSOR DEVELOPMENT

3.1 APPROACH

The CSSM is initialized with meteorological, cloud, and terrain data. To date, this data has been provided directly by the user either through single point or gridded input files. The generation of these fields is tedious and time consuming.

Additionally, many users have requirements to produce simulated cloud fields which are climatologically representative for a given area and time. For example, a war gamer many need a simulated cloud field for a typical summer day over Korea, or a weapons evaluator many need simulations that cover the full range of cloud scenes (worst cast to best case) in which the weapon system will operate.

The climatological preprocessor will operate as a front-end preprocessor to the CSSM to provide atmospheric and cloud data for a user-selected location, time, and climatological scenario (e.g., "typical" Korean summer day). Output from the preprocessor will be in a form compatible for easy ingest into the CSSM.

This section describes our plans and initial design for the climatological preprocessor. Future efforts will produce a final design and complete the design implementation and software development.

A suitable candidate database for use in the CSSM preprocessor must meet several criteria:

- Global spatial coverage
- High spatial and temporal resolution
- Consistency between cloud information and meteorological information.

The first two criteria are relatively straight forward and are discussed in more detail in the following subsections. The last criterion is more complex and is discussed next.

The need for consistency between cloud and meteorological information evolves directly from the CSSM. If the CSSM is initialized with inconsistent cloud and meteorological information, (e.g., a

meteorological profile from a convective day and cloud information with high cirrus), the model's results are unpredictable and unreliable.

The amount of information retained in climatological databases covers a broad spectrum. The database usually falls into one or two of the following categories:

- Large collections of raw data
- Detailed summary information with climatological statistics and distributions
- Gross summary information such as monthly means.

An ideal solution would employ cloud and meteorological databases from the same source that contain both raw data and detailed summary information. In that way, the consistency is maintained at the raw data level (i.e., both the meteorological and cloud observations will be coincident in time and space). The summary data can be used by the preprocessor to select (from a histogram, for example) a typical scenario. Then the raw data could be searched to find an observation that falls into the selected scenario.

While guaranteeing consistency between cloud and meteorological information, the above scenario is not realizable for several reasons. First, no databases exist from the same source that contain both cloud and meteorological information. Second, the amount of processing time and storage capacity required for such a system would be prohibitive.

The worst solution would employ databases that only contain gross summary information. Initializing the CSSM with averaged data will produce unrealistic results since these data do not represent atmospheric conditions at any given space and time. For example, frequency distributions of clouds for any given location are typically "U" shaped. When averaged, the cloud occurrence is approximately 50%. Using this average cloud occurrence will imply that clouds occurrence is actually 50% at all times, which is typically not the case.

3.2   SURVEY OF CLIMATOLOGICAL DATABASES

Our literature review revealed the following databases for possible inclusion in the climatological preprocessor. This section contains subsections which describe details of the meteorological, cloud, and topographic databases we examined. At the end of each subsection, a table compares the infor-

mation contained within each database. The structure of the table includes databases in the rows, with several features grouped into columns. These features include the data format, database specific requirements, the resolution, temporal span, quality control (QC), and statistical information. The columnar information is described below:

- Data formats describe the type of data available (e.g., gridded data, observational data (non-gridded), and algorithms)
- Database parameters applicable to CSSM indicates that the database contains parameters required for CSSM initialization. Includes the following:

    Standard parameters (meteorological databases)

    Cloud type, amount, base and top (cloud databases)

    Elevation data (topographic databases)

- High Resolution describes the database's resolution relative to a threshold determined for CSSM initialization. The thresholds for the spatial and temporal components are:

    Horizontal (x,y) – 1.5° x 1.5°

    Vertical (z) – 15 levels

    Temporal – output every 6 hours

- Temporal span indicates the database has a period of record of at least five years
- QC indicates that the data was checked for errors.
- Statistics describes the statistical information available. Can be one of four categories:

    None – no statistical summaries were produced

    Limited – few statistics with limited potential for CSSM impact

    Complete – monthly averages, distributions, with diurnal effects

    Unknown – statistics available, but the extent and usefulness is not known.

3.2.1 Meteorological Databases

Candidate meteorological databases must contain information in both the horizontal and vertical dimensions about the standard meteorological variables: temperature, moisture, pressure, and wind. Since this information is included in most meteorological analyses, several databases were identified which contain all of the standard parameters. This subsection provides details about the meteorological databases we reviewed. Table 9 at the end of this section compares the features of each database.

1. NCEP/NCAR Reanalysis Project

The NCEP/NCAR Reanalysis is a joint effort between the National Center for Environmental Prediction (NCEP) and the National Center for Atmospheric Research (NCAR) (Kalnay et al., 1996). The purpose of this project is to produce a global dataset of atmospheric variables in four dimensions (three spatial, one temporal 40 years in length). Currently, global analyses are available from January 1979 through March 1997. Data were gathered from several platforms, including rawinsondes, aircraft, satellite, and surface reports (land and ship) and integrated with a spectral data assimilation model for final output.

Output from the model is mapped onto a T62 gaussian grid (about 2.5° grid spacing) in the horizontal, with 28 sigma levels or 17 pressure levels in the vertical. To support multiple users, the output is produced in several forms, such as climatological data, synoptic analyses, and time series archives (output four times for each day of the analysis). Data output includes standard surface and upper air data, along with flux and radiation data. Subsets of the data are directly available on-line via the internet and through anonymous FTP at NCEP. The bulk of the reanalysis data is distributed through NCAR, the National Climate Data Center (NCDC), and the Climate Prediction Center (CPC).

2. ECMWF Reanalysis (ERA) Project

The European Center for Medium Range Weather Forecasting (ECMWF) has also created a global database of atmospheric data for the purpose of climatological studies (Gibson et al., 1994). The approach is very similar to that of the NCEP/NCAR Reanalysis. However, there are some differences between the programs. The ERA project uses a spectral data assimilation model, using the same data platforms to initialize the model as the NCEP/NCAR Reanalysis. However, the ERA model has a horizontal resolution of T106 (about 1.125°), compared to the T62 grid of the NCAR/NCEP Reanalysis. In the vertical, there are 31 hybrid model levels, or 17 pressure levels. The data are output every six hours, and the dataset spans from 1979 to 1993.

Output from the ERA include the standard surface and upper air variables, along with certain flux and radiation information. Additionally, climatological and statistical information are provided with the standard data. Subsets of the data output from the ERA are currently available through

anonymous FTP at NCAR (National Center for Atmospheric Research, 1998). Full datasets can be acquired on either tape or CD-ROM via NCAR as well.

3. NASA GEOS I GCM

NASA has produced a data assimilation system of its own for the purpose of climatic studies. The Goddard Earth Observing System (GEOS) General Circulation Model (GCM), like the ERA and the NCEP/NCAR Reanalysis, also uses a data assimilation model to create a climatological dataset (Schubert et al., 1993). Data are gathered from data platforms similar to the above analyses and is integrated by the model. The analysis model is global in extent, has a horizontal resolution of 2.0° x 2.5° and a vertical resolution of 20 sigma levels or 18 pressure levels. Data are output at least every six hours, with some variables output every three hours. The current dataset spans from 1985 to 1993 (Harnett, 1996).

Standard atmospheric parameters at the surface and upper levels are output from the model, with several other flux and radiation parameters available. Some monthly averaged data is also available. Data are freely available from the Goddard Distributed Active Archive Center (DAAC) on several forms of media, including tape and anonymous FTP.

4. UFAF High Resolution Analysis (HIRAS)

The United States Air Force (USAF) HIRAS database consists of standard upper-air and surface meteorological parameters (National Climatic Data Center, 1998). These data include pressure, height, temperature, moisture, and winds on all mandatory pressure surfaces (surface, 1000, 850, 700, 500, 400, 300, 250, 200, 150, 100, 70, 50, 30, 20, and 10 mb) mapped onto a global 2.5° x 2.5° resolution grid. Analyses are generated and archived for every six hours (00, 06, 12, and 18 GMT) This archive spans from 1985 to present. Data from HIRAS originates from the Air Force Global Weather Central's (AFGWC) model output.

5. Comprehensive Aerological Reference Data Set (CARDS)

NCDC has gathered a very large global dataset of radiosonde observations spanning from 1940-1990 (Eskridge et al., 1996). Analyses were available for 00 GMT and 12 GMT for most stations during their reporting period, with some observations available at 06 GMT and 18 GMT. Over 2300 stations and 20 million observations are stored in the database. The number of levels in the soundings vary

from station to station. On average, the vertical resolution is 50 mb from the surface to 200 mb, 25 mb from 200 to 100 mb, and 10 mb from 100 mb to 1 mb (Wang and Rossow, 1995). These figures may vary with the season, type of radiosonde used, and the location. Data recorded in the databases include the standard meteorological variables (temperature, moisture, pressure, winds).

Over 20 sources of meteorological data were employed to create the CARDS database. Since the datasets originated from several sources, the data were stored in their own proprietary format. A processor was written to quality control the data and to transform it into a universal format which the CARDS database employs. Manual quality control of the data was also necessary in several cases.

In addition to the standard radiosonde observations, statistical data have been compiled from the observations. These include mean, standard deviation, and the median for several parameters. Averages at 12 UTC and 00 UTC have been compiled for each month and archived along with the observations. Station histories are also available via the internet at NCDC (http://www.ncdc.noaa.gov/cards).

Table 9 Meteorological Database Outline

	DATA FORMAT	STANDARD PARAMETERS	HIGH RESOLUTION			LARGE TEMPORAL SPAN	QC	STATISTICS
			XY	Z	T			
NCEP/NCAR Reanalysis	Gridded	✓		✓	✓	✓	✓	Limited
ERA	Gridded	✓	✓	✓	✓	✓	✓	Unknown
GEOS I	Gridded	✓		✓	✓	✓	✓	Limited
HIRAS	Gridded	✓			✓	✓		None
CARDS	Obs	✓				✓	✓	Complete

3.2.2 Cloud Databases / Algorithms

The CSSM requires that the selected cloud database must contain information about the cloud base and cloud top height, cloud fraction, and cloud type. Few cloud databases provide all this information at high resolution. Therefore, several data sources may need to be selected. This subsection provides details on the cloud databases we reviewed. Table 10 at the end of this section compares the features of each database.

1. NCEP/NCAR Reanalysis

In addition to the meteorological information already mentioned (see above section), the NCEP/NCAR Reanalysis also contains cloud information. The database includes the total cloud fraction, and the low, middle, and high cloud base and top heights. These data, instead of being taken from observations are completely determined by the analysis model. A comparison of these variables with climatologies and observations indicate that the cloud information is useful. Although the model-derived cloud information does not contain the details necessary to initialize the CSSM (cloud type), these data can be estimated from supplementary meteorological information, such as precipitation rates and radiation data.

2. CHANCES Levels (CLVL)

The CLVL dataset consists of a multi-layer global cloud database for an initial period of 31 days in July, 1994 (Forsythe et al., 1996). This database is based on the Climatological and Historical Analysis of Clouds for Environmental Simulations (CHANCES) database. The CHANCES database contains visible and infrared imagery, along with cloud/no cloud fields. These fields are used in conjunction with meteorological databases (HIRAS, DATSAV2, SSM/I) and the U.S. Navy topographic database (ETOPO5) to produce cloud products every hour with spatial resolutions of 5 km in the horizontal and 1.5 km in the vertical. Eight levels exist in the vertical. Cloud tops are determined through satellite observations, while bases are estimated from surface observations and rawinsonde soundings.

Currently, the CLVL database is only one month long and is still in a "proof of concept" state of development. Initial analysis has revealed problems with the initial cloud base determination scheme (Rienke et al., 1997). The Cooperative Institute for Research in the Atmosphere (CIRA) has developed a new satellite-based technique for cloud base determination that shows significant improvement in the ability to estimate cloud bases.

3. Real-Time Nephanalysis (RTNEPH)

The AFGWC RTNEPH is a global cloud analysis model which produces real-time analysis of cloud amount, cloud type, and cloud height (Isaccs, 1994). This model has been operational since August 1983, when it replaced the 3DNEPH model. The output of the model is on a polar-stereographic grid

with a resolution of approximately 48 km, valid at 60° N and S latitude. Data input into the RTNEPH originates from the Defense Meteorological Satellite Program (DMSP) and polar orbiting satellites and surface observations. Data from the model is output every three hours.

Although the RTNEPH contains all of the cloud data necessary to initialize the CSSM, it has certain limitations. The emphasis of the RTNEPH is on cloud detection, rather than determination of specific cloud parameters, such as cloud height, thickness, and type. The RTNEPH assumes that every pixel is either totally cloudy or totally clear. This leads to an underestimate of the frequency of thin clouds and overanalyzes clear and totally cloudy scenes. Additionally, errors are common in data sparse areas, such as the ocean, due to the lack of supporting surface observations.

4. Support of Environmental Requirements for Cloud Analysis and Archive (SERCAA)

The SERCAA research and development program was a four-year effort to create algorithms which retrieve high-resolution cloud properties from data collected by several meteorological satellites, including the GOES-Next, DMSP, NOAA, GMS, and METEOSAT (Isaccs, 1994). The SERCAA algorithms rely on three basic tests to identify cloudy areas:

- Identification of temporal changes in cloud cover
- Detection of clouds in nearby pixels through identification of reflectance and/or thermal structures of new clouds.
- Identification of cloudy pixels through spectral discriminant testing.

Output from these algorithms include estimates of cloud base and top, cloud type, and cloud amount. Additionally, these algorithms calculate microphysical, optical, and radiative properties of clouds. The SERCAA algorithms are to be included in the USAF Cloud Depiction and Forecast System (CDFS-II) and will replace those algorithms already in the RTNEPH (Atmospheric and Environmental Research, Inc., 1998). Output from the CDFS-II / SERCAA algorithms are to be mapped onto a 24 km polar-stereographic Cartesian grid. Testing for the new CDFS-II system is to begin in 2001.

5. USAF Surface Observation Database (DATSAV2)

DATSAV2 contains worldwide surface meteorological observations for approximately 10,000 stations (synoptic, airways, and ship) dating back to 1973 (NCDC, 1998). These observations are recorded every hour; however, the number of observations varies. More observations are recorded at

75

the synoptic hours (i.e., 00, 03, 06... UTC) due to missing observations from the Eastern Block and Southern Hemisphere during the off-synoptic hours (Forsythe et al., 1996). Data from the DATSAV2 includes the standard meteorological parameters and some cloud layer information, including total cloud amount and cloud base height. These cloud data could be used in conjunction with other cloud databases for verification purposes, or to fill in possible data gaps.

6. High Resolution Infrared Sounder (HIRS)

A global cloud climatology has been produced from data collected by the HIRS sensor, aboard the NOAA polar orbiting satellites. This sensor specializes in measuring transmissive or semi-transparent clouds (typically cirrus) (Wylie et al., 1994). Past estimates of transmissive cloud cover were estimated from the longwave infrared window (10-12 microns) on polar orbiting and geostationary satellites and tended to be under-represented. Using multispectral techniques, the HIRS is able to separate the transmissive clouds from the opaque clouds.

The HIRS instrument uses a CO_2 slicing technique (using the 13-15 micron band) and its infrared bands to estimate the cloud top pressure and effective emissivity at a resolution of 20 km. In this climatology, all clouds that exhibit an effective emissivity less than 0.95 are labeled as cirrus clouds; all values greater than 0.95 are labeled as opaque clouds.

Currently, data from the HIRS instrument has been compiled into monthly data files spanning eight years (Wylie and Menzel, 1997). Cloud probabilities and frequencies are contained within each data file. Compilation of these monthly statistics is expected to continue for several more years.

7. International Satellite Cloud Climatology Project (ISCCP)

ISCCP was a project designated to create a dedicated database of various cloud parameters with global coverage at 280 km resolution (Rossow et al., 1996). The overall purpose of the project was to:

- Produce a global, reduced resolution, calibrated and normalized radiance dataset containing basic information on the properties of the atmosphere from which cloud parameters can be derived.

76

- To stimulate and coordinate basic research on techniques for inferring the physical properties of clouds from the condensed radiance dataset and to apply the resulting algorithms to derive and validate a global cloud climatology for improving the parameterization of clouds in climate models.

- To promote research using ISCCP data that contributes to improved understanding of the Earth's radiation budget and hydrological cycle.

Sources of the ISCCP data came from up to five geostationary satellites (measuring radiance) and two polar orbiters (measuring cloud properties). The cloud properties sampled include mean cloud amount, cloud top heights, optical depth, cloud water path, and cloud types. These variables are categorized by cloud type during the daytime and into cloud classes (low, middle, and high) at all times. Data were sampled every three hours (for any given location) and archived. Monthly summaries of these products were also produced and archived for public use. Frequency distributions and statistics were compiled over all hours (00, 03, 06...UTC) for each month to account for diurnal effects on the cloud properties.

8. Chernykh and Eskridge, 1995

A method for estimating cloud heights and amounts strictly from radiosonde observations has been developed for possible use in the CARDS project. The algorithms test for changes in temperature and relative humidity with respect to the height. Cloud layers are diagnosed when the second derivative of temperature with respect to the height is greater than or equal to zero and the second derivative of the relative humidity with respect to the height is less than or equal to zero. Cloud fractions are defined through a graphical method developed by Arabey (1975).

Although the test for the presence of clouds was developed from a purely statistical analysis (comparison of spline approximations of temperature and relative humidity to surface observations), this test also makes physical sense. Where clouds are present, one expects higher relative humidities in regions of clouds than in the layer above or below the cloud layer. Latent heat release from the condensation of clouds will allow the temperature to stop decreasing with height or to increase near the base of a cloud.

Results from this experiment indicate that the probability of correctly diagnosing cloud level was approximately 90%. The probability of correctly diagnosing both cloud level and fraction varied

77

with the level in the atmosphere; high clouds possessed a low probability, while low clouds possessed a high probability. Additionally, most testing was performed on layer type clouds. Due to a lack of observations, cumuliform type clouds did not undergo significant testing.

9. Wang and Rossow, 1995

A similar method to (8) for determining cloud levels was developed for use with radiosonde observations. This method uses only relative humidity (RH) profiles with respect to height to determine cloud base and top heights. RH thresholds were established to determine these cloud parameters. Algorithms for determining cloud amounts were not presented in this paper.

Radiosonde observations from 30 oceanic locations across the northern hemisphere were selected for analysis. Archived surface observations of clouds and ISCCP data were gathered for verification of the cloud levels. Results from this algorithm indicated that low and middle level clouds were represented well; high clouds tended to be underrepresented, with a third of them missing when compared to the surface observations and ISCCP data. Observations of multilayered clouds were quantitatively comparable to the surface observations.

10. Uddstrom and Gray, 1996

The National Institute of Water and Atmospheric Research in Wellington, New Zealand, developed a method for determining cloud classes through the use of satellites and radar. The data samples were drawn from 105 NOAA-11 and 152 NOAA-12 passes during most of 1994. Cloud classes were determined by separating the satellite data and radar data into several parts, including a Rain/No Rain flag (from the radar), infrared channel differences of temperature and radiance, and dimensions of cloudy areas. Additionally, gray level difference (GLD) statistics were used to measure the spatial characteristics of the cloud imagery.

To assist in the analysis of the cloud data, an interactive tool called ENHANCE is used to process data gathered from the AVHRR instrument on the NOAA satellites. From the diagnostics that ENHANCE produces on the AVHRR data, the analyst can produce plots on a pixel by pixel basis of cloud type. Cloud types that are produced include cumulus, cumulonimbus, stratus, nimbostratus, stratocumulus, altocumulus, and no cloud. High cloud identifications schemes are excluded from the algorithms presented.

11. Bankert and Aha, 1996

The intent of this project was to design a neural network that classifies clouds, given a set of satellite data. For this particular study, AVHRR local area coverage (LAC) scenes (512 x 512 pixels) were used as input into a probabilistic neural network (PNN) to classify 10 different cloud types, including clear sky. Sample areas of 16 x 16 pixels that contained at least 75% cloud coverage of a particular cloud type were labeled by analysts and processed by the neural network. Maritime areas were the only areas selected for study.

For each sample area, features were identified to more specifically describe the present cloud type. These included spectral, textural, and physical measures (204 total). Once the features are gathered, they are put through a feature selection algorithm. The object of feature selection is to *reduce the number of features used to characterize a dataset so as to improve an algorithm's performance on a given task* (Aha and Bankert, 1994). Included in a feature selection algorithm is a search algorithm, an evaluation function, and a classifier (the PNN). For this cloud classification case, a forward sequential selection (FSS) algorithm was used.

Results from this feature selection algorithm led to a reduction of features from 204 to 15. This would make the process of satellite cloud detection much easier for analysts. Overall, the accuracy of this algorithm was 86.8% in correctly detecting the 10 different cloud types. When these numbers were grouped into cloud classes (i.e., low, middle, high) the accuracy increased to 91.8%.

3.2.3 Terrain Database

The selected terrain database should contain standard gridded elevation data with a resolution at least that of the meteorological and cloud databases. High resolution databases are easy to obtain with the resolution being the only major difference between them. The terrain databases we evaluated are listed below. Table 11 at the end of this subsection outlines the features of each database.

Table 10 Cloud Database Outline

	DATA FORMAT	CLOUD PARAMETERS				HIGH RESOLUTION			LARGE TEMPORAL SPAN	QC	STATISTICS
		TYPE	AMT	BASE	TOP	XY	Z	T			
NCEP/NCAR Reanalysis	Gridded		✓	✓	✓		✓	✓	✓	✓	Limited
CLVL	Gridded		✓	✓	✓	✓		✓		✓	Complete
RTNEPH	Gridded	✓	✓	✓	✓	✓		✓	✓	✓	None
DATSAV2	Obs	✓	✓	✓				✓	✓	✓	None
HIRS	Gridded		✓		✓	✓	✓	✓	✓	✓	Complete
ISCCP	Gridded	✓	✓		✓		✓	✓	✓	✓	Complete
SERCAA	Algorithm	✓	✓	✓	✓					✓	None
Chernykh and Eskridge, 1995	Algorithm		✓	✓	✓					✓	None
Wang and Rossow, 1995	Algorithm			✓	✓					✓	None
Uddstrom and Gray, 1996	Algorithm	✓								✓	None
Bankert and Aha, 1996	Algorithm	✓								✓	None

1. Earth Topography – 5 Minute (ETOPO5)

ETOPO5 is a database of topographic and bathymetric data covering the globe at a 5 minute latitude, 5 minute longitude resolution (United States Geological Survey [USGS], 1997). Data was compiled from several sources, including the Defense Mapping Agency (DMA), U.S. Navy Fleet Numerical Oceanographic Center, and the U.S. Naval Oceanographic Center. ETOPO5 data may be obtained at the National Geophysical Data Center (NGDC) on tape, ftp, or CD-ROM.

2. TerrainBase Global Terrain Model

The TerrainBase data is the successor to the ETOPO5 data (National Geophysical Data Center [NGDC], 1994). Like the ETOPO5, the resolution is 5 arc seconds. Twenty-six regional and world-wide terrain models were used to create this terrain model. Since the terrain data originates from several sources, the height values given in the model are a "best estimate." Data from the TerrainBase can be obtained from the National Geophysical Data Center via ftp, tape, and CD-ROM.

3. GTOPO30

GTOPO30 is a global digital elevation model (DEM) compiled by the U.S. Geological Survey's (USGS) EROS Data Center (USGS, 1997). Data from this elevation database are stored at 30 arc seconds (approximately 1 km). Besides containing global topographic data, it also includes statistics for each topographic band, projection information, and shaded relief maps. GTOPO30 data is available via ftp and tape from the USGS.

Table 11 Terrain Database Outline

	DATA FORMAT	ELEVATION DATA	HIGH RESOLUTION	QC
ETOPO5	Gridded	✓	✓	✓
TerrainBase	Gridded	✓	✓	✓
GTOPO30	Gridded	✓	✓	✓

3.3   RECOMMENDATIONS

The most desirable climatological preprocessor would contain meteorological and cloud data derived from the same sources. However, only one database out of those researched contained both cloud and meteorological data (the NCEP/NCAR Reanalysis). Thus, analysis and quality control measures will need to be taken to ensure consistency between differing datasets (assuming the NCEP/NCAR Reanalysis is not utilized). If consistency is not achieved through these measures, results from the CSSM are unpredictable. For example, if the user is interested in typical clouds over Albania during March, the preprocessor is going to provide all the necessary inputs to the CSSM. If the preprocessor feeds the CSSM stratus cloud inputs with meteorological data indicative of cumulus clouds, the nature of the water content output will be unknown and unreliable. Ensuring consistency is therefore, of utmost importance.

Statistical information is also lacking in many of the researched databases. Although several meteorological and cloud databases contain statistics, most do not take diurnal effects into account. Those few that did contain complete statistics have other databases that may make them unsatisfactory for all users. If those databases are not acceptable, the climatological statistics will need to be compiled by hand and/or combinations of databases will need to be used.

Given the total number of databases available in each category, many different options exist for the creation of a climatological preprocessor. Each of these databases has advantages and disadvantages if applied to the climatological preprocessor. Table 12 outlines these advantages and disadvantages. When selecting databases, one must keep in mind that a desirable combination will be one which will satisfy all possible users of the climatological preprocessor. Each user has unique requirements. For example, some will only be looking for data to initialize the CSSM quickly, with data of sufficient quality to produce realistic results. Others may be looking for very high quality data at the highest resolution possible. To satisfy this broad range of users and to provide flexibility in implementation, we propose two solutions; a *simple* preprocessor and an *advanced* preprocessor.

3.3.1 Simple Climatological Preprocessor

The advantage to using a simple climatological preprocessor is that it will reduce the amount of time necessary to process the selected databases. To those users whom are only interested in pre-packaged CSSM inputs, this will be the better of the two solutions. It is unlikely that they will be interested in the highest quality data with the highest resolution possible. To reduce processing time and data storage requirements, statistical data should be used as much as possible. Our recommendations for a simple preprocessor are listed below.

- **Meteorological Data** — CARDS Database: The CARDS database is best for the simple preprocessor because statistical distributions have already been computed. Assuming the user is only interested in station data from locations scattered throughout the globe, this database will be easily applicable to the climatological preprocessor. Due to the nature of the dataset (station data), oceanic data will be lacking. If the user wants to use data other than at the station locations, an interpolation scheme will need to be applied.

- **Cloud Database** — ISCCP + HIRS + Chernykh and Eskridge, 1995: This three-part solution will be the easiest to integrate into the climatological preprocessor. ISCCP and HIRS have statistical distributions already compiled and complement each other very well. HIRS tends to underestimate low and middle clouds, but handles high clouds well. ISCCP handles low and middle clouds well, but underestimates high clouds. The algorithms of Chernykh and Eskridge are necessary because both ISCCP and HIRS do not contain any cloud base data. These algorithms can calculate the cloud levels with good accuracy. Another advantage to using these algorithms are that they were tested with data from the CARDS database. The use of three separate databases may present consistency problems, so additional QC may be necessary.

- **Terrain Database** — TerrainBase Global Terrain Model: All of the terrain models would be suitable for this task. The TerrainBase data was chosen over both the ETOPO5 and the GTOPO30 datasets for two reasons; the TerrainBase database is more up to date than the ETOPO5, and the GTOPO30 has a resolution which is higher than necessary for the climatological preprocessor.

Overall, this solution should satisfy those users that are only looking for CSSM initialization data. QC is necessary to ensure consistency between the databases.

3.3.2 Advanced Climatological Preprocessor

The advantage to using an advanced climatological preprocessor is that it will provide truly global coverage with the highest quality and resolution possible. However, the tradeoff is in the processing time and data storage requirements. Although the use of statistical data would be ideal, the resolution of the statistical datasets will not satisfy most users. Our recommendations for an advanced preprocessor are listed below.

- **Meteorological Database** — ECMWF Reanalysis: With a resolution of approximately 1.125°, the meteorological data output from this model is far superior to any other meteorological database. Extensive QC has already been computed on the data. Data from the model can be applied in several ways. If data storage is vast, then the user can store several years worth of data and randomly select days of any particular month to get the meteorological data. Otherwise, the user can compile the statistics on the data to reduce the data storage requirements. Compiling the statistics manually should be easily handled by most computer systems. Software to process the statistics will be developed in future efforts.

- **Cloud Database** — SERCAA: The SERCAA algorithms are one of only two databases/algorithms which produce all the necessary cloud parameters for CSSM initialization. The SERCAA algorithms were designed to produce data at a very high resolution (nominally 25 km) (Isaccs, 1994) which will complement the ERA very well. Given that inputs to the SERCAA include meteorological data and satellite data , the user must have satellite data at their disposal. Like the meteorological dataset, statistics will need to be compiled and/or random cloud data will be selected that complements meteorological data from the same day. One major advantage to this method is that consistency between the cloud data generated from the SERCAA algorithms and the meteorological data should not be a concern, since the meteorological data is already used as input into the SERCAA algorithms.

- **Terrain Database** — TerrainBase Global Terrain Model: This database will also be sufficient for the advanced user. The resolution is still high enough to satisfy the typical advanced user.

Although this solution for the climatological preprocessor will require significant computing and implementation resources, it will yield a very high resolution data initialization system for the CSSM. Consistency issues are partially resolved with this solution, since the SERCAA algorithms require meteorological inputs, which can be provided by the ERA. The creation and maintenance of this database will be performed in future efforts.

Table 12 Database Comments

	ADVANTAGES	DISADVANTAGES
NCEP/NCAR Reanalysis (meteorological)	High quality gridded meteorological data over a long period of time. Easy to apply to the climatological database.	Low horizontal resolution. Statistics are not compiled on the data
ERA	Very high spatial resolution for a global database. Gridded meteorological data will allow for easy application to a climatological database.	Little current information is currently available on the model and the data output.
GEOS I	Contains high quality gridded meteorological data for a long period of time. Data is readily available for free.	Low horizontal resolution. Statistical summaries have mean values, but lack standard deviations and frequency distributions.
HIRAS	Meteorological data is gridded and covers a long temporal span.	No quality control. Low spatial resolution. Statistics are not compiled on the data.
CARDS	Data has been extensively quality controlled and covers a very large time period. Climatological Statistics are compiled on the data.	Data is not gridded, making processing more difficult. Vertical resolution also varies from station to station.
NCEP/NCAR Reanalysis (cloud)	See previous reference	Cloud data grouped into classes (low, middle, high) rather than by type. Cloud data created by the model, not included in the observations. Statistics are not compiled on the data.
CLVL	Very high temporal and spatial resolution. Contains cloud level information and amounts.	Cloud data grouped into 8 different levels in the atmosphere, not by cloud type. Temporal span only one month. Data largely interpolated.
RTNEPH	Spatial and temporal resolution is high. All necessary cloud variables are included in the database.	Data largely persisted. Small number of data sources. Pre-compiled statistics are lacking.
DATSAV2	High temporal resolution. Large number of observations per temporal period.	Cloud amounts are reported by cloud class (low, middle, high). Cloud types and cloud tops not available. Pre-compiled statistics also not available.
HIRS	Very high spatial resolution. Statistics have been compiled on the data and are contained within the database.	Low and middle clouds underrepresented. If multi-layered clouds present, only top layer is measured. Cirrus clouds are the only type of cloud classified. Cloud base not available.

Table 12 Database Comments (Continued)

	ADVANTAGES	DISADVANTAGES
ISCCP	High temporal resolution. Statistics are compiled on the data which account for diurnal effects.	Spatial resolution very low. High clouds underrepresented. Cloud types only available during daylight hours.
SERCAA	Allow output to a high spatial resolutions grid. All necessary cloud information can be processed. Input data is employed from several sources.	Satellite data required for analysis. No database of cloud data processed by SERCAA algorithms available.
Chernykh And Eskridge, 1995	Meteorological data are only source of input necessary to output cloud data. Algorithms are accurate in test cases.	High clouds were not detected in 1/3 of all tested cases. Cloud types are not processed by algorithms.
Wang and Rossow, 1995	Meteorological data are only source of input necessary to output cloud data. Algorithms are accurate in test cases.	High clouds were not detected in 1/3 of all tested cases. Cloud types and amounts are not processed by algorithms
Uddstrom and Gray, 1996	Uses satellite imagery analysis techniques to obtain cloud type information.	Algorithms to detect high clouds were not developed. Cloud layers and amounts are not calculated by algorithms.
Bankert and Aha, 1996	Uses neural nets to accurately determine cloud types from satellite imagery	Large amount of user interaction required. Cloud layers and amounts are not calculated by algorithms.
ETOPO5	High spatial resolution (5 arc-minute)	No disadvantages identified
TerrainBase	High spatial resolution (5 arc-second)	No disadvantages identified
GTOPO30	High Spatial Resolution (30 arc-minute)	No disadvantages identified

4.   SUMMARY AND RECOMMENDATIONS

4.1   SUMMARY

The Cloud Scene Simulation Model, developed with the support of the U.S. Air Force Research Laboratory, was designed to generate high-resolution cloud imagery for use in a wide-range of DoD applications, including mission rehearsal, sensor testing, and scene validation. Improvement of the CSSM was the goal in this effort, with tasks devoted to improvement of the cirrus model, design of a climatological preprocessor, and software support. The first task of this effort focused on improving the CSSM's cirrus model. We tuned the internal model parameters to better replicate in situ cloud ice water content observations. We also researched and designed a new cirrus model capable of capturing the unique structures observed in "precipitating" cirrus clouds. In the second task, we researched and designed a climatological preprocessor to provide climatological inputs to the CSSM. The final task (not discussed in detail in this report) provided for software support, training, and testing.

The need for an improved cirrus model is evident. The baseline cirrus model was developed with statistical and fractal parameters estimated from values reported in the literature and on visual inspection. More accurate and realistic parameters are required to support radiometric validation and sensor test applications. This effort improves on the cirrus model by estimating model parameters on in situ ice water content values sampled by aircraft. We used ice water content values collected during the SUCCESS experiment to perform our parameter estimation and tuning. We examined other sources of cirrus data, but only the SUCCESS data set provided both the high resolution and supporting cloud and meteorological information we needed for parameter estimation.

From the SUCCESS dataset, we were able to update those parameters for the cirrus and cirrostratus cloud models. Samples of water content from cirrocumulus clouds were not available from the SUCCESS dataset; therefore, we did not tune the cirrocumulus model at this time. Descriptions of the analysis techniques and the process used to update the cirriform model parameters are included in this report.

Statistical analysis of the water content data revealed that the agreement between the observed and simulated water content paths was generally good. The cirrus mean water content values appear to be somewhat over-predicted by the CSSM. However, agreement between the observed and simulated Hurst parameters and autocorrelation functions were generally good. Cirrostratus agreement was also good, with the autocorrelation and the standard deviation agreeing well. Comparisons of the Hurst parameter for observed and simulated paths was poor, probably due to the limited number four of observed cirrostratus paths. The statistical analysis techniques utilized included the computation of basic statistical parameters (mean, standard deviation, etc.) and Tshebycheff inequalities. The use and application of these techniques are included in Section 2.4.

Other pertinent technical development included the design for a cirrus uncinus model. Some features that are unique to this cloud type include: a vertical velocity perturbation field, generating head region, and a particle trajectory model for precipitating ice crystals. This plan includes implementations of all these features into a future version of the CSSM and is documented in Section 2.2 of this report.

In addition to the development and improvement of the cirrus model, we developed a preliminary design for a climatological preprocessor. This design required that we research available meteorological, cloud, and terrain databases and identify applicable databases. Because we identified a large number of databases, a wide range of options was available for the creation of a climatological preprocessor. We offered two implementation plans; a *simple* and an *advanced* solution. The *simple* plan includes the use of CARDS, ISCCP, HIRS, algorithms from Chernykh and Eskridge (1995), and the TerrainBase Global Terrain Model. The *advanced* plan features the use of the ECMWF Reanalysis, SERCAA algorithms, and the TerrainBase Global Terrain Model datasets. These plans should satisfy most present and future users of the CSSM.

Various software modifications and improvements were employed to support CSSM users throughout the reporting period. Specifically, we installed and tested an updated baseline version of the CSSM on the client computer systems. Additionally, we debugged the CSSM when necessary and implemented new parameters into the model. Many additional computer programs were written in support of the data analysis and parameter estimation task. These included programs to extract simulated paths out of

87

CSSM water content fields, IDL scripts for statistical analysis and generation of one page summaries, and programs to convert the SUCCESS data into an easily managed ASCII format.

4.2 RECOMMENDATIONS

The CSSM employs a modular software design that is easily maintained and allows for future growth. Below we list a few recommendations for continued validation of CSSM output and suggestions for enhancements and growth.

Implement Enhanced Cirrus Model

We recommend the incorporation of the suggestions made in Section 2.2 for the cirriform model improvements. This would include developing an enhanced non-precipitating cirrus model along with building a precipitating cirrus uncinus model. Additionally, we recommend tuning cirrocumulus model parameters in the same way as described here for cirrus and cirrostratus cloud types. A cirrocumulus aircraft database would first need to be identified and analyzed to support this task.

Implement Climatological Preprocessor

We recommend the implementation of the climatological preprocessor as outlined in Section 3. In addition to gathering the recommended databases, data should be transformed into a universal format for easy data selection and entry into the CSSM. Additionally, the user should be able to select the meteorological data through a graphical-user interface (GUI).

Develop Fog Model

The current CSSM implementation does not support fog. We recommend the development of a stochastic fog model based on data reported in the literature.

Develop Enhanced Rain Model

The CSSM's rain model (documented in Cianciolo et al., 1996) provides a limited capability to simulate precipitation for nimbostratus and precipitating cumulus cloud types. We recommend the implementation and validation of an enhanced rain model as follows:

- Employ size distribution models to derive autoconversion rates from cloud water to rain water for stratiform and cumuliform clouds.

88

- Review and implement parametric scavenging, evaporation, and growth models for stratiform and cumuliform precipitation.

- Develop and enhanced cascade model to include advection processes, e.g., the effects of advection on parcel rain rates and rain shaft trajectories.

- Update the current "waterfall" mechanism to evaluate the amount of atmospheric moisture available to support rain rates and precipitation with time.

- Compare statistics of model-produced rain amounts to those of observed data.

Provide Software Support

The growing demand to integrate the CSSM and its output fields into distributed simulations and other simulation systems combined with the increasing complexity of the CSSM make it imperative that technical experts be available to assist with user integration efforts. We recommend the establishment of a task-order or level-of-effort type support contract through which customers can contribute directly to the costs involved with their integration efforts and receive individual assistance on an as-needed basis.

Enhance Fast-Map Post-Processor

The Fast-Map post-processor (documented in Cianciolo et. al., 1996) was intended as a proof-of-concept process to translate CSSM water content output fields into hardware-specific graphical parameters (e.g., transparency, absorptivity, and diffusivity). We believe the approach has great potential to rapidly provide the graphical quantities needed for real-time cloud scene visualization.

This page intentionally left blank

APPENDIX A
CIRRUS MODEL/DATA BIBLIOGRAPHY

The annotated bibliography for cirrus models and data follows. Note, that our search focused only on cirrus information relevant to CSSM development. For example, we selected references which included some discussion of high-resolution cirrus observations, parametric models of physical and optical properties, vertical and horizontal fine structure, etc. A list of the references that we reviewed follows. Each reference consists of citation, abstract, and summary of pertinent information for our model development process.

1. **Cohen I. D., Cirrus Particle Distribution Study — Part 5, Air Force Surveys in Geophysics 414, AFGL-TR-79-0155, AD-A077361, 81 pp., July 1979.**

Abstract:

On 19 March 1978 an MCE-130E aircraft obtained ice particle data in cirrus clouds near Albuquerque, NM. Some data were also obtained from a high altostratus layer below the cirrus. Printouts of particle size and average number distribution for consecutive 30-sec periods during the flight are presented. Additionally, graphical displays of average particle spectra and 2-D particle examples are given for five 3- to 5-min periods when cloud conditions were relatively homogeneous.

Pertinent Information:

- Same comments apply as written in Varley (1978, Part I). Average data are tabulated for 30-sec intervals for approximately 100 minutes.

- Measurements were taken for the two cloud layers (cirrus and altostratus) as well as the clear-air area between the layers. Results showed a large difference in the type and size of particles in the altostratus and cirrus cloud layers. Particles in the lower altostratus layer were relatively large with a variety of shapes. Particles in the higher cirrus layer were smaller with more regular shaped crystals.

- Ice water content (IWC) in the altostratus remained quite constant despite decreasing crystal sizes with altitude. However, crystal sizes remained nearly constant with altitude in the cirrus layer while water content increased.

2. Cohen I. D., and A. A. Barnes, Cirrus Particle Distribution Study — Part 6, Air Force Surveys in Geophysics 430, AFGL-TR-80-0261, AD-A096772, 106 pp., September 1980.

Abstract:

Cirriform clouds associated with a frontal system which passed through New Mexico on 4 and 5 April 1978 were sampled by a MC-130E which has been equipped with cloud physics instrumentation by AFGL. The clouds sampled were thin cirrus and cirrostratus layers in advance of the front on 4 April and behind the same front on 5 April. Particle sizes were small; maximum sizes on 4 April were approximately 700 mm. On 5 April, few clouds could be found, but one patch yielded particles as large as 1300 mm. Particle distribution curves are presented for three 5-min periods from the 4 April flight and one 5-min period from the 5 April flight. Additionally, consecutive 30-sec average distributions are presented for selected time periods from each of the flights. In addition to the visible cirrus clouds, particles were also found in clear air between the cirrus clouds. Some of the sub-visible cirrus particles seemed to come from clouds above the aircraft, but other instances of sub-visible cirrus occurred when there were no visible cirrus above the aircraft suggesting that the particles had developed in situ.

Pertinent Information:

- Same comments apply as written in Varley (1978, Part I). Average data are tabulated for 30-sec intervals for approximately 75 minutes on each of two flights (the flights occurred on two consecutive days) intended to characterize pre-frontal and post-frontal cirrus clouds. 5-min averages are also presented for four periods.

- Very little cloud was encountered during the second flight on 5 April; however, sub-visible cirrus was present as detected by the cloud probe. Particles ranging from 100-300 mm were observed.

- Nearly a constant background of small particles (2-4 mm) was observed throughout the two flights as well as on previous flights by this aircraft (as detailed in this series of reports).

- Cirrus clouds were measured at temperatures of -40° C and altitudes greater than 30,000 ft. Much of the previous research had been done in cirrus clouds at lower altitudes and warmer temperatures.

- There seems to be no clear cut boundary between visible and sub-visible cirrus, rather, conditions change continuously from one to the other.

- The approach of the front led to a greater variety of particle types, but did not seem to have much effect on the IWC or maximum particle size.

92

3. **Cohen I. D., Cirrus Particle Distribution Study — Part 8, Air Force Surveys in Geophysics 437, AFGL-TR-81-0316, 110 pp., October 1981.**

Abstract:

The AFGL instrumented MC-130E sampled thin cirrus clouds on 3, 4, and 5 February 1979. In some cases, there was no visible cirrus, but some particles were detected. During this period, the upper air pattern was dominated by southwest to northeast flow, while two surface systems moved from north to south. The first of these left thin cirrus in eastern New Mexico; the second pushed south to the Gulf of Mexico, leaving the cirrus studied on the previous two flights. Most of the particles observed were less than 100 mm. As a rule, the opacity of the cirrus seemed related more closely to the density of particles in the 20- to 200-mm range. On examination, the form factor appeared to be higher (indicating more consistent sized particles) in cirrus of non-frontal origin than in cirrus associated with strong surface weather systems. This report is the last in a series of cirrus particle distribution studies.

Pertinent Information:

- Same comments apply as written in Varley (1978, Part I). Average data are tabulated for 15-sec intervals for periods of varying length over the three days studied.

- Thin cirrus was studied on the 3 February flight. Cirrus particles were quite uniform during the 3 February flight, with high form factors, particles sizes detected almost exclusively by the scatter (2-30 mm) and cloud (30-300 mm) probes, and uniform water content. Four 5-min periods were selected from this flight and are presented in greater detail in the report.

- Thin cirrus was studied on the 4 February flight. Two types of sub-visible cirrus were detected: that consisting of ice crystals which have fallen from a higher level and that which has formed in situ. The form factor was lower for those areas of sub-visible cirrus formed by fallout, reflecting a wider variety of particle sizes. Four 5-min periods were selected from this flight and are presented in greater detail in the report.

- A variety of cirrus clouds were sampled on the 5 February flight during the long flight from New Mexico to Ohio. Six 5-min periods were selected from this flight and are presented in greater detail in the report.

4. **Danne, O., G. G. Mace, E. E. Clothiaux, X. Dong, and T. P. Ackerman, Observing Structures and Vertical Motions Within Stratiform Clouds Using A Vertical Pointing 94-GHz Cloud Radar, Beitr. Phys. Atmosph., vol. 69, no. 1, pp. 229-237, February 1996.**

Abstract:

Cloud properties derived from a 94-GHz Doppler radar include the vertical distribution of liquid and ice water hydrometeors and a measure of their radial velocity relative to the radar. A temporal record of the vertical distribution of cloud particles can

lead both to information on the vertical distribution of clouds and to the significant structures present within them. A time-space conversion method to derive the horizontal spatial scales of the observed dominant structures within stratiform clouds, such as cirrus, altostratus and stratocumulus, is considered. The method utilizes the Taylor transformation: the clouds that advect over the radar are assumed to be fixed in shape, and wind speeds derived from nearby wind profilers are used for the advecting cloud velocities. This method is shown to produce accurate retrievals even for significant uncertainties in the velocities of the profiler-derived wind speeds. It is applied to radar returns obtained from two different time periods when stratiform cirrus and altostratus clouds were present. The vertical motion of the cloud droplets derived from the radar during a case of cirrus uncinus clouds embedded in a cirrostratus layer lend support to a conceptual model of cirrus convection based on prior observations obtained from aircraft and centimeter-wavelength radar with lower temporal and vertical resolution. These applications of the radar are pertinent to validating models of micro- and mesoscale dynamics within stratiform clouds and are intended to be illustrative of the capabilities of a millimeter-wave Doppler radar. The analysis of large datasets in a statistical manner will ultimately lead to improved cloud parameterization schemes in general circulation models.

Pertinent Information:

- Three datasets are used in their analysis (taken with Penn. State 94 GHz radar): (1) cirrus data from the Nov/Dec 1991 FIRE II program in Coffeyville, Kansas, (2) cirrus data from the April 1994 Remote Cloud Sensing Intensive Operational Period of the ARM Program in north central Oklahoma, and (3) stratiform cirrus data from the same April 1994 field campaign.

- To date only a limited amount of data has been analyzed, the authors mention performing a statistical analysis based on a large set of data to develop a microphysics parameterization sometime in the future.

- They use a result from Starr and Cox (1985) that shows that changes of cloud water content averaged over a horizontal distance of 6.3 km are typically less than 30% within time periods of 5 minutes.

- By transforming the spectral peaks identified by the radar, the authors found dominant horizontal spatial scales of 2, 1.32, 5, 2.86 km for cirrus clouds and 11, 7.26, 4.17, 1.7, 1.2 km for altostratus.

- Dominant horizontal scales of upward motion roughly estimated to be 500 to 1500 m.

5. Ebert, E. E., and J. A. Curry, A Parameterization of Ice Cloud Optical Properties for Climate Models, J. of Geophys. Res., vol. 97, no. D4, pp. 3831-3836, March 20, 1992.

Abstract:

We present a new parameterization of the optical properties of ice crystal clouds which is suitable for use in climate models. Five spectral intervals in the shortwave and five intervals in the infrared are employed, with the ice cloud optical properties parameterized in terms of ice water path (IWP) and the effective radius (r_e) of the ice crystal size distribution. The parameterization thus allows the flexibility of varying the ice water path and effective radius independently of each other. The parameterized optical properties are used to calculate the bulk reflectivity, transmissivity, and emissivity for cirrus clouds with realistic ranges if IWP and r_e. For a given change in cloud optical depth, a change in r_e alone is more effective than a change in IWP alone in altering the shortwave reflectivity and therefore in altering the strength of the cloud albedo feedback.

Pertinent Information:

- Goal of this effort is to build a parameterization between radiative and microphysical properties of cirrus clouds to support studies of the effects of cirrus clouds on climate.

- Paper presents a parameterization of optical properties (i.e., shortwave optical depth, single scattering albedo and asymmetry factor, and longwave mass absorption coefficient) as a function of IWC and ice particle size distribution effective radius (at resolutions typical of radiation codes employed in climate models).

- IWC and particle size information are derived from size distributions reported elsewhere (by Takano and Liou).

- We may be able to use the parameterizations for shortwave optical properties (optical depth, single scattering albedo, and asymmetry factor) in future implementations of the Fast-Map processor.

- Parameterizations for bulk radiative properties (reflectivity, transmissivity, emissivity) are also given and may be of use for future Fast-Map implementations.

6. Heymsfield, A. J., Ice Crystal Growth in Deep Cirrus Systems, in Proc. of the Conference on Cloud Physics of the Am. Met. Society, Tucson, AZ, pp. 311-316, October 1974.

Abstract:

An early study of the microstructure of cirrus clouds was undertaken by Weickmann (1947). He determined the particle characteristics of different cirrus types from direct in-flight samplings. The primary crystalline form in convective cirrus clouds was found to be the bullet rosette, and in cirrostratus eroded single bullets, columns, and

plates. The crystal habit thus appears to be primarily related to the vertical velocity. The natural seeding of lower clouds by cirrus crystals was documented by Braham and Spyers-Duran (1967), who found that cirrus crystals can fall into the tops of growing cumuli in concentrations of 105 m^{-3}. The microstructure of cirrus clouds was studied by Heymsfield and Knollenberg (1972). They measured ice crystal spectra with a particle size spectrometer and collected ice crystals in different cirrus types. The concentrations of crystals larger than 150 mm were found to be 1x10^{-2} to 2.5x10^{-2} cm^{-3}, and the ice water content from 0.106 to 0.26 g/m^3 in cirrostratus, and 0.15 to 0.39 g/m^3 in cirrus uncinus.

In the present study, particle spectra were measured through cirrus systems with a cloud depth in excess of 5 km. There were thirteen case studies in several different synoptic types. Two of the cases will be discussed in detail.

Pertinent Information:

- Average IWC data for cirrostratus and cirrus uncinus were reported.
- Three probes were used to collect data: 2-30 mm, 20-300 mm, 200-3000 mm.
- Horizontal paths approximately 15 miles long were recorded every 2000 vertical feet through the clouds. Flights took place in the Pacific Northwest, Midwest, and East Coast of the US.
- Two cases are detailed in this paper.
- Cloud IWC was calculated from the particle spectra and observed crystal habit.
- Case 1 (Oregon): IWC varied from 1x10-3 — 0.7 g/m3 with even greater values lower in the cloud due to orographic effects. Graph is included.
- Case 2 (Connecticut): IWC varied from approximately 1x10-3 — 0.5 g/m3. Graph is included.
- Over all 13 cases studied, changes in IWC seemed to be primarily related to the vertical velocity structure within the cloud.
- Thin (nearly invisible) cloud layers were observed on all flights at the tropopause level.
- Calculated IWC values were frequently higher than the difference between water and ice saturation at the temperature of the level. This suggests that the vertical flux of moisture was adding a significant contribution to the ice water content.

7. **Heymsfield, A. J., Precipitation development in stratiform ice clouds: a microphysical and dynamical study, J. of Atmos. Sciences, vol. 34, pp. 367-381, February 1977.**

Abstract:

Aircraft microphysical measurements in ice clouds associated with warm frontal over-running systems, warm frontal occlusions, closed lows aloft and the jet stream were

combined with Doppler radar measurements in four case studies. Good agreement was obtained between aircraft calculations of the radar reflectivity factor and air velocity, and radar measurements and calculations of these parameters. Vertical velocities typically ranged from 10 cm/s in warm frontal overrunning systems to in excess of 50 cm/s in clouds associated with a closed low aloft, longitudinal rolls and isolated convective cells. Ice crystal seeding in trails emanating from longitudinal rolls were measured to extend over 7 km in the vertical and over 100 km in horizontal distances. Several general results were deduced from the aircraft measurements. Vertical velocities generally in excess of 50 cm/s at temperatures lower than -5°C were found to be necessary for liquid water occurrence in deep stratiform ice clouds. Water saturation was not necessary for nucleation to occur. The IWC and ice crystal concentration, parameterized in terms of the vertical air velocity and temperature, were found to be directly dependent on the vertical velocity. Ice crystal concentrations were found to be 2-4 orders of magnitude higher than ice nuclei concentrations at temperatures warmer than -15°C.

Pertinent Information:

- Cirrus generating cells have considerably higher IWC values and precipitation rates than in stratiform ice clouds over the same temperature range.

- Doppler radar is useful for determining vertical velocity magnitudes, however, aircraft data is required to study cloud microphysics.

- Heymsfield (1975) found IWC to range between 0.025 and 0.16 g/m3 at temperatures lower than -20°C. Highest values were in clouds with embedded convective cells. This paper relates cloud microphysics and precipitation to the magnitude of the vertical velocity (and thus the presence of convective cells).

- Aircraft sampling was performed to collect data on the vertical distribution of cloud microphysics. Sampling passes were parallel to wind direction, approx. 25 km long, taken in 600m steps down from cloud top.

- Longitudinal rolls: isolated bands occasionally extended over 100 km. Vertical velocities were measured at ±50 cm/s. Upward-moving region of a roll was typically 1.2 km deep. Band orientation was within several degrees of the wind direction. Liquid water existed within the rolls at temperatures as low as -30°C.

- Convective cells: cells were estimated to be 1 km in the horizontal and 2 km in the vertical dimension. Vertical velocities of ±50 cm/s were noted. Liquid water was observed in the cells.

- Presence of liquid water is dependent on the magnitude of the vertical velocity.

- Graph of IWC verses temperature is shown for varying categories of vertical velocity. Equations showing IWC = f(T, vertical velocity) are given. Unfortunately, within the CSSM, we do not have access to vertical velocity, therefore we cannot make use of these parameterizations.

- IWC values were calculated as averages along the 25 km passes through a constant cloud layer. IWC is calculated from pass-average particle size spectra and ice crystal habits. IWC generally increased from about .001 g/m3 at a temperature of -60°C to 0.5 g/m3 at 0°C, with a wide scatter at any given temperature due to differing vertical velocity magnitudes.

- A discussion of ice crystal habit as a function of temperature and vertical velocity magnitude is included.

- Derived relationships are included: between radar reflectivity and IWC and precipitation rate and IWC. Such relationships can be useful in estimating cloud microphysical parameters from remote sensing and ground-based measurements.

- Calculation for IWC using particle spectra and habit information is included in an appendix.

8. **Heymsfield, A. J., Cirrus Uncinus Generating Cells and the Evolution of Cirriform Clouds. Part I: Aircraft Observations of the Growth of the Ice Phase, J. of Atmos. Sciences, vol. 32, pp. 799-808, April 1975.**

Abstract:

The growth of the ice phase in cirrus uncinus and cirrostratus clouds was studied through aircraft measurement of cloud particle spectra at different altitudes. Five different cirrus uncinus clouds were studied; one of the cirrus uncinus evolved into cirrostratus. The temperature range of sampling was -19 to -58°C. In cirrus uncinus heads, crystals were determined to be nucleated and grown in the upshear region, before being carried into the trail regions of the head downshear as a result of wind shear. The updraft region is upshear, and the downdraft region downshear. A "hole" was found to separate the up- and downshear regions of the head, with a horizontal extent of about 150 m. The concentrations of crystals in the head regions were on the order of 0.5 cm^{-3}, with 0.025-0.05 cm^{-3} longer than 100 mm. Accumulation of particles in the updraft region was noted. The mean length of crystals longer than 100 mm (precipitation size particles) ranged between 0.5 and 1.0 mm, and crystals as long as 2 mm were found at temperatures as low as -56°C. The average IWC was found to be 0.15-0.3 g/m^3 in the head. The cirrostratus clouds sampled had their nucleation regions near the top of the clouds; crystals sedimented and grew from the source region near the top to near the base, and then evaporated to the base. The crystal concentrations were about 0.2 cm^{-3}, with 0.01 cm^{-3} longer than 100 mm. The mean length of

crystals larger than 100 mm ranged between 0.2-0.5 mm. The IWC ranged between 0.01-0.16 g/m³.

Pertinent Information:

- The primary crystalline form found in the five different cirrus clouds studied was the bullet rosette.

- In a previous (1972) study, average ice crystal concentration within cirrus generating cells (for crystals longer than 150 mm) was 0.1-0.25 cm-3, average IWC was found to be 0.15-0.25 g/m3. These IWC values are significantly higher than those predicted by the Feddes model currently implemented within the CSSM. Most likely, the difference is due to the fact that Heymsfield's values are appropriate for generating cells specifically.

- Particle spectra were measured in this study. The related microphysical properties (including IWC, precipitation rate, radar reflectivity) were calculated.

- No appreciable liquid water was found.

- Cirrus uncinus: heads were divided into two regions separated by a "hole" (a minimum) in the particle concentrations. Smaller particles were found in the base of the head of the upshear region, increasing in size with height in the head. Particles were larger near the top of the head in the downshear regions and decreased in size toward the base of the head. This points to the fact that particles are rising in upshear regions and falling in downshear regions. Convective turrets were embedded in some uncinus trails (approx. 1 km across). The IWC in the turrets was less than in the original cell and particle sizes were smaller. Particle size and concentration are a function of temperature, with sizes decreasing and concentrations increasing with decreasing temperature. IWC did not seem to be related to temperature, but rather, may be a function of dynamics instead.

- Cirrostratus: cirrostratus clouds exhibited lower particle concentrations and IWCs than did cirrus uncinus clouds. The mean and maximum crystal lengths were found to increase from near the cloud top to the cloud base.

- Cirrus uncinus heads ranged in vertical extent from 0.3 to 1.4 km, in horizontal extent from 0.8 to 2.0 km, and typical length-to-depth ratios of 2:1 to 5:1. The typical lifetime of an individual cloud was 15-25 min.

- IWC values measured in this study agree with data taken previously by Rosinski et al. (1970).

9. **Heymsfield, A. J., Cirrus Uncinus Generating Cells and the Evolution of Cirriform Clouds. Part Ii: The Structure and Circulations of the Cirrus Uncinus Generating Head, J. of Atmos. Sciences, vol. 32, pp. 809-819, April 1975.**

Abstract:

The structure and circulations of the cirrus uncinus generating head were determined from aircraft measurements of the temperatures, horizontal wind velocities and particle spectra at different altitudes. Stable layers were found to exist directly above and

below the head. The head was found to exist in a region with a dry adiabatic lapse rate. Waves were observed in the stable layer below the head. The head was found to be divided into two regions in active cirrus uncinus. The upshear part of the head is the updraft region, and the downshear part the downdraft region. A region containing almost no crystals was found to separate the up- and downdraft regions. This "hole" was typically 150 m across.

The vertical velocities in cirrus uncinus were determined from aircraft and Doppler radar measurements. Typical vertical velocities were estimated to range from 100-200 cm/s from aircraft particle measurements, and determined from Doppler radar measurements to range from 120-180 cm/s. Typical downdraft velocities of 50 cm/s were determined from the aircraft measurements and from the Doppler measurements to be a maximum of 80 cm/s, with 20-40 cm/s the typical velocity.

Two mechanisms are suggested from the formation of cirrus uncinus clouds. For cirrus uncinus oriented in lines almost perpendicular to the wind direction, it is suggested that there is layer lifting and that convective cells develop along the lifting line. In the case of isolated cirrus uncinus, it is suggested that a wave in the stable layer below the head region causes a perturbation in the head region which results in convection in the layer. Two mechanisms are suggested for the formation of new generating cells upwind or downwind of the original cell, which significantly increases the lifetime of the cloud. Evaporative cooling in the trail region may induce the formation of new turrets above the trail of an original cell. A second possible mechanism is the formation of a convergent and divergent region at the stable layer below the head region induced by the downdraft in the trail region of the head.

Pertinent Information:

- Paper presents a possible dynamical model for the structure and evolution of cirrus uncinus generating heads.
- Visual observations of the cirrus uncinus cloud indicate that it is usually composed of a head and trail. Typical dimensions of the head are 300 m or more vertically and 1-2 km horizontally. Trail is composed of ice crystals falling out of the head. Trails without a head have been observed and it is assumed that the cloud is in a decaying stage.
- Extended discussion of the vertical velocity structure in the upshear and downshear regions in the head is presented. A conceptual model for crystal motion within the head is presented.

10. **Heymsfield, A. J., Cirrus Uncinus Generating Cells and the Evolution Of Cirriform Clouds. Part III: Numerical Computations of the Growth of the Ice Phase, J. of Atmos. Sciences, vol. 32, pp. 820-830, April 1975.**

Abstract:

Equations were developed to calculate the growth of the ice phase in cirrus clouds. Calculations indicated that nucleation of ice crystals in cirrus uncinus heads forming at temperatures lower than -35°C generally should occur near the upwind base of the head, and in cirrostratus clouds at the top of the cloud.

The growth of ice crystals and the resulting shape of cirrus uncinus clouds with an updraft velocity of 100 cm/s were calculated. With an initial crystal concentration of 0.025 cm^{-3} and a nucleation temperature of -40°C, crystals of 0.45 mm length, and a maximum IWC of 0.3 g/m^3 were predicted.

Latent heat release due to the ice crystal growth increased the initial updraft velocity only slightly. A downdraft velocity comparable in magnitude to the original updraft velocity was calculated to occur in the downshear part of the cirrus uncinus head.

Pertinent Information:

- The cirrus uncinus generating cell is defined as a region containing large ice crystals and well-defined circulations in the head region during the active part of a cloud's lifetime.
- Empirical relationships can be used to estimate terminal velocity of single bullet crystals and rosettes.
- Equations are presented for the change in height of a crystal with a given terminal velocity in an updraft region and the horizontal distance that a particle travels for a given wind velocity.
- Model for the growth of ice crystals is combined with trajectory model and results are shown. The model produced realistic values of IWC, particle sizes and overall cloud shape.

11. **Heymsfield, A. J., and J. L. Coen, Parameterization of Cirrus Microphysical and Radiative Properties in Larger-Scale Models, Downloaded From the ARM Web Page, October, 1996.**

Abstract:

This study exploits measurements in clouds sampled during several field programs, including the Atmospheric Radiation Measurement (ARM) Program, to develop and validate parameterizations that represent the physical and radiative properties of convectively generated cirrus clouds in intermediate and large-scale models (including cumulus ensemble models and general circulation models). We focus on cirrus anvils

because they occur frequently, cover large areas, and play a large role in the radiation budget. Because of a lack of knowledge about how anvils develop, age, and decay, preliminary work focuses on understanding the physical (microphysical, radiative, and dynamical) processes that occur in these clouds.

Pertinent Information:

- This paper presents a brief discussion of ongoing improvements to the Lagrangian ice crystal trajectory-growth model developed previously. This model is too complex and CPU intensive for use in the CSSM.

12. Heymsfield, A. J., and L. J. Donner, A Scheme for Parameterizing Ice-Cloud Water Content in General Circulation Models, J. of the Atmos. Sciences, vol. 47, no. 15, pp. 1865-1877, 1 August 1990.

Abstract:

The optical properties of ice clouds are a primary issue for climate and climate change. Evaluating these optical properties in three-dimensional models for studying climate will require a method to calculate the IWC of such clouds. A procedure is developed to parameterize IWC as a function of large-scale meteorological characteristics for use in circulation models in which the IWC is not calculated by means of a three-dimensional prognostic equation for condensed water. The technique identifies large-scale flows in which ice clouds exist and calculates their IWC by reconstructing the trajectory associated with cloud formation. As the cloud forms, its ice content changes both by deposition of ice from water vapor and by ice removal by sedimentation. The sedimentation process is found to modify significantly the IWC expected from deposition alone. IWCs predicted by the parameterization are compared with aircraft observations collected in the middle latitudes and the tropics, and show reasonable agreement over four orders-of-magnitude of IWC. A parameterization for the sublimation of ice crystals settling into ice-subsaturated environments is also presented.

Pertinent Information:

- IWC is basic to calculating radiative transfer associated with ice clouds. Platt and Harshvardhan (1988) suggest that cloud optical depths (IR and visible) are primarily dependent on the IWC and mode radius of the particle size spectrum; the mode radius can be related to the IWC.

- This paper presents a simple parameterization for deriving the vertical distribution of IWC from the vertical velocity and temperature at grid points in a GCM. (It is intended for use with GCMs that do not carry prognostic condensed water.) The CSSM could be modified to use vertical velocity as an input parameter, thus allowing us to estimate the vertical distribution of IWC.

- Three data sources are used for comparison: (1) 1970's cirrus data sampled during the Environmental Definition Program which consisted of 25-km-long constant altitude flight legs oriented to the wind direction, (2) FIRE data sampled during spiral descents through cirrus clouds with horizontal distances covered by each loop of the spiral of 5 to 10 km, (3) data from 6 tropical ice clouds near Kwajalein, Marshall Islands in which sampling was conducted from cloud top to bottom in a manner similar to the EDP data. Measurements from the aircraft included particle size spectra. IWC is derived.

- Individual IWC data from the three datasets are presented for several ranges of vertical velocity. IWCs depends primarily upon temperature, varying by four orders of magnitude over temperatures found in the troposphere. Increasing vertical velocity produces less than linear increases in IWC.

13. Heymsfield, A. J., R. G. Knollenberg, Properties of Cirrus Generating Cells, J. of Atmos. Sciences, vol. 29, pp. 1358-1366, October 1972.

Abstract:

Particle size spectra were measured during 20 hours of sampling in cirrus generating cells (uncinus, stratus, spissatus, thunderstorm anvil) and the particle concentration, mean crystal length, ice water content, reflectivity factor, and precipitation rate were calculated from these spectra. Average values of the physical properties in the generating cells were:

- Ice crystal concentration: 10,000-25,000 m-3
- Mean crystal length: 0.6-1.0 mm
- Particle habit: bullet, rosette, column (75%) — plate (25%)
- Ice crystal density: 0.6-0.9 g/m3
- Ice water content: 0.15-0.25 g/m3
- Reflectivity factor: 5.0-20.0 mm6/m3
- Precipitation rate: 0.5-0.7 mm/hr.

Growth was found to be downward, reaching a maximum ice water content just below the base of the generating cell. The maximum ice water contents (not including the thunderstorm anvil) were found in cirrus uncinus. Liquid water was not found throughout the cirrus sampling by measurement with the Johnson-Williams hot wire

liquid water meter; however, we believe that liquid water is present as a transient phase.

Pertinent Information:

- Data were taken by the Univ. of Chicago Cloud Physics Laboratory and identified a consistent pattern in cirriform characteristics. Emphasis is on generating cells which were found in all cirrus studied except the cumulonimbus anvils.

- Description of IWC calculation is presented along with a discussion of sources of error in the computation.

- Methodology of computing radar reflectivity factor and precipitation rate is also provided.

- Graphs of 1-sec average IWC values for 6 flight paths are presented.

- Data show that most cirrus clouds contain generating cells. Cells were typically 1-2 km in diameter and 1 km thick.

- IWC within cirrus uncinus reached maximum values just below the base of the generating cell.

- Maximum IWC values were found in cirrus uncinus cloud type (not including cumulus anvils).

- Cirrostratus clouds have large IWC too, but contain lower numbers of particles than uncinus.

- Cumulonimbus anvils have IWC values in excess of 1.0 g/m3.

- Relatively large particles typify cirrus generating cells.

14. Heymsfield, A. J., K. M. Miller, and J. D. Spinhirne, The 27-28 October 1986 FIRE IFO Cirrus Case Study: Cloud Microstructure, Monthly Weather Review, vol. 118, pp. 2313-2328, November 1990.

Abstract:

The temperature and wind field structures and hydrometeor composition of cirrus clouds sampled by the NCAR King Air and Sabreliner aircraft on 28 October 1986 near Madison, Wisconsin are described as part of a case study that examines cirrus cloud radiative and microphysical properties. Two cloud layers were sampled from top to base. The upper layer was found at altitudes between 8.5 and 11.5 km and the lower between 6.0 and 8.5 km. Vertical velocities calculated from the increase in ice mass flux with height were typical of synoptic scale lifting. Stronger vertical velocities were measured in convective cells at the top of the lower layer.

The total ice particle concentration was dominated by particles < 200 mm. Mean particle size and IWC increase with decreasing altitude. The largest particles, exceeding 1000 mm in the upper layer and 1500 mm in the lower layer, probably resulted from aggregation, even at cold temperature. Cloud emissivity and optical depth were calculated from the ice particle size spectra.

The distribution of ice mass was narrow at cloud top and broadened with decreasing altitude. At the highest levels of the upper cloud, one-half of the mass was in particles < 150 mm. In this region, we underestimate the mass by a significant fraction presumably contained in particles too small to detect. In the lower levels, one-half of the mass was in particles < 200-400 mm. In the cloud sample by the King Air, one-half of the mass was in particles < 400-600 mm. Up to 10% of the mass in the higher cloud and up to 30% in the lower cloud was contained in particles > 500 mm.

We relate the microstructure of a shallow liquid water layer associated with altocumulus to lidar observations. Thirteen separate episodes of liquid water were sampled at about -30°C. Mean droplet dimensions were < 9 mm, and the liquid water contents were low. Virtually no ice particles were detected within and below the layer. We surmised that under such conditions these liquid water clouds remained colloidally stable. Kelvin-Helmholz waves may have produced the undulations observed at cloud top.

Pertinent Information:
- Two cloud layers were studied, an upper and lower. Conditions were typical of synoptic scale lifting.
- Mean particle size and IWC increased with decreasing altitude.
- Two convective cells were encountered near cloud top (about 0.5 km across).
- Graphs of temperature, potential temperature, and horizontal wind speed vs. altitude are included.
- Upper cirrus layer extended from 9-11.5 km. Much or all of the lower structure appears to result from precipitation of ice crystals from a thin layer above 11 km.
- Images of ice particles and a summary of ice particle habit vs. temperature are presented.
- Graph showing ice particle concentration vs. altitude for all size categories shows decreasing concentration with increasing particle size (typical of cirrus clouds).
- Total concentration was dominated by smallest particles (25-200 mm).
- Trend from smaller size particles at colder temperatures near cloud top to larger sizes at base was evident.

- IWC was calculated from particle size spectra and habit percentages by relationship presented in Heymsfield (1977). Graphs are included.

- Graphs of IWC show wide horizontal variability. Values vary by as much as a factor of 10 (e.g., 0.015 — 0.15 g/m3). Increasing IWC with decreasing altitude is clearly seen.

- Liquid water was identified and measured. Normally it's rarely discussed when analyzing cold clouds. Its presence may be important for radiation calculations.

- Cloud optical depth, t, was calculated (for visible wavelengths) from two-dimensional imaging probe data to be equal to 2.3. Bulk contributions to t were from particles > 150 mm.

- Infrared emissivity was calculated from e = 1 — exp(-tvis/3), where 3 is a rough factor used to convert from visible to infrared optical depth. e was calculated to be 0.53.

- Data shows aggregation of particles in temperatures as low as -56 °C.

- Growth by aggregation can transfer mass efficiently into an evaporative environment thus lowering cloud base.

15. Heymsfield, A. J., and L. M. Miloshevich, Relative Humidity and Temperature Influences on Cirrus Formation and Evolution: Observations From Wave Clouds and FIRE II, J. of Atmos. Sciences, vol. 52: pp. 4302-4326, December 1996.

Abstract:

Measurements in orographic wave clouds, and in cirrus sampled during FIRE II, are used to investigate ice nucleation in the upper troposphere. The dynamically and microphysically simpler, quasi-steady state wave clouds provide relatively ideal conditions for observing characteristics of ice nucleation. We apply conclusions from the wave cloud study to help understand the formation and evolution of ice in the cirrus clouds observed during FIRE II.

The wave cloud study extend analyses reported by the authors in 1993 down to -56°C, in part by using an improved droplet size spectrometer with a detection threshold of 0.4 mm and a Video Ice Particle Sampler with a detection threshold of 5-10 mm. The measurements show a rapid transition from solution droplets to ice crystals characteristic of homogeneous ice nucleation, through the temperature range -35°C to -56°C. The temperature dependence of the relative humidity (RH) and the droplet sizes when ice nucleation occurs is consistent with theoretical and experimental expectations for homogeneous freezing. An expression is given for the peak RH with respect to water in the wave clouds (RH_{hn}), which decreases from 100% above -39°C to 73% at -56°C; RH_{hn} represents the condition required for ice nucleation in the wave clouds, and is shown to be more consistent with the homogeneous freezing of sulfuric acid solution droplets than ammonium sulfate solution droplets.

Aircraft measurements made in cirrus during FIRE II show highly ice-supersaturated regions in clear air, placing a lower bound on the RH required for cirrus formation approximately equal to $(RH_{hn}-10)$%. Measurements from a balloon-borne formvar ice crystal replicator are reported which show the vertical structure of cirrus to generally consists of three microphysically distinct regions: a highly ice-supersaturated ice production region near cloud top, an ice-supersaturated ice crystal growth region, and a sublimation region near cloud base formed by fallout of ice into ice-subsaturated air.

A negative feedback is observed, and studied numerically, between ice crystal concentration and ice-supersaturation: the RH condition for new ice nucleation in cirrus is most likely to occur near cloud top, when existing ice concentrations are low. A second relationship wherein the ice production rate depends on the RH leads us to propose a conceptual model of the formation and evolution of cirrus clouds.

Pertinent Information:

- This paper is full of information concerning the dynamical evolution of cirrus clouds and the various processes that control that evolution.

- It investigates both the observed and theoretical temperature-dependencies of relative humidity and droplet size upon ice nucleation.

- Analysis of Wave90 data produced the following relationship between the peak RH observed (RHhn) and temperature (in °C): $RHhn = 188.92 + 2.81T + 0.013336T2$.

- The authors found that ice nucleation in clear air will occur whenever $RH > (RHhn — 10)$%.

16. Heymsfield, A. J., and C. M. R. Platt, An Empirical Model of the Physical Structure of Upper-Layer Clouds, Atmos. Research, vol. 26, pp. 213-228, 1991.

Abstract:

A data set obtained in cirrus clouds has been examined to deduce any dependencies of the particle size spectral form or the crystal habit on the temperature. It was found that both form of the spectra and crystal habit changed systematicllay with temperature, the largest change occurring between -40 and -50 °C. These findings are consistent with previously found dependencies between lidar backscatter measurements and temperature.

A preliminary scheme for parameterizing the cirrus particle size spectra for crystal dimensions greater than 20 mm in terms of the temperature and the IWC is described. The visible extinction in cirrus is estimated.

Pertinent Information:

- This study uses data from Heymsfield (1977).

- IWC was calculated from pass-averaged particle spectra, crystal habits, and concentrations.

- Data shows that IWC values increase with increasing temperature. Average IWC values (calculated from the Heymsfield data) are binned by temperature ranges and included in a table. We may be able to use these data to replace the average IWC values in the Feddes model.

- Main finding is that the shapes of the cirrus crystal size distributions (at least for dimensions greater than 20 mm) and the distribution of crystal habits depend to a large extent on the ambient temperature.

- The cirrus particle spectra was shown to be a function of both temperature and IWC. Equations are included to show how to calculate the spectra.

17. Kosarev, A. L., and I. P. Mazin, An Empirical Model of the Physical Structure of Upper-Layer Clouds, Atmos. Research, vol. 26, pp. 213-228, 1991.

Abstract:

An empirical model of the structure of upper-layer clouds is suggested which includes data on the frequency of occurrence, amount, temperature, height, phase structure, and microstructure of cirrus clouds. The microstructure involves integral characteristics (cloud particle concentration, visible light attenuation coefficient, total liquid water content) and particle size distribution. The part concerning phase structure and microstructure is mostly based on field experiments made in the USSR. The model parameters are presented as plots, tables, and empirical relations.

Pertinent Information:

- Paper includes global statistics of frequency of occurrence of cirrus clouds.

- Includes summaries of statistics on cloud base and top heights, cloud thickness, and cloud base temperature.

- Microphysical quantities including: total water content (W), light attenuation coefficient (e), particle concentration, and size distribution parameters were measured over European territory of USSR from 1974-1984.

- W (sum of liquid and IWC) may sometimes exceed 0.1-0.2 g/m^3.

- Average W = 0.01 g/m^3.

- Clouds were defined as regions where W > 0.005 g/m^3.

- Wn (cumulative) = A0n + A1n |T| + A2nT2, where n corresponds to the cumulative percentile of interest. Graphs of W vs. T for various levels of n are shown, and Ain coefficients are tabulated.

- Similar graphs and parametric fits are provided for e, concentration, and size distribution parameters.

18. Kosarev, A. L., I. P. Mazin, and A. N. Nevzorov, The Empirical Model of the Structure of Cirrus Clouds in Middle Latitudes, Annalen der Meteorologie, A.M. Offenbach, vol. 2, no. 25, 1988, pp. 482-484.

Abstract:

This brief paper reports on the macrostructure and microstructure of cirrus clouds observed in European territory of what was previously the USSR. A parameterization of frequency of occurrence of cirrus is presented based on the data of Zak and Baranov (1960's). A parameterization of cumulative IWC, particle concentration, and size spectra are presented based on aircraft measurements of cirrus performed in the same territory during 1974-1984.

Pertinent Information

- All parameterizations are covered in a later paper by Kosarev and Mazin (1991, listed previously in this bibliography). That paper is more clearly written.

19. Marshak, A. , W. Wiscombe, and A. Davis, On the Analysis of the Multifractal Properties of Cloud Liquid Water Data, Proceedings of IRS '92, Keevailik and Karner (Eds.), pp. 116-119.

Abstract:

The multifractal properties of liquid water content data measured by aircraft from the 1987 FIRE marine stratocumulus experiment are studied. The simplest possible random models —log-binomial and log-normal models with fractional integration to get power spectrum equal to the one of liquid water data, fractional Brownian motion, and Weierstrass-Mandelbrot function —are compared with the observed liquid water data.

The similarity dimension of both liquid water data and fractal models is calculated to find the region of parameters in primary multifractal models. The well-known f(a) singularity analysis is applied to the gradient field and the 'raw' data. It has allowed us to get the values of p in the log-binomial and s in the log-normal model which gives the similar singularity properties as the observed liquid water data.

Pertinent Information:

- Specifics of this paper pertain to stratocumulus clouds observed during FIRE 1987, however, the general discussion of multifractal models and analysis provides background information for the CSSM modeling effort.

- Authors mention a method by Higuchi that offers an improvement to measuring fractal dimension. We might use something similar in our data analysis of liquid and IWC time (i.e., spatial) series.

20. **Matrosov, S. Y., B. W. Orr, R. A. Kropfli, and J. B. Snider, Retrieval of Vertical Profiles of Cirrus Cloud Microphysical Parameters from Doppler Radar and Infrared Radiometer Measurements, J. of Applied Meteorology, vol. 33, pp. 617-626, May 1994.**

Abstract:

This paper describes a new method to retrieve vertical profiles of the parameters of cirrus cloud microphysics that are important for the estimation of climatic feedback. These parameters are the particle characteristic size and ice mass content. The method also allows calculations of vertical profiles of particle concentrations and ice mass flux. The method uses measurements of radar reflectivities and Doppler velocities from the ground-based zenith-viewing radar combined with measurements of down-welling brightness temperatures from an infrared radiometer operating in the "window" (10-12 mm) region. The proposed method is illustrated on data obtained on 26 November 1991 during FIRE II in Coffeyville, Kansas. This paper also presents estimates of uncertainties of parameter retrieval due to different a priori assumptions about particle shapes, distributions, fall velocity-size relationships and due to errors in measurements. Comparisons with in situ measurements showed reasonable agreement.

Pertinent Information:

- Goal is to develop better understanding of cirrus cloud properties for inclusion into climate models.

- Authors develop a technique to relate ice mass content (IMC) and radar reflectivity that allows for independent variation of particle size and concentration.

- Radiometer provides vertically averaged cloud parameters.

- Radars and lidars can provide vertical profiles of cloud parameters.

- Graph of vertically averaged median particle diameter is presented (data taken during FIRE II).

- Graphs of vertical profiles of median particle diameter and IMC are presented (data taken during FIRE II).

- Empirical relationship between IMC and radar reflectivity (suggested by Sassen, 1987) is reproduced; $IMC = 0.037\ z_i^{0.696}$.

- Assuming we will not have access to radar or radiometer data to initialize the CSSM, the techniques described in this paper do not apply to our CSSM development effort.

110

21. Minnis, P., D. F. Young, K. Sassen, J. M. Alvarez, and C. J. Grund, The 27-28 October 1986 FIRE IFO Cirrus Case Study: Cirrus Parameter Relationships Derived from Satellite and Lidar Data, Monthly Weather Review, vol. 118, pp. 2402-2425, November 1990.

Abstract:

Cirrus cloud radiative and physical characteristics are determined using a combination of ground-based, aircraft, and satellite measurements taken as part of the FIRE Cirrus Intensive Field Observations (IFO) during October and November 1986. Lidar back-scatter data are used with rawinsonde data to define cloud base, enter, and top heights and the corresponding temperatures. Coincident GOES 4-km visible (0.65 mm) and 8-km infrared window (11.5 mm) radiances are analyzed to determine cloud emittances and reflectances. Infrared optical depth is computed from the emittance results. Visible optical depth is derived from reflectance using a theoretical ice crystal scattering model and an empirical bi-directional reflectance model. No clouds with visible optical depths greater than 5 or infrared optical depths less than 0.1 were used in the analysis.

Average cloud thickness ranged from 0.5 km to 8.0 km for the 71 scenes. Mean vertical beam emittances derived from cloud-center temperatures were 0.62 for all scenes compared to 0.33 for the case study (27-28 October) reflecting the thinner clouds observed for the latter scenes. Relationships between cloud emittance, extinction coefficients, and temperature for the case study are very similar to those derived from earlier surface-based studies. The thicker clouds seen during the other IFO days yield different results. Emittances derived using cloud-top temperature were ratioed to those determined from cloud-center temperature. A nearly linear relationship between these ratios and cloud-center temperature holds promise for determining actual cloud-top temperature and cloud thicknesses from visible and infrared radiance pairs.

The mean ratio of the visible scattering optical depth to the infrared absorption optical depth was 2.13 for these data. This scattering efficiency ratio shows a significant dependence on cloud temperature. Values of mean scattering efficiency as high a 2.6 suggest the presence of small ice particles at temperatures below 230K. The parameterization of visible reflectance in terms of cloud optical depth and clear-sky reflectance shows promise as a simplified method for interpreting visible satellite data reflected from cirrus clouds. Large uncertainties in the optical parameters due to cloud reflectance anisotropy and shading were found by analyzing data for various solar zenith angles and for simultaneous AVHRR data. Inhomogeneities in the cloud fields result in uneven cloud shading that apparently causes the occurrence of anomalously dark, cloudy pixels in the GOES data. These shading effects complicate the interpre-

tation of the satellite data. The results highlight he need for additional study of cirrus cloud scattering processes and remote sensing techniques.

Pertinent Information:

- Using data from 71 FIRE cases, the authors have derived values for cloud base, center, and top heights along with corresponding temperatures from lidar and rawinsonde data.
- Average cloud thickness (for all 71 scenes) ranged from 0.5 to 8 km.
- GOES imagery was used to compute emittance and reflectance variables.
- Optical depths were computed.
- Resulting data were used to derive parametric relationships between cloud emittance, extinction coefficients, scattering efficiency, reflectance, optical depth and cloud top/center temperatures.

22. **Mitchell, D. L., S. K. Chai, Y. Liu, A. J. Heymsfield, and Y. Dong, Modeling Cirrus Clouds. Part I: Treatment of Bimodal Size Spectra and Case Study Analysis, J. of Atmos. Science, vol. 53, no. 20, pp. 2952-2966, 15 October 1996.**

Abstract:

A model has been developed that predicts the evolution of bimodal size spectra in cirrus clouds. This was done by predicting two size distributions: one for ice particles less than about 150 mm and another for larger particles. The sum of these two distributions yielded the composite, bimodal size distribution, which was predicted from the growth processes of vapor deposition and aggregation. Predicted size spectra were directly compared with size spectra measured during a cirrus cloud case study sampled during a Lagrangian spiral descent. Favorable agreement was obtained between predicted and measured size distributions, especially at ice particle sizes < 150 mm.

The aircraft sampling technique and conditions characterizing the case study were well suited for evaluating the effect of aggregation on ice particle growth. Model calculations indicated that aggregation growth increased mean ice particle sizes by up to 50 mm and reduced concentrations by up to 60% during the case study. The cloud-averaged aggregation efficiency was estimated to be 0.5, which is comparable with values estimated for frontal clouds. It was suggested that ice crystals referred to as planar polycrystals, which exhibit complex three-dimensional shapes, may be precursors for aggregation in cirrus clouds.

The physical mechanisms governing the evolution of the small particle size distribution were investigated using ice particle replicator data from two case studies. Combining the replicator data with theoretical work on the evolution of size distributions,

112

evidence indicates that the mean size in the small ice particle size distribution is relatively small and constant when vapor deposition growth dominates, implying pristine hexagonal crystal types. When aggregation growth involving planar polycrystals occurs, this mean size tends to become larger and can vary widely. Aggregation growth in the small particle distribution may act to e distribution may act to diminish bimodal behavior.

Estimated contributions of unmeasured small ice particles (D<50 mm) to cloud optical depth, t, were shown to vary widely with conditions and were at least about a factor of five less than estimates from an earlier study. The overall impact of the aggregation process on t, relative to t for diffusion growth only, was estimated. For the case study considered, aggregation attenuated t by 10-20%.

Finally, the microphysical properties were predicted from analytical expressions. This may make it possible to incorporate this model into large-scale models without excessive increases in computation time.

Pertinent Information:

- Dynamical model predicts evolution of bimodal size spectra in cirrus clouds. Model is 1-d. Assumes horizontally homogeneous, steady-state water contents. Principal model input is the vertical distribution of the IWC (one of the cloud descriptors we are trying to find).

- Gamma distributions used to describe number-size distributions for large (>150 mm) and small (<150 mm) particles are presented. Author states that for most cases, it appears possible to describe the full cirrus size distribution as the composite of the small and large size distribution models.

- Provides information on how to back IWC out of measured size distribution parameters to initialize the model.

- As a part of the results, one graph of IWC vs. altitude is included showing the initial water content vertical profile (derived from measured size distribution information sampled on 1 November 1986 of FIRE I) and the resulting portion of that predicted to be associated with large cirrus particles.

- A fair amount of general information is included that may be of use when designing models of size spectra for the CSSM and Fast-Map.

23. Mitchell, D. L., A. Macke, and Y. Liu, Modeling Cirrus Clouds. Part II: Treatment of Radiative Properties, JAS, vol. 53, no. 20, pp. 2967-2988, 15 October 1996.

Abstract:

A new radiation scheme, suitable for two-stream radiation transfer models, was developed for cirrus clouds. Analytical expressions were derived for the extinction and

absorption coefficients and the asymmetry parameter. These are functions of the ice particle size distribution parameters, ice particle shapes, and wavelength. The ice particle shapes considered were hexagonal plates and columns, bullet rosettes, and planar polycrystals. These appear to be the principal crystal types found in cirrus clouds. The formulation of radiative properties accounts for the size distribution projected area and the distance radiation travels through ice particles. For absorption, refraction and internal reflection of radiation were parameterized.

By assuming an idealized cirrus cloud, the dependence of the single scatter albedo, reflectance, and emissivity on wavelength, ice particle shape, and size distribution was demonstrated. Reflectance and emissivity exhibited a strong dependence on ice particle shape, with planar polycrystals and bullet rosettes often being twice or more reflective than hexagonal columns and plates.

The radiation scheme was tested with microphysical and radiation measurements from two cirrus cloud field studies. It was shown for both case studies that by matching observed and predicted albedo-emissivity curves, the radiation scheme could predict the observed mean ice particle size and ice water path (IWP), provided the dominant ice particle shape was known or inferred. Retrieved IWP values differed from measurement-derived values by <= 15% for the first case study and 18% on average for the second case study. Hence, it may be feasible to retrieve realistic IWP estimates from satellite data for a given ice particle shape.

Other radiation schemes have not been able to explain the second case study, which was characterized by relatively high albedos. These high albedos appeared to result from unusually small hexagonal plate crystals having asymmetry parameter values similar to those of cloud droplets.

An improved treatment of the asymmetry parameter was not the primary reason for the good agreement between theory and observations. Rather, key factors appeared to be improved treatments of ice particle photon path, projected area and mass, and the omission of certain physical processes included in Mie theory that may not be appropriate for ice particles.

The radiative properties were predicted from analytical expressions, making this scheme useful for predicting radiative properties in large-scale models without excessive increases in computation time.

Pertinent Information:

- Analytic expressions were derived for extinction coefficient, absorption coefficient, and asymmetry parameter as functions of size distribution parameters, particle shapes, and wavelength.

- Resulting scheme is capable of predicting ice water path.

- Expressions are suitable for inclusion in a two-stream radiative transfer model and are not well suited for a highly parametric model such as the CSSM.

24. Orr, B. W., and R. A. Kropfli, Estimation of Cirrus Cloud Particle Fallspeeds From Vertically Pointing Doppler Radar, Proc. of 26th Annual Conference on Radar Meteorology, Norman, OK, May 24-28, 1993, pp. 588-590.

Abstract:

FIRE II was conducted in Coffeyville, Kansas, in late 1991 to study microphysical and radiative properties of cirrus clouds. A variety of active and passive remote sensors were employed, including an 8-mm-wavelength cloud sensing Doppler radar developed at the Wave Propagation Laboratory (WPL). The radar, having excellent sensitivity to cloud particles (-30 dBZ at 10km), good spatial resolution (37m), and velocity precision (.05 m/s) is an excellent tool for observing cirrus clouds. Having this radar directed toward the zenith for long periods of time during FIRE II permitted the reflectivity-weighted particle fallspeed to be related to reflectivity which allowed a separation of ice particle fallspeeds from vertical air motions. Additionally, such relationships have proved useful in other multi-sensor techniques for determining vertical profiles of ice particle size and IWC in cirrus clouds. This paper discusses the analysis method and the results of applying it to cirrus cloud reflectivity and velocity data collected during FIRE II.

Pertinent Information:

- Authors developed a method to derive cirrus particle fallspeed from radar reflectivity values.

- Results are of minimal immediate use for our model development unless we include a radar pre-processor to provide more complete initial information about cloud shape.

- One graph of average vertical fallspeed vs. radar reflectivity is presented.

- All three FIRE II cases analyzed show general trend of higher fallspeeds at cloud base. Ranges for fallspeeds are presented.

- Two graphs of fallspeed vs. altitude are shown.

115

25. Piironen, A. K., E. W. Eloranta, Convective Boundary Layer Mean Depths and Cloud Geometrical Properties Obtained from Volume Imaging Lidar Data, J. of Geophys. Res., vol. 100, D12, pp: 25569-25576, 1995.

Abstract:

This paper presents automatic methods for obtaining convective boundary layer mean depths, cloud base altitudes, cloud top altitudes, cloud coverages, and cloud shadows using the University of Wisconsin Volume Imaging Lidar (VIL). These methods provide mesoscale observations representing the 70 km² scanning area of the VIL. All data obtained with the VIL during the 1989 FIFE field experiment are analyzed and the results are summarized. The reliability of these methods is verified by comparing the results with radiosonde profiles, satellite images, and visual estimates from Range Height Indicator scans of the VIL.

Pertinent Information:

- Methods to calculate cloud base and top altitudes can be used in our data analysis task.

26. Platt, C. M. R., A parameterization of the Visible Extinction Coefficient of Ice Clouds In Terms of the Ice/Water Content, J. of Atmos. Sciences, vol. 54, pp. 2083-2098, August 1997.

Abstract:

This article describes a parameterization of the visible extinction coefficient of cirrus and frontal ice cloud in terms of the ice/water content. The parameterization is based on the discovery that the ice cloud particle size spectra from a particular dataset tended to fall into three separate well-defined regions. These regions were a Marshall-Palmer distribution covering particles with dimensions larger than between 100 and 1400 mm, depending on the cloud temperature; a Heymsfield-Platt type power-law distribution for the smaller particles (dimensions from 20 mm to somewhere between 100 and 800 mm); and a different spectrum of the smallest particles of sizes less than 20 mm. The dataset chosen had been obtained from aircraft in situ observations of cloud particle size spectra in ice clouds and covered the entire spectral range from 2 to 3000 mm, thus allowing a study of every important spectral region. Part of this dataset was used originally in a previous study by Heymsfield and Platt. The data used in the present study covered cirrus clouds overlying deep frontal clouds together with a reanalysis of the Heymsfield-Platt set for "dry" cirrus clouds.

In the present study, the visible extinction coefficient s was parameterized in terms of the ice/water content W. A model of cylindrical ice particles was used. It was found

that the dependence of s on W followed a power law of the from, $s = jW^k$, where k had a value that depended on the temperature range.

The size spectra, although measured in certain cirrus and frontal ice clouds, were also used as surrogate spectra to estimate similar s-W relations for water clouds.

The s-W relations for cirrus ice clouds were found to agree reasonably with those obtained recently by other workers. The relations also indicated, conversely, that the cloud ice/water content of cirrus cloud be retrieved from a measure of the cloud volume extinction coefficient to within an uncertainty of about 30%.

Pertinent Information:

- The aim of this study was to calculate the water content (W) and extinction coefficient (s) as functions of cloud temperature and to relate the values of W to s.

- This study uses the old Heymsfield data (average pass values for size distribution at incremental steps through a cloud layer).

- The authors derive W from size distribution parameters using two models for the number concentration; a power law over the range 20-100 mm (N=ADB), and a Marshall-Palmer law for values above 500 mm (N=N0 exp(-lD)).

- A graph of W vs temperature is included containing W values calculated in this effort, along with other experiments and models for reference. This is a very useful graph to compare to the Feddes curve and to the CSSM output fields. How close do we come to the values presented on this graph?

27. **Platt, C. M. R., and A. C. Dilley, Remote Sounding of High Clouds. IV: Observed Temperature Variations in Cirrus Optical Properties, J. of Atmos. Sciences, vol. 38, pp. 1069-1082, May 1981.**

Abstract:

The results of a ruby lidar (0.694 mm wavelength) and infrared radiometer (10-12 mm) study on cirrus clouds are reported for a period covering the autumn and winter months at Aspendale (38°S, 144°E). The lidar and radiometer data have been used to study the temperature dependence of the gross structure and optical properties of cirrus clouds. Well-defined correlations are found between the mid-cloud temperature and cloud depth, infrared absorption coefficient, infrared emittance, backscatter to extinction ratio and ratio of the visible extinction coefficient at 0.693 mm to the infrared absorption coefficient at 10-12 mm. For instance, as the mid-cloud temperature varies from -70 to -30 °C, the mean cloud depth increases from 1 to 3.5 km and the mean infrared absorption coefficient from 0.04 to 0.25 km^{-1}. These two factors together cause a change in emittance from 0.11 to 0.42. The increase in absorption coef-

ficient with temperature can be attributed to the presence of larger ice particles in the deeper clouds. Over the same temperature range the effective backscatter to extinction ratio has a fairly complex behavior with values of 0.25-0.3 below -45 °C, but with a rapid increase to 0.45 at -40 °C. The multiple scattering factor is found to increase from 0.54 at -60 °C (approx. 11 km altitude) to 0.76 at -20 °C (approx. 5.5 km altitude). Some cases of very high anomalous lidar backscatter occur for clouds of mean temperature $\geq$ -35° and emittance $\geq$ 0.6. The depolarization ratio of the lidar backscattered radiation also shows complicated variations with temperature.

The observed changes in backscatter to extinction ratio are attributed to a change in the ice crystal habit from simple spatial crystals at temperatures < -40 °C to more complex aggregates at greater temperatures. This is based on the fact that supercooled water cannot exist at temperatures below -40 °C. The high anomalous backscatter is attributed to specular reflection from horizontally oriented plate crystals or from supercooled water droplets. Changes in depolarization ratio at temperature greater than -40 °C are attributed variously to the presence of mixed-phase clouds, to crystal aggregates and to horizontally oriented hexagonal crystals.

Changes in the multiple-scattering factor with temperature (i.e., altitude) are found to agree qualitatively with theoretical predictions, the main effect being a reduction in the multiple-scattering factor (leading to a more transmitting cloud) as the range or altitude of the clouds increases.

Pertinent Information:

- Primary goal of this research effort is to seek possible temperature-dependent variations in optical properties throughout cirrus clouds.

- A systematic increase in cloud depth with temperature is observed (T > -37.5° C) indicating that as the cloud thickens, the cloud base height decreases.

- Definite temperature (or altitude) trends in optical properties have been identified.

28. **Platt, C. M. R., and Harshvardhan, Temperature Dependence of Cirrus Extinction: Implications for Climate Feedback, J. of Geophys. Res., vol. 93, no. D9, pp. 11051-11058, Sept. 20, 1988.**

Abstract:

The measured temperature dependence of infrared absorption in cirrus cloud obtained from previous extensive lidar and radiometer (LIRAD) observations of cirrus is used to investigate the sensitivities of changes in cirrus optical properties to changes in global temperature. Values of infrared absorption and IWC calculated previously from observations of cirrus cloud microphysics are also used to investigate climate

sensitivities. The values of calculated mean infrared absorption give a very similar temperature dependence, and thus climate sensitivity, to the LIRAD results. Values of mean IWC calculated from the observations of cloud microphysics are compared with the available IWC calculated from moist adiabatic ascent through a vertical cloud depth of 300 m, and a similar temperature dependence is found in both cases. However, taking into account the observed cloud depths of cirrus, considerable dilution of IWC below adiabatic values is obviously occurring. The temperature sensitivities of extinction (or absorption) coefficients (calculated from a combination of LIRAD and microphysics results) are found to be generally less than the temperature sensitivities of IWCs, due to an increase in cloud particle model radius with temperature. The temperature sensitivity of cirrus extinction is found to vary from 0.033 $°C^{-1}$ at -22.5 °C to 0.200 $°C^{-1}$ at -72.5 °C. Equivalent sensitivities for cirrus optical depth are influenced by observed changes in cirrus cloud depth with temperature and vary from 0.003 $°C^{-1}$ at -22.5 °C to 0.241 $°C^{-1}$ at -72.5 °C. As high cold cirrus clouds are considered to cause a positive feedback with global temperature change, such a feedback is seen to become particularly strong at the lowest temperatures. A simple method of parameterization of cirrus visible and infrared optical properties in terms of cloud temperature is presented, thus making it possible to introduce cirrus optical properties into a numerical model without requiring knowledge of the IWC.

Pertinent Information:

- Authors point out the need to understand the distribution with altitude of cirrus clouds, as well as an accurate specification of optical properties for climate modeling.

- Current models (GCMs) have only a crude prediction of cloud liquid water content. Most models achieve a diagnostic cloud, when either a layer in the atmosphere becomes saturated, or, has a specified humidity. A fractional cloud amount is assigned and cloud optical properties are assigned.

- This paper uses an alternative approach in which cloud optical properties are parameterized as a function of temperature or pressure and cloud liquid water content is thus bypassed. The authors mention the parameterization of Feigelson (1978), but use data from Platt and Dilley (1981) and Platt et al. (1987).

- Platt (1984) and Platt et al. (1987) show from a year's extensive LIRAD observations that, when averaged over many cases, the cirrus infrared absorption coefficient is a well-defined monotonic function of atmospheric temperature.

- Refer to Platt et al. (1987) for cirrus cloud depth information (range from 1 to 4 km with some dependence on cloud temperature). In a nutshell, for midlatitude clouds, cloud depth is given by the following:

  h(km) = 0.0456 T + 4.7 (-72.5 °C < T < 35 °C)

  h(km) = -0.0650 T + 0.725 (-35 °C < T < -15 °C)

- IWCs are calculated from a model of uplift and condensation for a constant cloud depth. Results indicate a rapid decrease in liquid water content with temperature. The resulting average IWCs are somewhat greater than those which were calculated in Heymsfield and Platt (1984) from cirrus cloud microphysics data (probably due to greater cloud depths in the latter).

29. Poix, C., G. Febvre, A. Fouilloux, H. Larsen, and J. F. Gayet, The Retrieval of Cloud Microphysical Properties Using Satellite Measurements and an in Situ Database, Annales Geophysicae, vol. 14, pp. 98-106, 1996.

Abstract:

By combining AVHRR data from the NOAA satellites with information from a database of in situ measurements, large-scale maps can be generated of the microphysical parameters most immediately significant for the modeling of global circulation and climate. From the satellite data, the clouds can be classified into cumuliform, stratiform and cirrus classes and then into further sub-classes by cloud top temperature. At the same time a database of in situ measurements made by research aircraft is classified into the same sub-classes and a statistical analysis is used to derive relationships between the sub-classes and the cloud microphysical properties. These two analyses are then linked to give estimates of the microphysical properties of the satellite observed clouds. Examples are given of the application of this technique to derive maps of the probability of occurrence of precipitating clouds and of precipitating water content derived from a study within the International Cirrus Experiment (ICE) held in 1989 over the North Sea.

Pertinent Information:

- Paper makes reference to APOLLO cloud classification scheme which may be useful in building a cloud pre-processor.

- Database of in-situ measurements consists of about 500 hours of flight time (about 10000 km of in-cloud distance) by French atmospheric research aircraft flying through mid-latitude clouds over Western Europe.

- Data consist of thermodynamical and microphysical parameters averaged over "homogeneous" regions through the cloud. Average length of a homogeneous cloud length was 5 km.

- In situ parameters include: vertical cloud extent, cloud top temp., temp. at measurement level, liquid water content, droplet concentration, mean volume diameter, concentration of cloud particles larger than 100 mm, precipitating water content of particles greater than 100 mm (for T < 0 °C, precipitating water content is equivalent to IWC), and cloud type.

120

- Graph of precipitating water content vs. cloud top temperature is shown for all cloud types. Two curve fits to the data (one for cumuliform cloud types and one for stratiform/cirriform) are included. We can use these fits to predict mean IWC as a function of cloud top temperature for the CSSM cirrus clouds. The stratiform/cirriform fit is given by the following:

for $-35 < T < 6$ °C $IWC = 6.1e-2 - 6.8e-3\ T - 5.7e-4\ T^2 - 1.3e-5\ T^3 - 8.1e-8\ T^4$

for $-50 < T < -35$ °C $IWC = 1e-2$

where T is the cloud top temperature (in °C), and IWC is the IWC in (g/m³). Note that these values are less (by about a factor of 2-5) than the IWC values predicted by the Feddes model for all cirrus cloud types and temperatures.

30. **Quante, M., E. Raschke, F. Albers, A. Grattzki, P. Scheidgen, and Y. Zhang, The International Cirrus Experiment (ICE) — Results from the Pilot Experiment 1987, Conference on Atmos. Radiation, 7th, San Francisco, CA, July 1990, Preprints (A92-13901 03-47), Boston, MA, American Society, 1990, pp. 30-37.**

Abstract:

Consideration is given to the major scientific objectives of ICE, namely, investigate the physical processes contributing to the life cycle of cirrus, improve cirrus parameterizations in general circulation and models, and upgrade cloud retrieval from satellite observations (particularly to verify ISCCP results). Results which were obtained from during the pilot experiment 1987 are reported, and some of accompanying modeling activities are presented. Aircraft measurements of radiative, microphysical, and dynamical quantities sampled in extended cirrus fields are reported. The findings indicate the complexity of structure and a complex particle structure combined with the many different processes involved in the dynamical organization of the observed clouds.

Pertinent Information:

- Review of the ICE objectives and equipment is provided.
- This paper analyzes one specific case study taken on 1 October 1987 in a target area about 200 km east of the British coast.
- Maximum IWC measured was 0.1 g/m³.
- Typical range of values is 0.01 -0.04 g/m³.
- Measurements show complex internal structure within the cirrus layer with impulses of one to a few kilometers embedded within a mesoscale organization (10-15 km).
- Graphs of particle size distribution, particle concentration and vertical velocity for the case study are also presented.

- Variations of horizontal motions within the cloud layer exceed variations in the vertical by a factor of more than 10. The distribution of small scale variances (<500m) in wind, temperature, and humidity increase toward the cloud base region.

31. Randall, D. A., and K. M. Xu, Use of ARM Data to Test an Improved Parameterization of Upper Tropospheric Clouds for Use in Climate Models, Final Report to the U.S. DOE, March 1995

Abstract:

Report includes status of five research tasks that comprise the project:
- Develop, implement, and test an improved parameterization of upper tropospheric cloudiness, with emphasis on cloud formation, maintenance, and destruction.
- Conduct tests of the new parameterization in the SCM, including tests in which the one-dimensional model is "forced" with observations (e.g., of large-scale vertical motion) collected at ARM sites.
- Use the CEM to perform further tests of the parameterization, in part by simulating observations collected during ARM, and to suggest model-development strategies.
- Perform climate simulation with the full three-dimensional version of the CSU GCM.
- Make the improved parameterizations available and adaptable for use in other models.

Pertinent Information:

- Authors have developed a new cloud microphysics parameterization for use in climate models.
- The parameterization predicts cloud amount in terms of predicted large-scale average mixing ratios of cloud water and cloud ice.
- Cloud amount is then used for radiative transfer and microphysics, as well as in the parameterization of cloud dynamics.
- Research is not applicable to our model development.

32. Sassen, K., Ice Cloud Content from Radar Reflectivity, Applied Meteorology, vol. 26, pp. 1050-1053, August 1987.

Abstract:

The ice equivalent radar reflectivity factor ($Z_i = 5.3\ Z_e$) is found from previous measurements to be related to the precipitation rate (R, mm/hr) and ice mass content (M, g/m^3) of ice crystal clouds by $R = 0.067\ Z_i^{0.804}$ and $M = 0.037\ Z_i^{0.696}$. Comparison with other empirical equations suggests that changes in the ice crystal size distribution accompanying the formation of precipitation particles begin to modify these relations within deep ice clouds and lead to a different class of relations for snowfall. Accord-

ingly, the above equations are considered valid for $Z_i \leq 10$ dbZ, and should be particularly appropriate for short-wavelength radar observations of cirrus clouds.

Pertinent information:

- Relationship between radar reflectivity and ice mass content could be useful in validation studies where radar data are available. In those cases, we could derive IWC values for comparison with CSSM-produced clouds.

33. Sassen, K., D. O'C Starr, T. Uttal, Mesoscale and Microscale Structure of Cirrus Clouds: Three Case Studies, J. of the Atmos. Sciences, vol. 46, no. 3, pp. 371-396, February 1989.

Abstract:

The structure and composition of three basic cirrus cloud types are examined through coordinated aircraft and ground-based polarization lidar and radar measurements. The cloud systems consist of a multilayered orographic cirrus, a 6-km deep cirrostratus, and a group of fibrous cirrus bands at the tropopause. The data reveal the presence of mesoscale generating regions with horizontal dimensions ranging from ~15 km in narrow cloud bands up to ~100 km in cirrostratus. These generating regions appear to be composed of complexes of much smaller convective structures, presumably on the ~1-km scale of cirrus uncinus cells, and so are termed Mesoscale Uncinus Complexes (MUC). Accumulations of ice particles within cirrus, commonly referred to as precipitation trails, are associated with generating regions at or near cloud tops, but are also created by the local production of ice crystals within embedded convective impulses. Supercooled cloud droplets large enough to be detected by aircraft probes (≥5 mm diameter) were sampled in embedded convective cells near cloud base at temperatures ranging from -12° to -36° C. Ice particle nucleation at colder temperatures is assumed to involve the homogeneous freezing of haze particles too small to be detected by the aircraft probes employed, although they appear to have been detected by the polarization lidar technique under some conditions. Average ice mass contents are temperature dependent in a manner consistent with the conversion of a relatively small amount of excess water vapor (corresponding to ice supersaturations of a few percent) to ice mass.

Pertinent Information:

- There is growing evidence that spherical liquid droplets are important in determining the scattering and microphysical properties of cirrus. Liquid water may be present in cirrus clouds with temperatures warmer than -40° C (e.g., about half of midlatitude cirrus observed in Australia have midcloud temperatures warmer than -40° C).

- Measurements used in this paper were taken from ground-based polarization lidar, Doppler radar, and research aircraft.

- Average aircraft parameters for each flight leg of two of the three case studies are presented (including concentration, particle size, and mass content).

- Aircraft data for several flight legs are shown (including vertical velocity, concentration, and mass content).

- Summary ice crystal distributions for each of the three case studies are presented (averaged over 5° C temperature bins).

- Average concentrations and mass contents for each of the three case studies are also presented (averaged over 5° C temperature bins).

- Uniform-appearing cirrostratus case study showed surprising amount of internal structure dominated by several mesoscale cirrus-particle generating regions (identified by sheared ice particle trails in the radar data). Data suggests that generating regions are composed of complexes of individual cells, presumably displaying the 1 km dimensions typical of cirrus uncinus. Evidence is lacking for the organization of these generating cells into cloud bands.

- Vertical distribution of ice mass content gradually increases during descent through the cloud and reaches a maximum near cloud base.

- Fibrous cirrus clouds were aligned to distinct and relatively narrow bands, which were from a few to several hundred kilometers long.

- Generalizations made from analyzing these three different cirrus cloud types were: clouds were surprisingly dynamic, cloud structures ranged in size from 1-100 km. The 1km unit presumably represents a basic convective cell. Cells are organized into MUC with dimensions ranging from 15 km (narrow cirrus bands) up to 100 km in deep cirrostratus. Liquid water was detected unambiguously. Ice crystal data are consistent with previously reported microphysical data parameterizations, and display a clear temperature dependency. Size distributions are similar to those of Heymsfield and Platt (1984), but their ice mass contents exceed the authors values for temperatures warmer than -40° C. Leg-averaged ice mass contents ranged from 0.5 to 16.4 mg/m³, compared to peak values of 150 and 45 mg/m³ (from aircraft and radar, respectively). Vertical distributions of ice mass content are similar to the patterns generated by a cirrus cloud model by Starr and Cox (1985).

34. Soden, B. J., and L. J. Donner, Evaluation of a GCM Cirrus Parameterization Using Satellite Observations, J. of Geophys. Res., vol. 99, no. d7, pp. 14401-14413, 20 July 1994.

Abstract:

This study applies a simple yet effective methodology to validate a general circulation model parameterization of cirrus ice water path. The methodology combines large-scale dynamic and thermodynamic fields from operational analyses with prescribed occurrence of cirrus clouds from satellite observations to simulate a global distribution of ice water path. The predicted cloud properties are then compared with the corresponding satellite measurements of visible optical depth and IR cloud emissivity to

evaluate the reliability of the parameterization. This methodology enables the valida-
tion to focus strictly on the water loading side of the parameterization by eliminating
uncertainties involved in predicting the occurrence of cirrus internally within the pa-
rameterization. Overall the parameterization performs remarkably well in capturing
the observed spatial patterns of cirrus optical properties. Spatial correlations between
the observed and the predicted optical depths are typically greater than 0.7 for the
tropics and northern hemisphere mid-latitudes. The good spatial agreement largely
stems from the strong dependence of the ice water path upon the temperature of the
environment in which the clouds form. Poorer correlations (r =0.3) are noted over the
southern hemisphere mid-latitudes, suggesting that additional processes not accounted
for by the parameterization may be important there. Quantitative evaluation of the pa-
rameterization is hindered by the present uncertainty in the size distribution of cirrus
ice particles. Consequently, it is difficult to determine if discrepancies between the
observed and the predicted optical properties are attributable to errors in the param-
eterized ice water path or to geographic variations in effective radii.

Pertinent Information:

- Methodology determines total ice water path (IWP) in large-scale cirrus clouds using sat-
  ellite observations. Visible optical depth and IR emissivity are derived and compared to
  GCM parameterizations.

- Typical cirrus cloud thickness varies from about 100 m to 3 km.

- Optical depth, t, is related to IWP by the following: tl = 3 Ql IWP / 4 re rice (where re is
  effective radius and rice is the density of ice, Ql is the effective extinction efficiency,
  l=0.6 mm for visible, and 15 mm for infrared, re is assumed to be 10 mm).

- w, p, and G are used to estimate the vertically averaged IWC (IWC) using model of
  Heymsfield and Donner (1990). Because that model requires a computationally intensive
  iterative solution, a look-up table was built for selected values of those variables. Once
  IWC is determined, IWP can be calculated simply by multiplying IWC by the cloud
  thickness. Is the look-up table built for this analysis generally available? We could use a
  similar approach to calculate average IWC and then introduce fractally-generated pertur-
  bations to the average value.

35. **Starr, D. O'C., S. K. Cox, Cirrus Clouds. Part I: A Cirrus Cloud Model, J. of Atmos. Sci-
ences, vol. 42, no. 23, pp. 2663-2681, 1 December 1985.**

Abstract:

A two-dimensional (x, z) time-dependent, numerical cloud model is developed for the
purpose of investigating the role of various physical processes involved in the main-
tenance of cirriform clouds. In addition to accounting for dynamic and thermody-
namic processes including phase changes of water, effects due to microphysical com-

position and radiative processes are also explicitly incorporated into the model. Diagnostic parameterizations for the local radiative properties of cloudy volumes and the gravity induced relative fall speed of the contained ice water are presented. Results of a simulation of a thin cirrostratus cloud are given. Features of the simulated cloud structure are quite realistic. Quantitative agreement is found between the simulated IWC and vertical motions and comparable observations. It is shown that radiative effects may be very significant in the maintenance of cirrus. The effects of the gravity-induced relative fall speed of ice crystals are found to be of critical importance in the evolution of the cloud layer.

Pertinent Information:

- Cloud model is used to investigate the physical processes involved in cirrus formation and maintenance.

- Two-dimensional numerical cloud model includes dynamic and thermodynamic and radiometric processes. Uses bimodal size distribution. Grid domain: 100 m grid spacing, 6.3 x 3.1 km domain.

- Simulates IWC as a function of position and time. Graphs are included showing time-dependent behavior and vertical profiles of average IWC.

- Average values are compared with cirrus data reported in a collection of technical reports by Varley, et al. and Heymsfield. Simulated cirrostratus means and maximum IWC values compare well with observation. (e.g., means between 3 and 8 mg/m^3, a value of 5 mg/m^3 within the cloud generator region, and max. values of 10 and 20 mg/m^3).

- Model produces horizontal embedded structures and multi-layered structure in cirrostratus as observed in nature.

- Model doesn't apply well to temperatures > -25°C or in cases of high shear.

36. Starr, D. O'C., S. K. Cox, Cirrus Clouds. Part II: Numerical Experiments on the Formation and Maintenance of Cirrus, JAS, vol. 42, no. 23, pp. 2682-2694, 1 December 1985.

Abstract:

The numerical cirrus cloud model of Starr and Cox is used to investigate the role of various physical processes in the formation and maintenance of cirrus. Effects due to microphysical composition, i.e., crystal habit and size distribution, are found to be quite important in determining the overall cloud water budget. Radiative processes are also shown to affect the organization and bulk properties of the cloud. Substantial differences between simulation of thin cirrus under midday and nighttime conditions are found with the cloud being less dense overall (=20%) but more persistently cellular during the day with all other environmental factors being the same. Cloud-scale interactions and feedbacks between dynamic, thermodynamic and radiative processes and

the microphysical composition are significant and strongly modulate the properties of the simulated clouds. A comparison is made between simulation of weakly forced cirrostratus and non-precipitating altostratus (liquid phase) under comparable environmental conditions. Five times more cloud water is maintained in the altostratus case where the updraft wind speeds are greater by a factor of 10. The role of the large-scale ascent or descent is also examined. Inferences are drawn from these results with respect to the parameterization of cirrus in large-scale forecast of climate models.

Pertinent Information:

- Cirrus cloud layer is more cellular during the day than at night with all other environmental conditions being equal. Midday cirrus also have higher peak mixing ratios, although overall mean values are approximately 20% lower.

- Daytime convective elements tend to persist throughout the day. Equivalent nighttime cells form and dissipate much faster (with a period of approximately 20 minutes). Cellular elements tend to be vertically elongated in shape.

- Author concludes that any attempt to represent cirrus by simple analogy to stratus cloud types is too simplistic.

- Author analyzes the results of varying ice water relative fallspeed on model output. For example a graph showing time-dependence of average IWC is constructed for varying fallspeeds.

- To emphasize the processes that are distinctly important for cirrus clouds, a simulation was also performed for a liquid phase altostratus cloud layer. Cellular regions are also present in altostratus, but are more horizontally elongated than their cirrus counterparts. They also occur higher within the cloud layer than cirrus cells.

37. Starr, D. O'C., D. P. Wylie, The 27-28 October 1986 FIRE Cirrus Case Study: Meteorology and Clouds, Monthly Weather Review, vol. 118, pp. 2259-2287, November 1990.

Abstract:

Detailed descriptions of the rawinsonde-resolved meteorological (3-hourly soundings) associated with a succession of five distinct mesoscale cirrus cloud regimes, which were observed intensely over 36-hour period, is given. The synoptic scale systems in which these features were embedded are described and a brief overview of the experiment is given. Regional analyses of the static stability structure and vertical motion are presented and interpreted with respect to the characteristics of the corresponding cloud fields as deduced from satellite and lidar observations. The cloud fields exhibited a high degree of persistent mesoscale organization on scales of 20-500 km reflecting corresponding scales of dynamic and thermodynamic structure/variability as on the synoptic scale. Cloud generation was usually confined to layers less than 1 km deep (typically 0.5 km in depth) and cellular organization was

evident in most cases irrespective of the thermal stratification. Multi-layered development was prevalent (2-3 layers) and was associated with vertical structure of the temperature and moisture fields resulting primarily from vertical gradients in horizontal advection. One convective generation layer usually present. Destabilization resulted primarily from advective processes that also led to the formation of a transient stable layer above and/or below the convective layer. Though resembling elevated frontal surfaces, the stable layers were not extensions of surface features. Cloud processes, primarily ice particle fall-out and evaporation, but also including cloud top detrainment, contributed to generating the multilayered structure. Two cases of clouds spawned from an overlying cloud deck were seen where one involved natural seeding of an ice-saturated and conditionally unstable layer in which vigorous convective development was subsequently observed. Subvisual cirrus in the lower stratosphere were found to be associated with prior tropopause features (upwind) where denser cirrus existed. Inferences are drawn with respect to the parameterization of cirrus in large-scale models. In particular, vertical resolution on the order of 0.5 km will probably be required to adequately resolve the forcing required for implementation of a physically-based parameterization. Greater understanding of the nature and causes of the observed mesoscale structure is also needed.

Pertinent Information:

- Authors describe the environmental conditions during the FIRE IFO. No discussion of cloud microstructure microphysics included. This paper serves as supporting information for all of the modeling efforts which use the 27-28 October 1986 FIRE data.

38. Sundqvist, H., A Parameterization Scheme for Non-Convective Condensation Including Prediction of Cloud Water Content, Quarterly J. R. Met. Soc., vol. 104, pp. 677-690, 1978.

Abstract:

A model for non-convective condensation processes has been developed. The model allows condensation to begin before relative humidity reaches 100%. The liquid water content of clouds is a prognostic variable of the model. The rate of condensation is a function of relative humidity and moisture flux convergence. The micro-physical processes involved in the formation of clouds and precipitation are parameterized by assuming that the rate of precipitation formation is a function of the amount of cloud water. Evaporation from falling rain is taken into account.

Quantitative tests with the model indicated that it yields reasonable evolution times and water content of clouds, and gives reasonable precipitation amounts.

Pertinent Information:

- Author describes a condensation model that could be incorporated into a large-scale dynamical model. The dynamical model provides the inputs to the condensation model (e.g., wind, temperature, moisture).

- No specific relevance to cirrus cloud precipitation.

39. Varley, D. J., Cirrus Particle Distribution Study — Part 1, Air Force Surveys in Geophysics 394, AFGL-TR-78-0192, AD-A061485, 71 pp., August 1978.

Abstract:

Cirrus particle distribution data are presented for a flight that was made by the AFGL instrumented MC-130E aircraft near Denver, Colorado on 29 October 1977. The data were gathered in support of an Air Force Weapons Laboratory project. The report briefly describes some previous cirrus research and also outlines the basic cloud physics instrumentation aboard the aircraft, particularly the PMS 1-D and 2-D spectrometer equipment. Data averages are given for consecutive 30-sec periods during a 27-min flight through varying thicknesses of cirrus clouds. Besides tabular data, graphs are presented that show the temporal variations of liquid water content and particle concentration as a function of size. The 2-D data indicated most of the cirrus particles were not recognizable according to any standard classification system, although many were bullet rosettes.

Pertinent Information:

- A discussion of particle habits as a function of temperature is presented.

- A summary of Heymsfield's measurements in cirrus generating cells is presented. Average particle size, shape, length, concentration, and IWC measured are given.

- The author mentions Knollenberg study that found cirrus contrails were similar to natural cirrus as regards crystal size spectra.

- Total mass or liquid water content of the particles recorded by the cloud and precipitation probes is calculated by equivalently "melting" all ice particles in a unit volume (1 m³). Particles measured by the scattering probe are considered to be round and to have a mass equal to equivalent sized liquid drops. Diameters used in the LWC calculation are estimated based on particle type and are included in a table.

- Measurements were taken for a period of approximately 30 minutes. Measurements include: particle size, concentration, and derived liquid water content. Aircraft altitude, temperature, dewpoint, and true airspeed are also reported. Data were averaged over 30-sec intervals which, given the typical air speed of the aircraft, corresponds to roughly 3 km paths through the cirrus clouds. The 30-sec averages are included in an appendix.

- The 30-sec average data could be compared with CSSM model output over large simulation domains. The collection of time series data presented in all eight of these AFGL reports could be analyzed to extract fractal model parameters and other useful information. However, due to the coarse spatial resolution (approx. 3 km) of the data, our analysis would be limited since the data would not support parameter estimation or validation at the higher resolutions used commonly in the CSSM.

40. Varley, D. J., and D. M. Brooks, Cirrus Particle Distribution Study — Part 2, Air Force Surveys in Geophysics 399, AFGL-TR-78-0248, AD-A063807, 108 pp., October 1978.

Abstract:

This report presents particle spectrometer data obtained by the AFGL instrumented MC-130E aircraft during a flight through various types of cirriform clouds in the Albuquerque area on 26 February 1978. The data consist of average particle concentration figures as a function of size for consecutive 30-sec periods during the 96-min sampling mission. Additionally, data for some particular 15-sec segments of the flight are closely examined. These segments, selected to represent various cirriform conditions, such as dense cirrostratus and thin cirrus, are documented with aircraft nose camera photographs of clouds and with plots of resulting particle concentrations and calculations of liquid water content.

Pertinent Information:

- Same comments apply as written in Varley (1978, Part I). Average data are tabulated for 30-sec intervals over a 96-min sampling period.

- In addition, eight examples of higher-resolution 15-sec average data are presented (corresponding to approximately 1.5 km spatial resolution). A graph of 15-sec average liquid water content data is shown covering the whole 96-min sampling period.

- Care was taken to sample cirrus particle conditions near cloud base and top.

- Several different cirrus cloud types were observed (including cirrostratus bases and tops, thick cirrostratus, and fibrous cirrus), therefore some comparisons can be made. Data compare well to studies by Heymsfield and Knollenberg, although those other studies reported higher water content values in most cases.

41. Varley, D. J., Cirrus Particle Distribution Study — Part 3, Air Force Surveys in Geophysics 404, AFGL-TR-78-0305, AD-A066975, 67 pp., December 1978.

Abstract:

This report describes particle spectra in thin cirrus clouds that were sampled on 18 March 1978 southwest of Albuquerque. The sampling aircraft, and MC-130E, flew near 31,000 ft (9.4 km) and acquired cloud particle data with its three PMS spec-

trometer probes. Ice crystals larger than 50 mm were recorded for only about 17 min, but smaller ones were measured by an axial scattering probe for several more minutes. Listings of particle concentration versus size, averaged over consecutive 30-sec intervals for 75 min, are included.

Pertinent Information:

- Same comments apply as written in Varley (1978, Part I). Average data are tabulated for 30-sec intervals over a 75-min sampling period taken from the 2 hour 45 min flight.

- Cirrus clouds were very thin, however, the scattering probe (measuring the smallest particles) continued to identify particles even while "outside" of any visible cloud layer when visibility was excellent. The cloud and precipitation probes (which measure larger particles) recorded the presence of larger particles for more limited periods totaling approximately 17 minutes of in-cloud time.

- The bulk of cirrus clouds were above the service altitude of the MC-130E aircraft.

42. Varley, D. J., and A. A. Barnes, Cirrus Particle Distribution Study — Part 4, Air Force Surveys in Geophysics 413, AFGL-TR-79-0134, AD-A074763, 91 pp., June 1979.

Abstract:

This is the fourth in a series of reports presenting particle distribution data acquired in cirrus clouds over the western U.S. The data herein were obtained 21 March 1978 by an instrumented MC-130E near Albuquerque, NM. The area was under the influence of a slight upper level ridge, and the cirrus appeared related to jet stream winds. No significant surface weather was present at the time. Results include the following: (1) the largest particles measured were near 2500 mm, but there were only one or fewer of these per m^3; (2) occasional particles as large as 1300 mm were recorded in what visually was cloud-free air; (3) few of the particles could be recognized in any know classification system but those most frequently recognized were bullet rosettes; (4) the PMS 2-D data revealed particle-type changes occurring in 5 seconds or less of flight time; (5) a halo around the sun was periodically seen when mixed-type crystals containing bullet rosettes were recorded; (6) varying numbers of small particles (1 to 28 mm) were recorded almost continually, even in clear air, while the aircraft was between 23,000 ft (7.0 km) and 27,300 ft (8.3 km) MSL; (7) computed IWC values generally decreased with height and increased with temperature in the cirriform clouds sampled; (8) particle size spectra were seldom exponential for particles smaller than approximately 250 mm; and (9) bimodal peaks were frequent in the population distribution near 100 and 250 mm.

Pertinent Information:

- Same comments apply as written in Varley (1978, Part I). Average data are tabulated for 30-sec intervals over a 94-min sampling period.

- Largest particles observed in this and previous flights have been approx. 2500mm measured near the base of thick cirrostratus. Data agree with previous findings by other authors that ice mass in cirrus tends to increase with increasing temperature.

- In agreement with previous authors (e.g., Chylek and Pinnick et al.), higher values of IWC, particularly those due to the presence of the largest particles (as identified by the precipitation probe) are accompanied by lower visibilities. The variation of visibility with IWC appears to correlate best with that of the precipitation probe and only poorly or not at all with the water contents determined from the scattering probe measurements.

- The scattering probe continued to detect cirrus particles even when in supposedly clear air. The probe was measuring sub-visible cirrus.

43. **Varley, D. J., I. D. Cohen, and A. A. Barnes, Cirrus Particle Distribution Study — Part 7, Air Force Surveys in Geophysics 433, AFGL-TR-80-0324, AD-A100269, 82 pp., October 1980.**

Abstract:

Particle data obtained during C-130 cirrus sampling flights on 28 and 29 January and 2 February 1979 over the southwestern United Sates are described. The first flight sampled cirriform clouds ahead of a developing storm; the second flight obtained data in the tops of the cirriform clouds of a fully developed storm; and the third examined cirrus formed by a weak polar front and strong upper level winds. All flights sampled a variety of densities of cirrus; however, those sampled on 29 January were the most complex and also at the lowest altitude. This flight provided numerous samples having as many at 350,000 particles per cubic meter in the 47-4700 mm size range. The largest particle sizes were generally less than 1100 μm, but some cirrus particles as large as 2.5 mm were detected at altitudes between 5.9 and 7.7 km. Generally, the calculated IWC values were 0.04 g/m³ or less, with a maximum of 0.10 g/m³ in the active storm situation. On the other two days, the cirrus was of varying density with most particles less than 1400 mm and IWCs of 0.03 g/m³ or less. Particles as large as 2.5 mm were detected in the cirrus on all three flights. The in-flight meteorologist's characterization of heavy or thin clouds is better correlated with total particle number than particle size. Several atmospheric and particle spectral properties are tabulated for consecutive 15-sec data samples for the three flights.

Cloud free periods were examined; some showed the presence of the two types of subvisible cirrus. The first type consisted of a background of small particles less than a few tens of microns; the second type consisted of large subvisible cirrus particles of

the order of 100 mm or larger. The density of subvisible particles larger than 100 mm during a cloud-free period on 2 February 1979 was 7 mm^{-3}.

Pertinent Information:

- Same comments apply as written in Varley (1978, Part I). Average data are tabulated for 15-sec intervals over three separate flights on three separate days.

- Emphasis for this report was on cirrus particle spectra data and sub-visible cirrus measurements. This is the first of the series of reports to describe total particle counts, maximum particle size, and form factor (a parameter which helps to describe the shape of the particle spectra). Such information may be useful for Fast-Map development and characterization of particle sizes in that model.

44. Wiscombe, W., A. Davis, and A. Marshak, Two Complementary Multifractal Analysis Techniques for Non-Stationary Atmospheric Processes With an Application to Cloud Liquid Water Content, Downloaded from the ARM Web Page, October 1996.

Abstract:

Standard Gaussian-type statistics are not really adequate to describe atmospheric variability; this traditional approach implicitly dismisses fluctuation as "noise" of use only in computing a standard deviation which, together with the mean, presumably varies so little in space and time that one can meaningfully speak of "climatological" values. In geophysics, unfortunately, this approach often fails. Means and standard deviations not only exhibit no "climatology," but depend on the scale of space/time sampling.

We adopt the opposite viewpoint; variability is in fact the signal, not the noise. This variability teaches us about the fundamental physics at work. Even simple laboratory or computational systems (and a fortiori geophysical systems) are typically attracted into dynamical equilibrium characterized by a large range of length- and/or time-scales, power-law energy spectra, and fractal geometrical properties. For such systems, the concepts of scale-invariance and/or mutifractality provide the most productive framework for data analysis and simulation.

Typical atmospheric signals exhibit non-stationary behavior. Our first task is therefore to define the most interesting stationary aspects of such non-stationary datasets. One method for doing this, called "singular measures," focuses on the absolute values of the gradient field, which is more likely to be stationary, as we progressively degrade the resolution r of this field, taking powers q and averaging, the results appear as power-laws in terms of the resolution r where the exponent is a function of q. Another method, called "structure functions," focuses on the absolute values of the dif-

ferences that occur in the data over arbitrarily large or small scales. Both of these methods are discussed in terms of analyzing cloud liquid water data available through the ARM Program.

Pertinent Information:

- Paper emphasizes that Gaussian statistics (e.g., mean and variance parameters) are not capable of fully describing cloud structures.
- Points out that multifractal techniques can also be used to analyze cloud observation data.
- Similar techniques have been applied previously by the authors to marine stratocumulus cloud fields. This brief paper recommends further investigation.

45. Zinn, J., A model of the Microphysical Evolution of a Cloud, Downloaded from the ARM Web Page, October 1996.

Abstract:

The earth's weather and climate are influenced strongly by phenomena associated with clouds. Therefore, a general circulation model that models the evolution of weather and climate must include an accurate physical model of the clouds. This paper described our efforts to develop a suitable cloud model. It concentrates on the microphysical processes that determine the evolution of droplet and ice crystal size distributions, precipitation rates, total and condensed water content, and radiative extinction coefficients.

We assume a fixed temperature, a cloud vertical thickness, and concentrations and size distributions of cloud condensation nuclei and ice condensation nuclei. The computation starts at time t=0 with a given concentration of precipitable water entirely in the form of vapor. As time advances, we compute the evolution of the number and size distributions of the liquid droplets and ice crystals along with their evaporation/condensation rates, collision rates, vertical falling rates, and rates of loss from outfluxing. We then compute the resulting evolution of the cloud water vapor, liquid and ice concentrations. As a byproduct, the precipitation rate and the cloud optical extinction coefficient are computed.

Pertinent Information:

- Author outlines a general-purpose dynamic cloud model. No application to the type of parametric model we will build for CSSM.

APPENDIX B
AIRCRAFT DATA SUMMARIES

Aircraft data summaries for each of the 29 water content paths that we selected for analysis. Each summary shows water content distributions along the path, the autocorrelation function, log-log plots of the fractal dimension, and a histogram of the water content along the path.

Aircraft Path 2-1: 04/21/96 182753-183006 GMT
Cloud Type: Cirrostratus

Path Height: 7315 m
Average Speed: 169 m/s

Cloud Base: 6570 m
Cloud Top: 9090 m

Mean Water Content: 0.061 g/m³
Standard Deviation: 0.017 g/m³
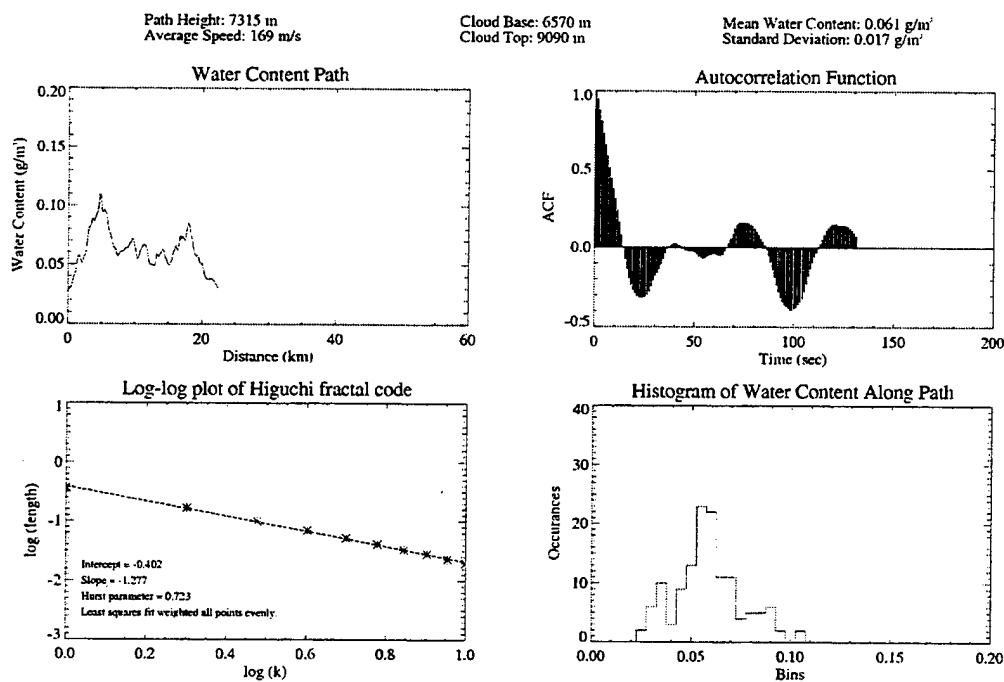
Aircraft Path 2-2: 04/21/96 183006-183247 GMT
Cloud Type: Cirrostratus

Path Height: 7316 m
Average Speed: 169 m/s

Cloud Base: 6870 m
Cloud Top: 10065 m

Mean Water Content: 0.043 g/m³
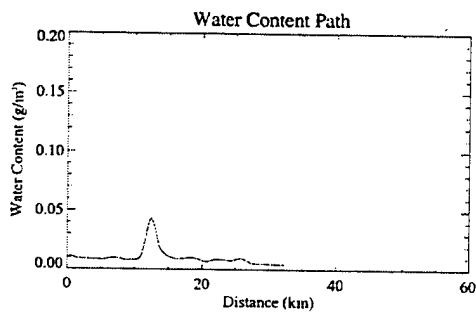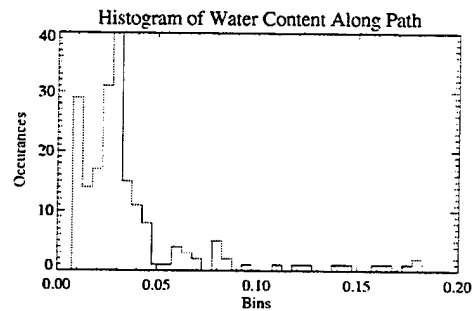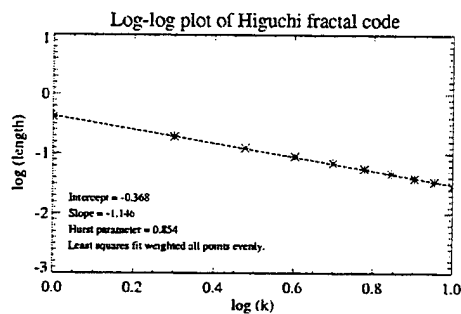Standard Deviation: 0.007 g/m³
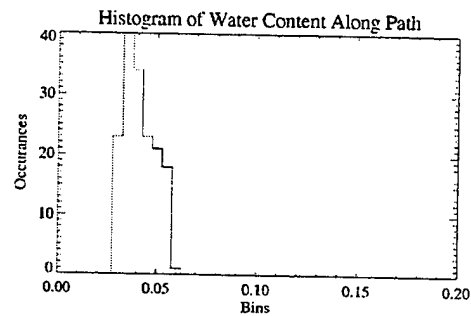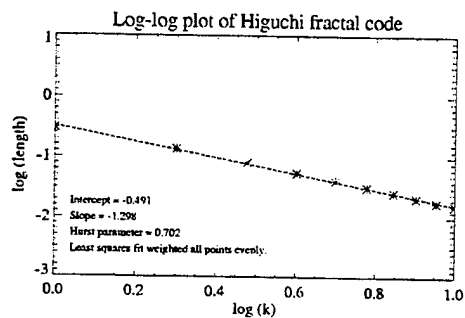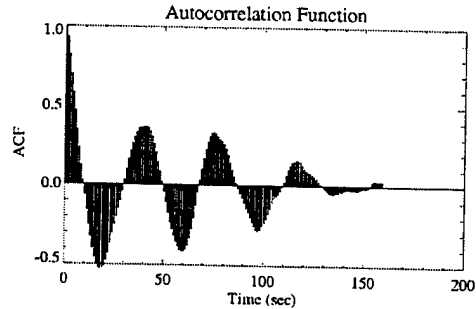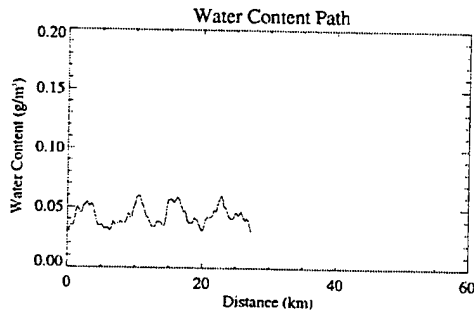
Aircraft Path 3: 04/21/96 184434-184712 GMT
Cloud Type: Cirrostratus

Path Height: 9144 m
Average Speed: 234 m/s

Cloud Base: 7500 m
Cloud Top: 11115 m

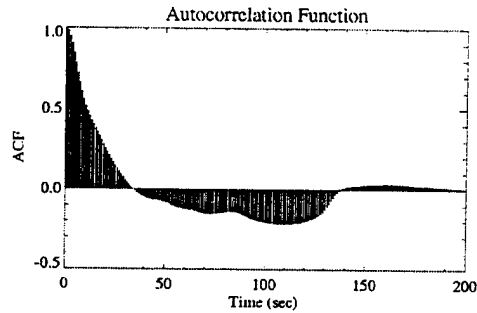Mean Water Content: 0.027 g/m³
Standard Deviation: 0.006 g/m³

136
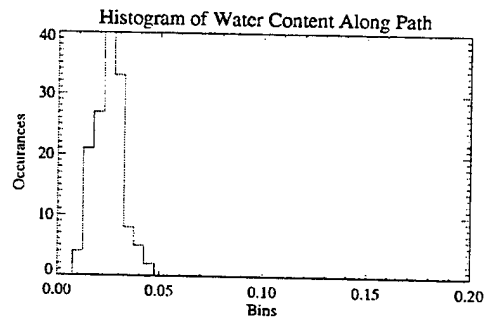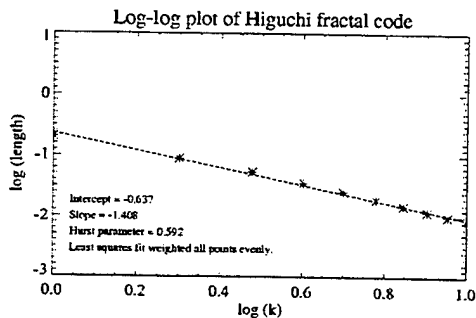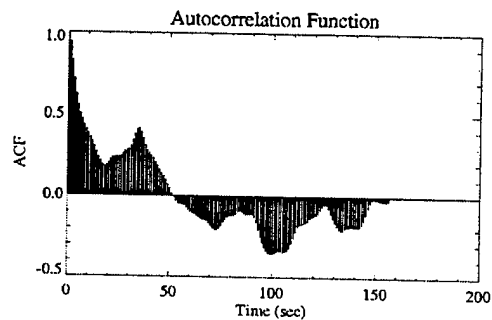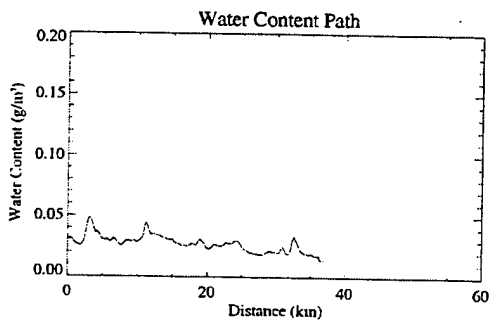
Aircraft Path 1: 04/27/96 181917-182330 GMT
Cloud Type: Cirrostratus

Path Height: 6107 m
Average Speed: 221 m/s

Cloud Base: 5400 m
Cloud Top: 8550 m

Mean Water Content: 0.174 g/m³
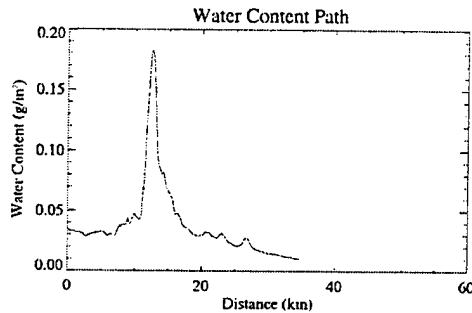Standard Deviation: 0.019 g/m³

Water Content Path

Autocorrelation Function

Log-log plot of Higuchi fractal code

Intercept = -0.548
Slope = -1.358
Hurst parameter = 0.642
Least squares fit weighted all points evenly.

Histogram of Water Content Along Path
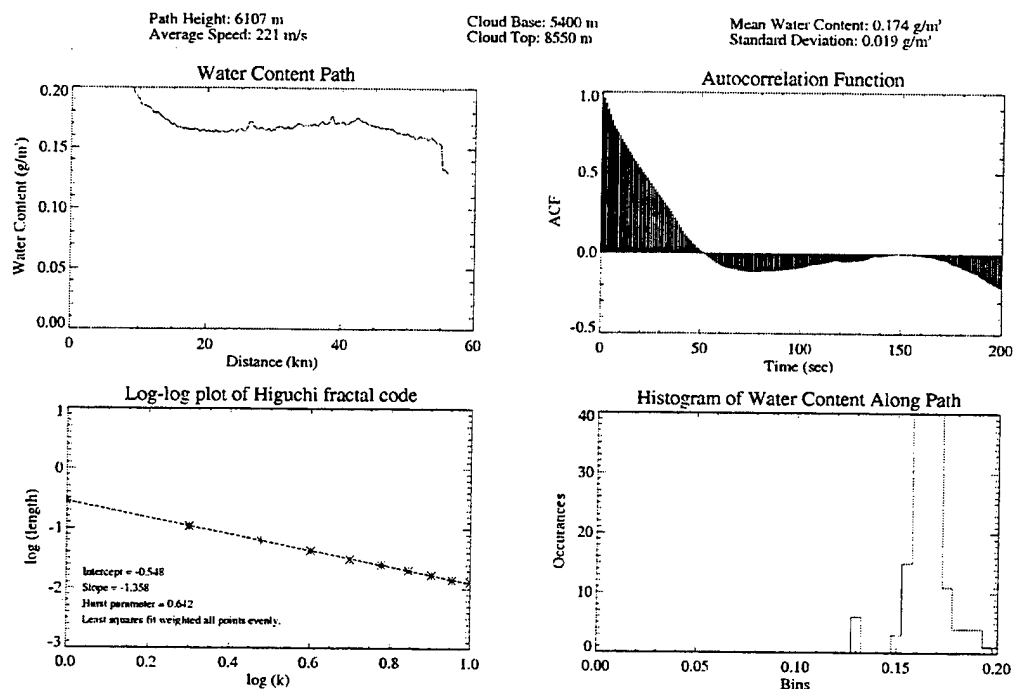
Aircraft Path 4-1: 04/20/96 175031-175315 GMT
Cloud Type: Cirrus

Path Height: 9754 m
Average Speed: 186 m/s

Cloud Base: 7620 m
Cloud Top: 9855 m

Mean Water Content: 0.017 g/m³
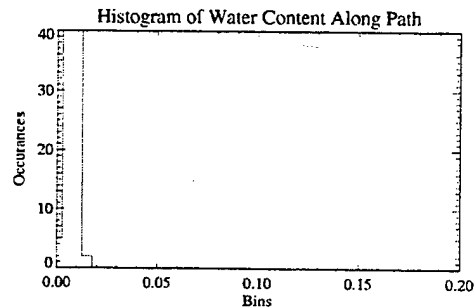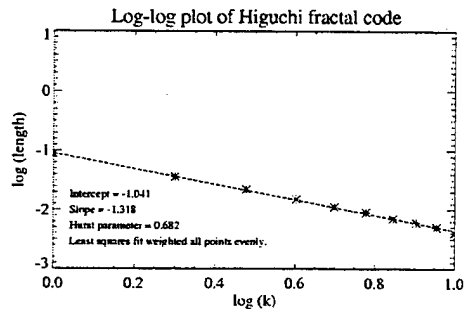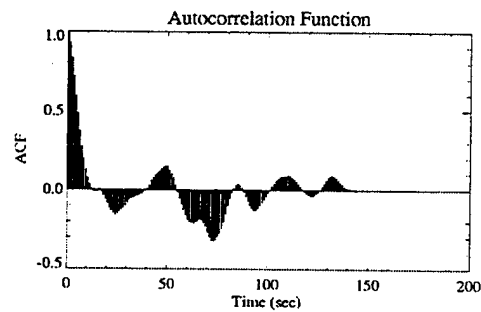Standard Deviation: 0.009 g/m³

Water Content Path

Autocorrelation Function

Log-log plot of Higuchi fractal code

Intercept = -0.623
Slope = -1.103
Hurst parameter = 0.897
Least squares fit weighted all points evenly.

Histogram of Water Content Along Path

137
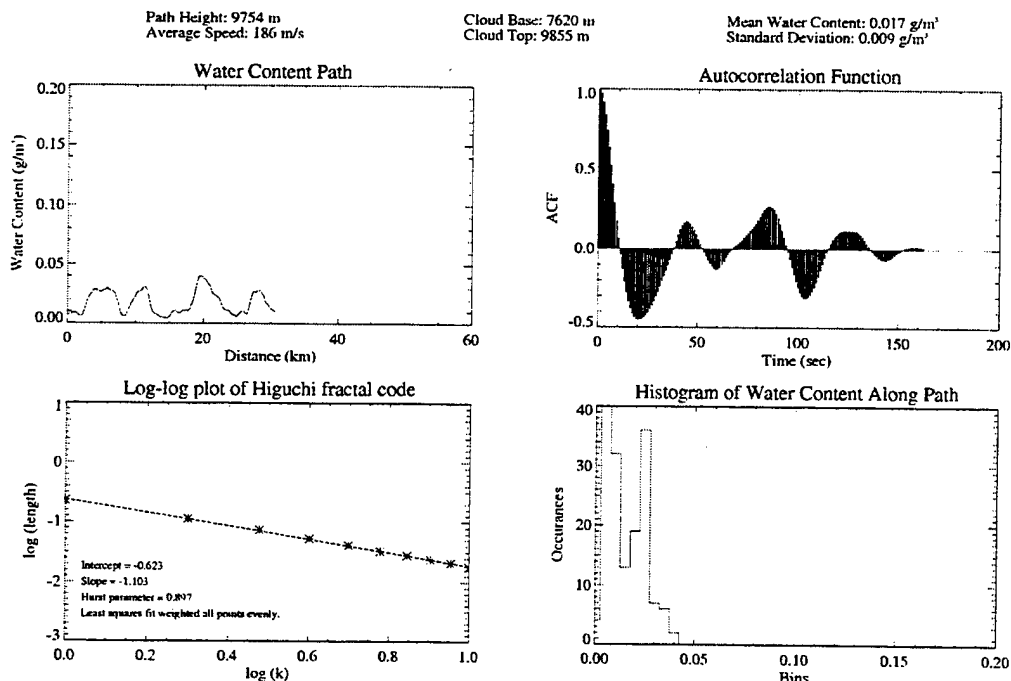
Aircraft Path 4-2: 04/20/96 175316-175612 GMT
Cloud Type: Cirrus

Path Height: 9753 m
Average Speed: 186 m/s

Cloud Base: 8175 m
Cloud Top: 9825 m

Mean Water Content: 0.015 g/m³
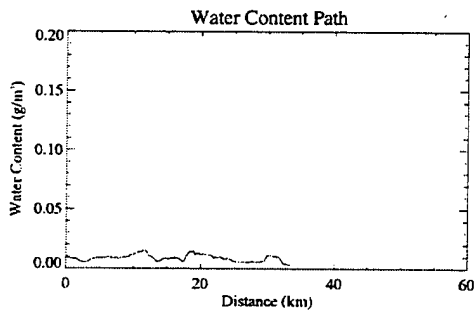Standard Deviation: 0.014 g/m³

Water Content Path

Autocorrelation Function

Log-log plot of Higuchi fractal code

Intercept = -0.462
Slope = -1.143
Hurst parameter = 0.857
Least squares fit weighted all points evenly.

Histogram of Water Content Along Path
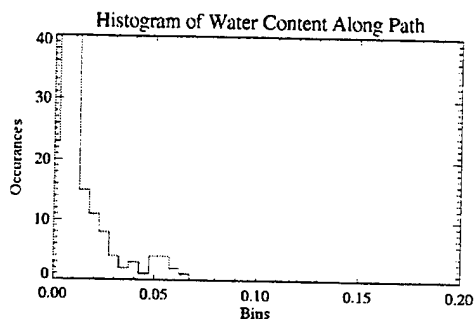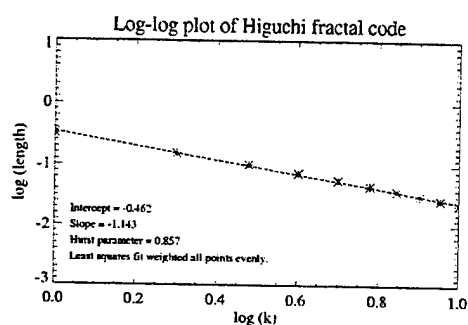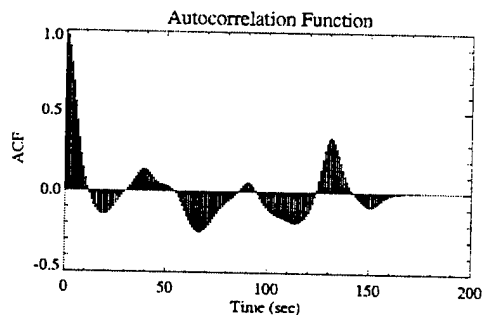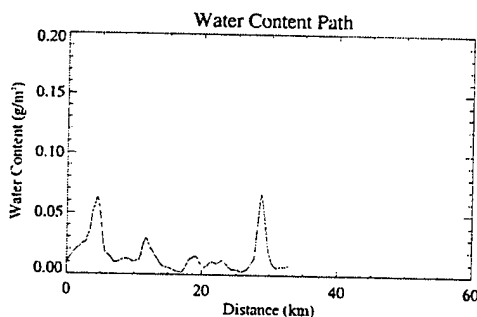
Aircraft Path 5-1: 04/20/96 181741-181931 GMT
Cloud Type: Cirrus

Path Height: 9748 m
Average Speed: 250 m/s

Cloud Base: 6900 m
Cloud Top: 9855 m

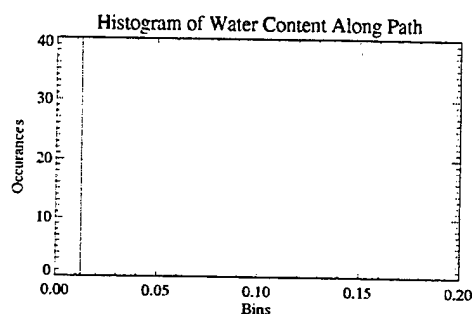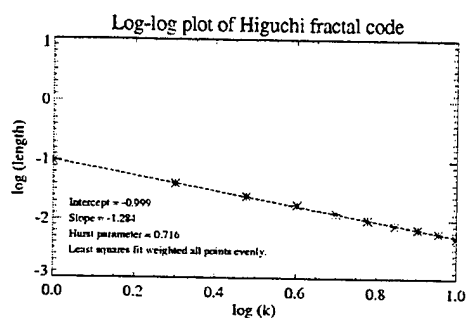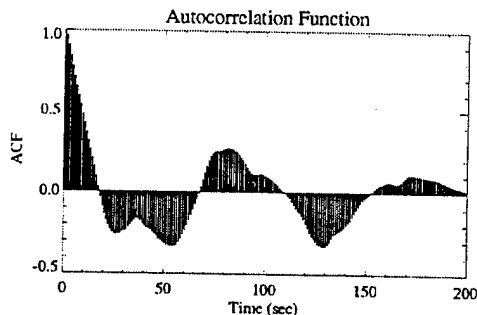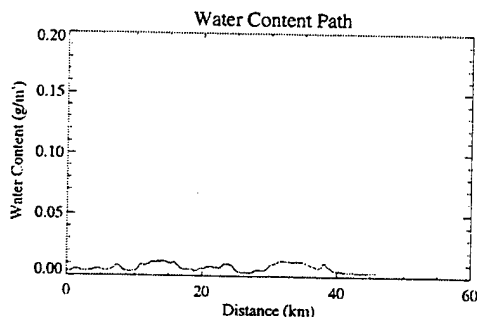Mean Water Content: 0.053 g/m³
Standard Deviation: 0.038 g/m³

Water Content Path

Autocorrelation Function

Log-log plot of Higuchi fractal code

Intercept = -0.490
Slope = -1.099
Hurst parameter = 0.901
Least squares fit weighted all points evenly.

Histogram of Water Content Along Path

138
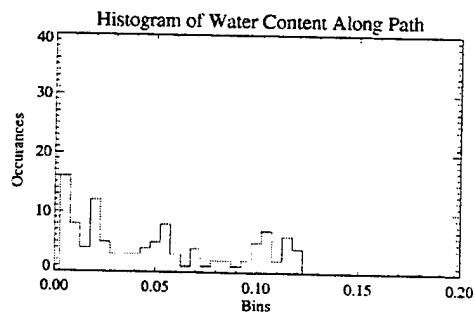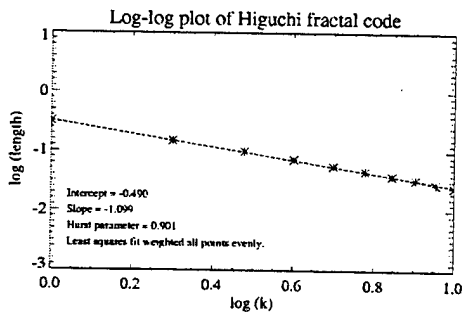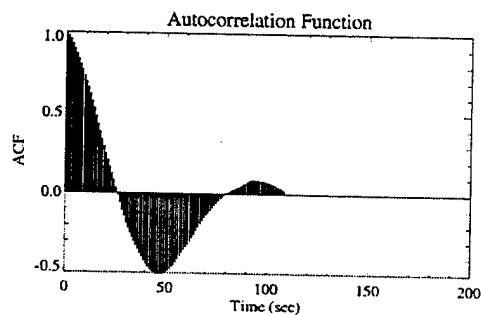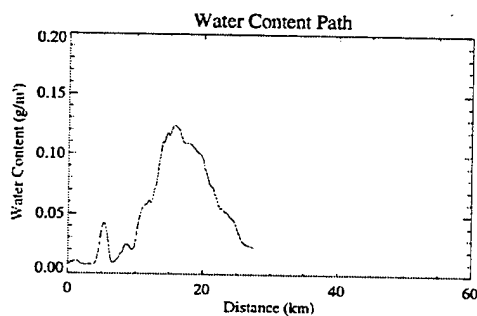
Aircraft Path 5-2: 04/20/96 181932-182247 GMT
Cloud Type: Cirrus

Path Height: 9748 m　　　　Cloud Base: 6900 m　　　　Mean Water Content: 0.020 g/m³
Average Speed: 250 m/s　　　Cloud Top: 9855 m　　　　Standard Deviation: 0.012 g/m³

Intercept = -0.431
Slope = -1.145
Hurst parameter = 0.855
Least squares fit weighted all points evenly.

Aircraft Path 5-3: 04/20/96 182248-182418 GMT
Cloud Type: Cirrus

Path Height: 9747 m　　　　Cloud Base: 6900 m　　　　Mean Water Content: 0.031 g/m³
Average Speed: 248 m/s　　　Cloud Top: 9855 m　　　　Standard Deviation: 0.018 g/m³

Intercept = -0.428
Slope = -1.201
Hurst parameter = 0.799
Least squares fit weighted all points evenly.

139
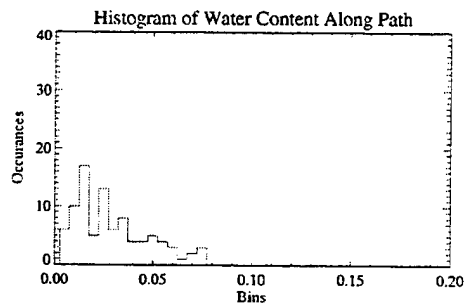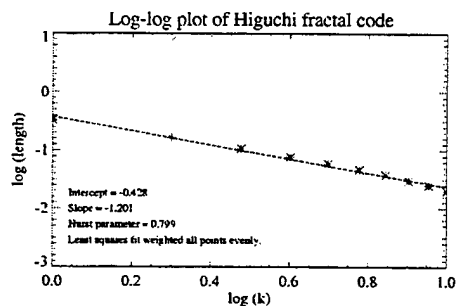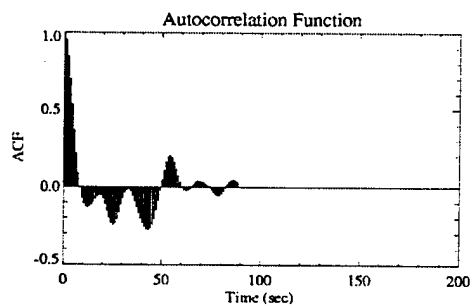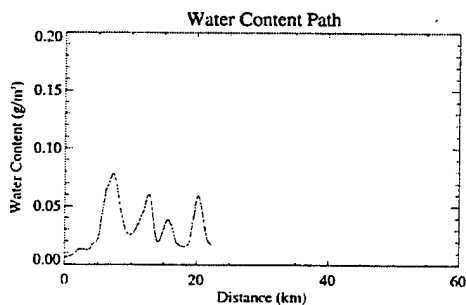
Aircraft Path 5-4: 04/20/96 182502-182720 GMT
Cloud Type: Cirrus

Path Height: 9747 m
Average Speed: 249 m/s

Cloud Base: 7335 m
Cloud Top: 9975 m

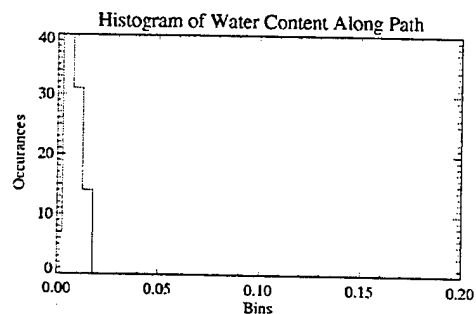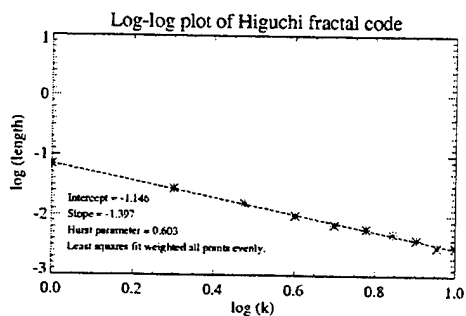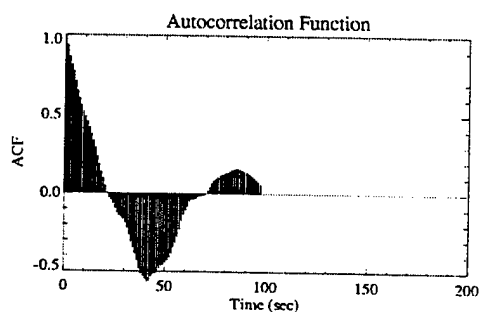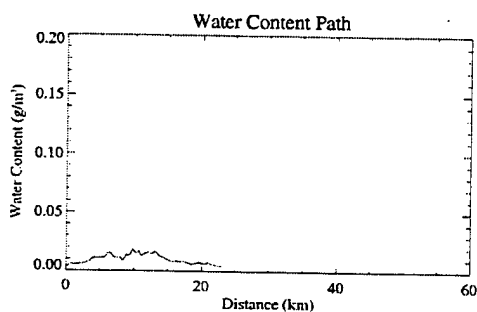Mean Water Content: 0.017 g/m'
Standard Deviation: 0.016 g/m'

Water Content Path

Autocorrelation Function

Log-log plot of Higuchi fractal code

Intercept = -0.404
Slope = -1.220
Hurst parameter = 0.780
Least squares fit weighted all points evenly.

Histogram of Water Content Along Path
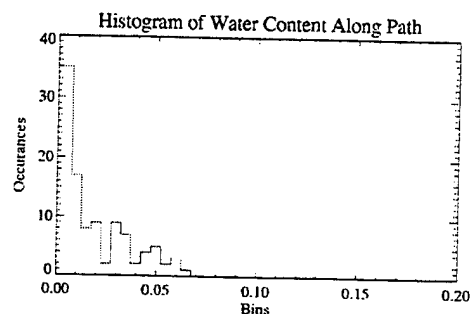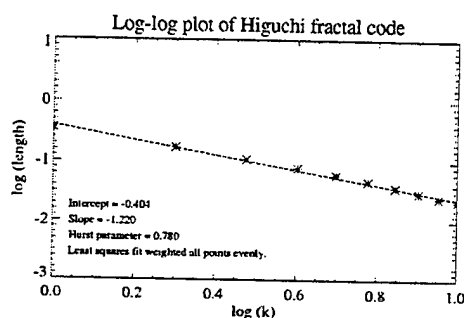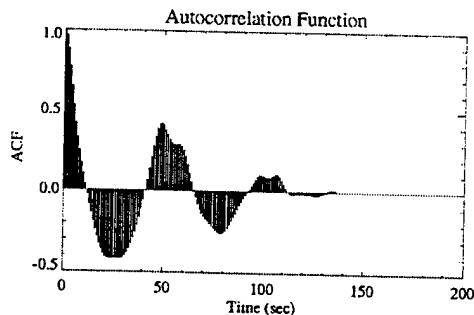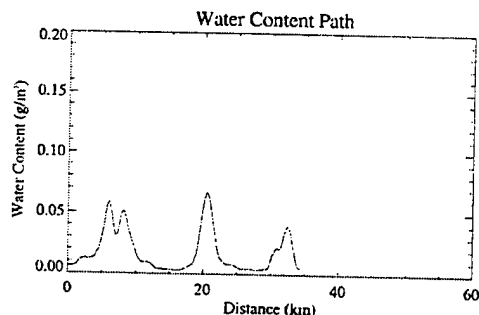
Aircraft Path 5-5: 04/20/96 182722-182923 GMT
Cloud Type: Cirrus

Path Height: 9747 m
Average Speed: 249 m/s

Cloud Base: 7335 m
Cloud Top: 9975 m

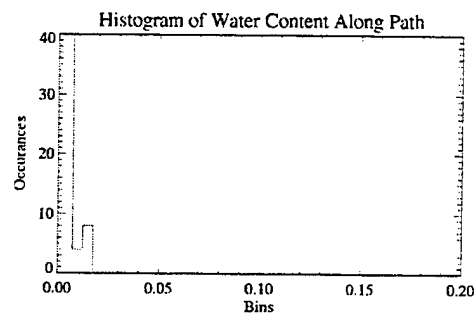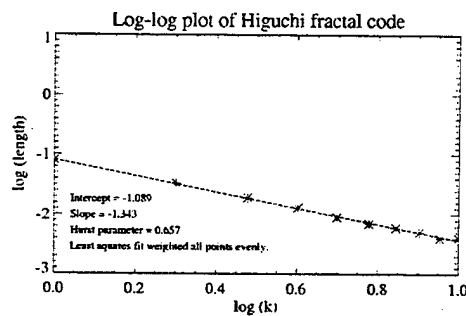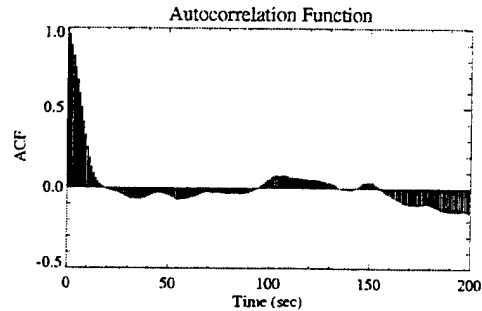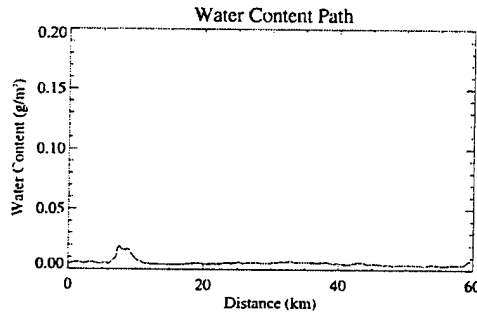Mean Water Content: 0.021 g/m'
Standard Deviation: 0.021 g/m'

Water Content Path

Autocorrelation Function

Log-log plot of Higuchi fractal code

Intercept = -0.542
Slope = -1.281
Hurst parameter = 0.719
Least squares fit weighted all points evenly.

Histogram of Water Content Along Path

140
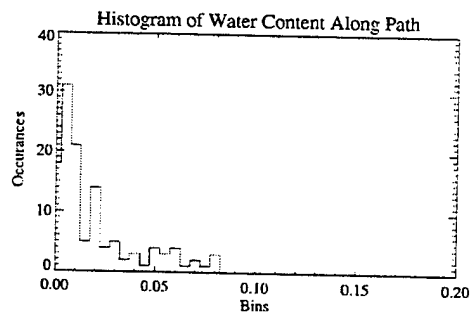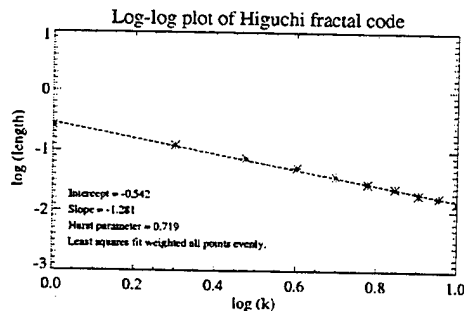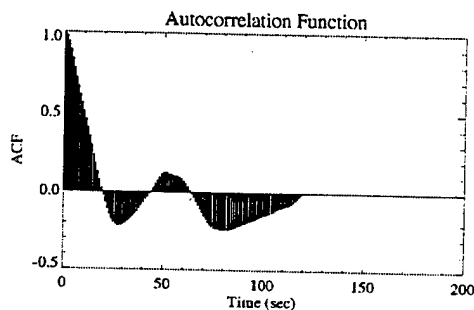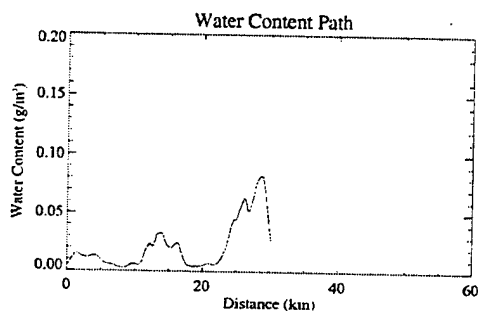
Aircraft Path 7: 04/20/96 184057-184221 GMT
Cloud Type: Cirrus

Path Height: 9724 m   Cloud Base: 7785 m   Mean Water Content: 0.022 g/m³
Average Speed: 216 m/s   Cloud Top: 9855 m   Standard Deviation: 0.005 g/m³

Water Content Path

Autocorrelation Function

Log-log plot of Higuchi fractal code

Intercept = -0.847
Slope = -1.325
Hurst parameter = 0.675
Least squares fit weighted all points evenly.

Histogram of Water Content Along Path
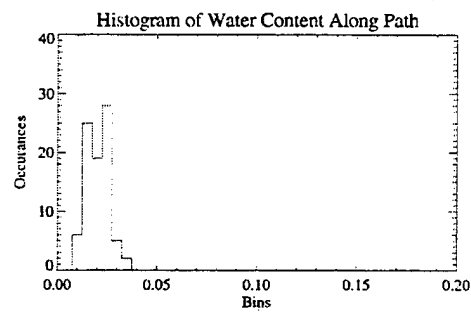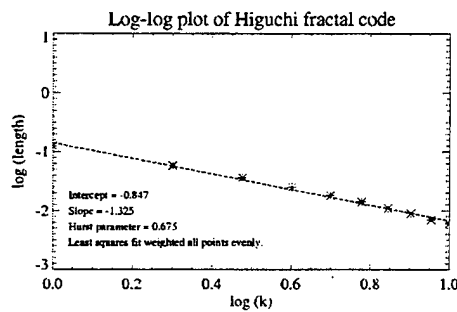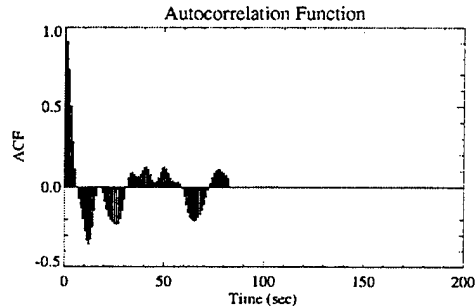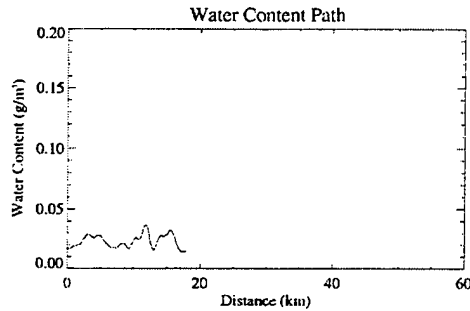
Aircraft Path 8: 04/20/96 184252-184407 GMT
Cloud Type: Cirrus

Path Height: 9724 m   Cloud Base: 7785 m   Mean Water Content: 0.005 g/m³
Average Speed: 213 m/s   Cloud Top: 9855 m   Standard Deviation: 0.001 g/m³

Water Content Path

Autocorrelation Function

Log-log plot of Higuchi fractal code

Intercept = -1.612
Slope = -1.210
Hurst parameter = 0.790
Least squares fit ignored the last 5 data points.
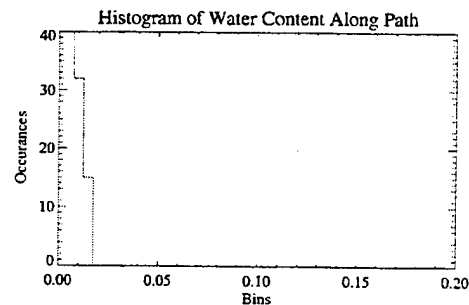
Histogram of Water Content Along Path
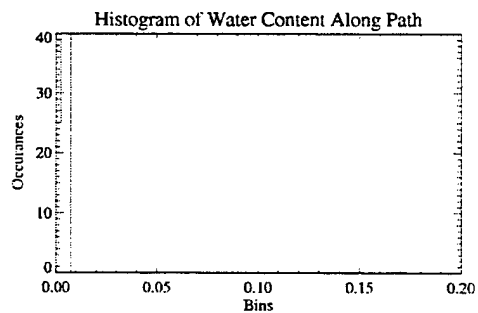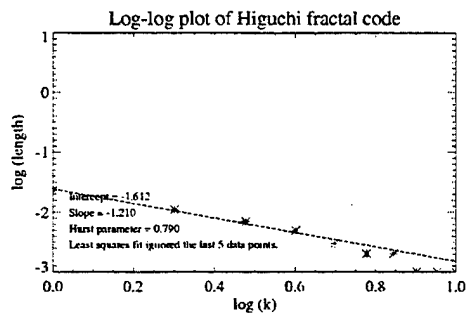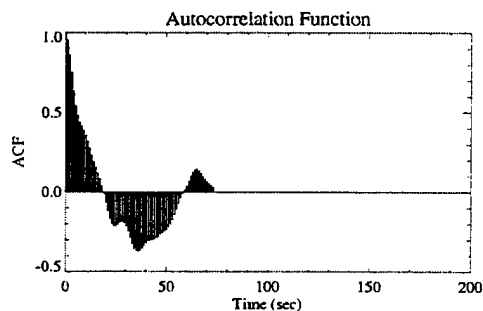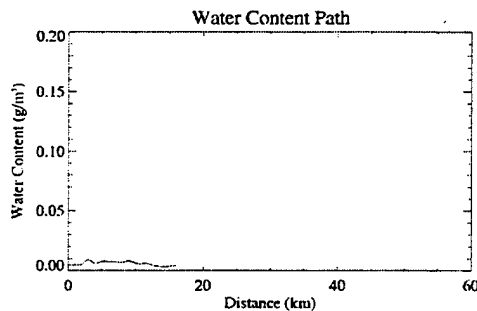
Aircraft Path 9: 04/20/96 184456-184615 GMT
Cloud Type: Cirrus

Path Height: 9723 m
Average Speed: 212 m/s

Cloud Base: 7785 m
Cloud Top: 9855 m

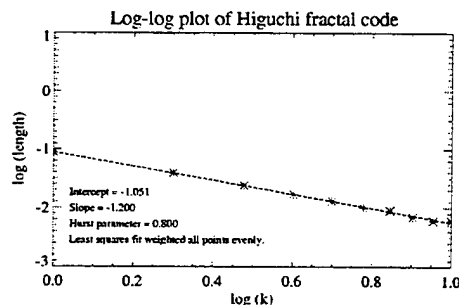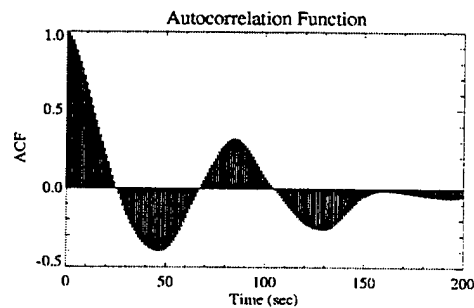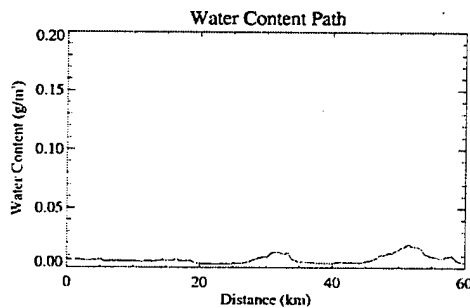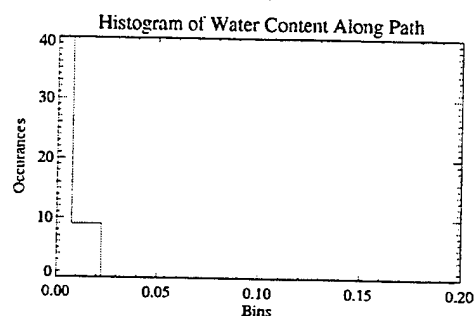Mean Water Content: 0.040 g/m³
Standard Deviation: 0.021 g/m³

Water Content Path

Autocorrelation Function

Log-log plot of Higuchi fractal code

Intercept = -0.522
Slope = -1.272
Hurst parameter = 0.728
Least squares fit weighted all points evenly.

Histogram of Water Content Along Path
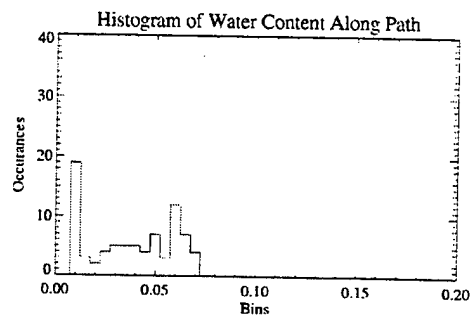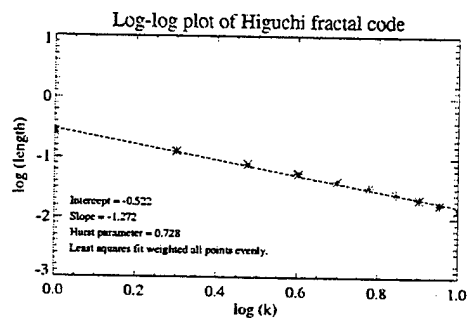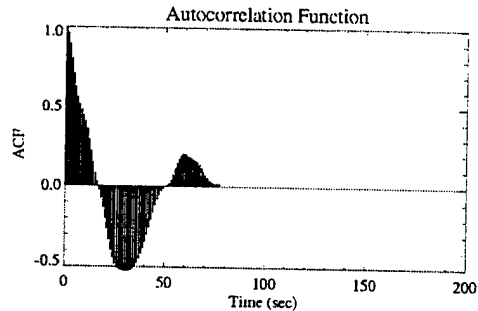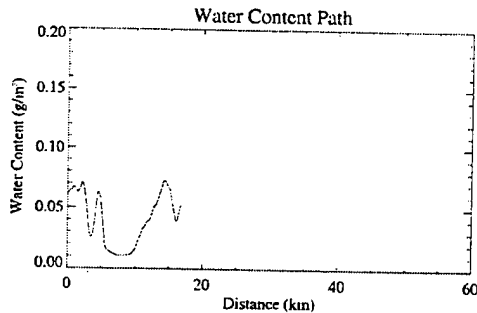
Aircraft Path 10: 04/20/96 184659-184818 GMT
Cloud Type: Cirrus

Path Height: 9725 m
Average Speed: 213 m/s

Cloud Base: 7575 m
Cloud Top: 9900 m

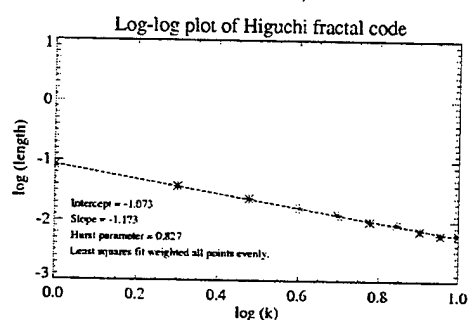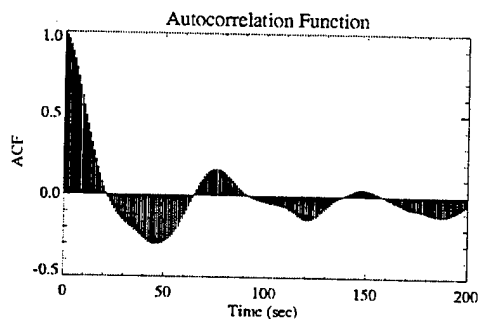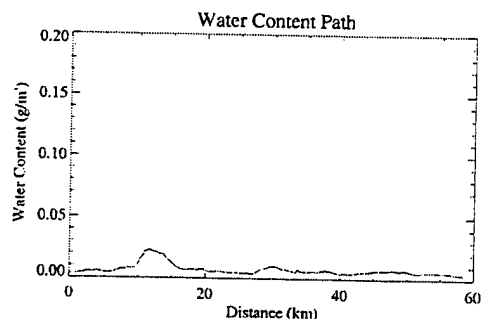Mean Water Content: 0.022 g/m³
Standard Deviation: 0.020 g/m³

Water Content Path

Autocorrelation Function

Log-log plot of Higuchi fractal code

Intercept = -0.733
Slope = -1.075
Hurst parameter = 0.925
Least squares fit weighted all points evenly.

Histogram of Water Content Along Path

142
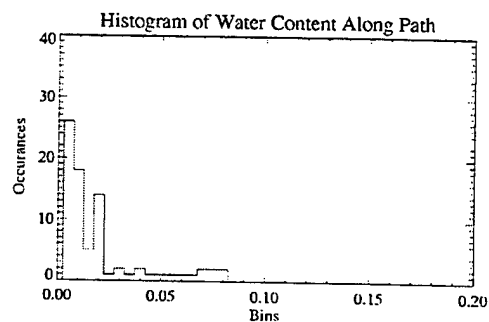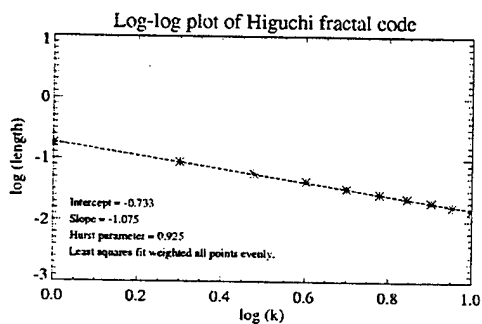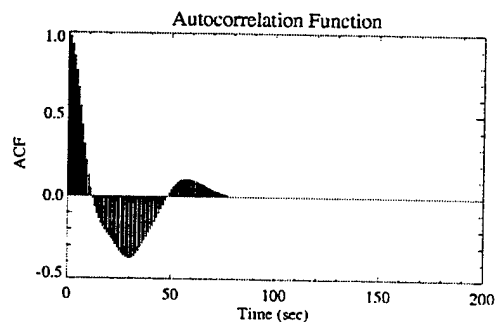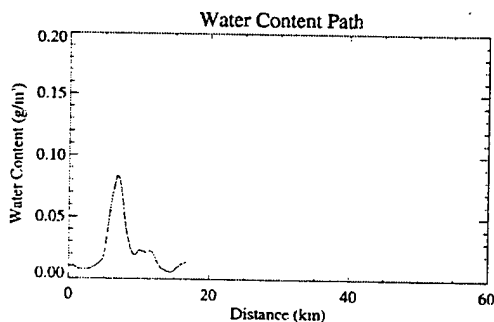
Aircraft Path 11: 04/20/96 190358-190619 GMT
Cloud Type: Cirrus

Path Height: 6714 m
Average Speed: 169 m/s

Cloud Base: 5925 m
Cloud Top: 8910 m

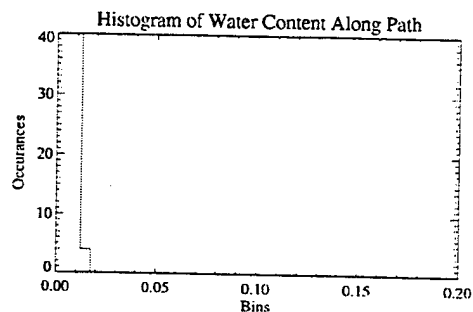Mean Water Content: 0.149 g/m³
Standard Deviation: 0.083 g/m³

Water Content Path

Autocorrelation Function

Log-log plot of Higuchi fractal code

Intercept = -0.203
Slope = -1.067
Hurst parameter = 0.933
Least squares fit weighted all points evenly.

Histogram of Water Content Along Path
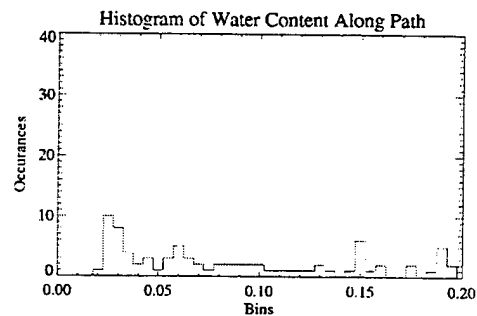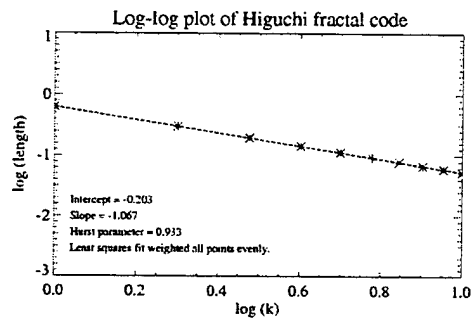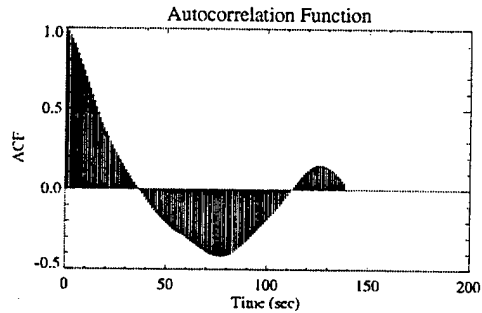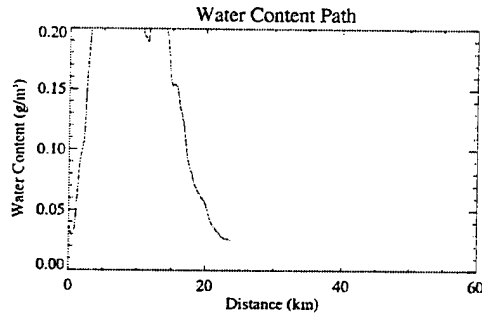
Aircraft Path 12-1: 04/20/96 192706-192944 GMT
Cloud Type: Cirrus

Path Height: 8222 m
Average Speed: 237 m/s

Cloud Base: 7650 m
Cloud Top: 10245 m

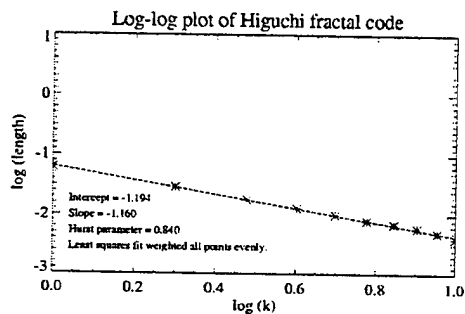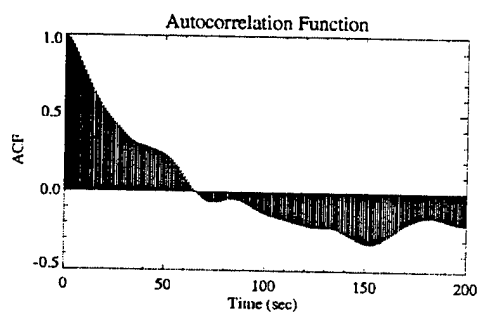Mean Water Content: 0.047 g/m³
Standard Deviation: 0.017 g/m³
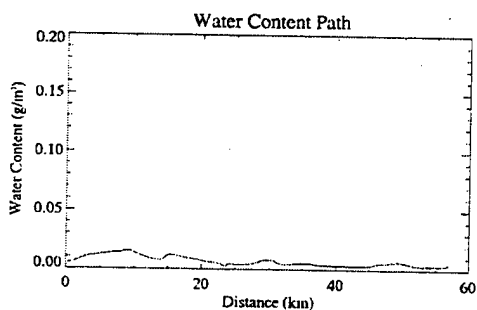
Water Content Path

Autocorrelation Function

Log-log plot of Higuchi fractal code

Intercept = -0.385
Slope = -1.322
Hurst parameter = 0.678
Least squares fit weighted all points evenly.

Histogram of Water Content Along Path

143
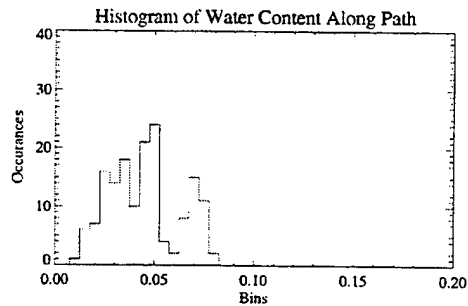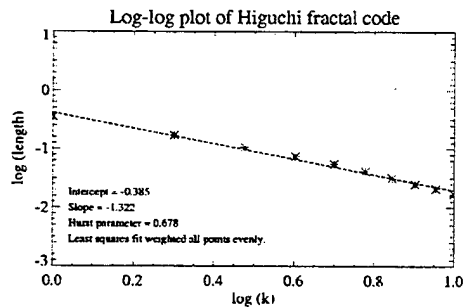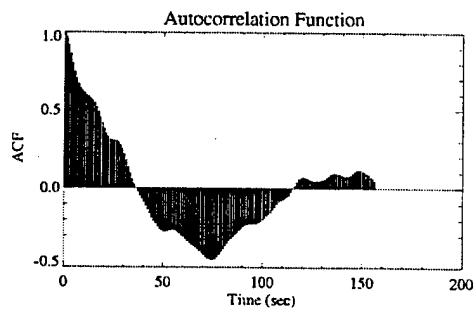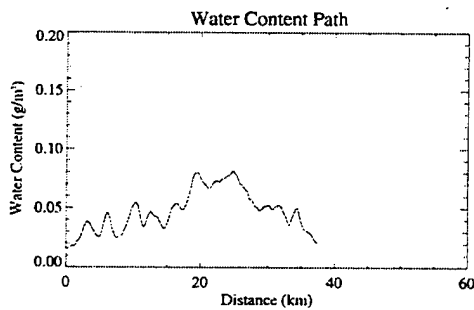
Aircraft Path 12-2: 04/20/96 192945-193301 GMT
Cloud Type: Cirrus

Path Height: 8222 m
Average Speed: 233 m/s

Cloud Base: 7320 m
Cloud Top: 10125 m

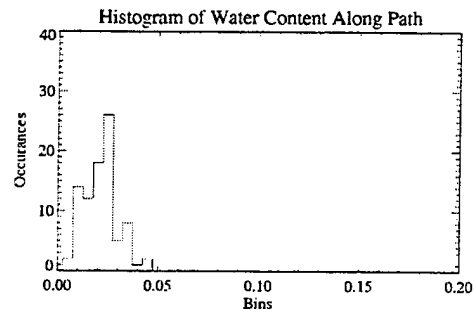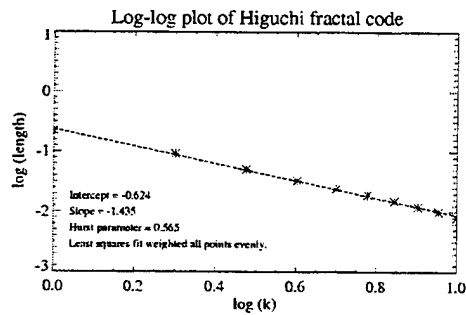Mean Water Content: 0.055 g/m³
Standard Deviation: 0.036 g/m³

Water Content Path

Autocorrelation Function

Log-log plot of Higuchi fractal code

Intercept = -0.080
Slope = -1.252
Hurst parameter = 0.748
Least squares fit weighted all points evenly.

Histogram of Water Content Along Path
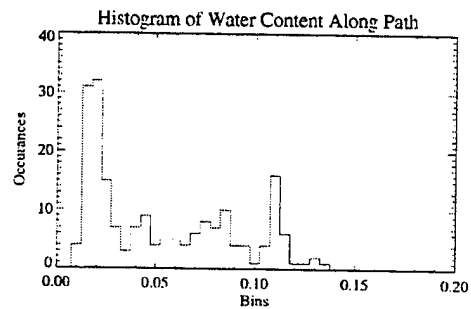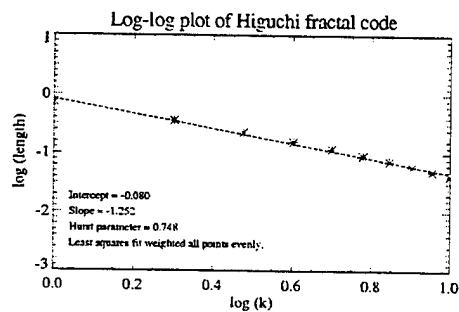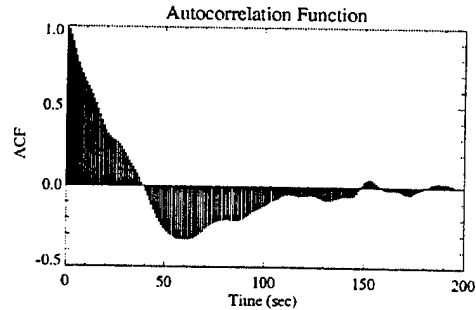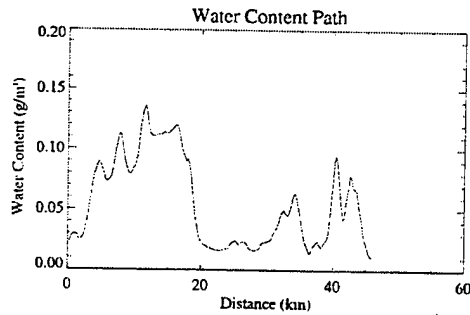
Aircraft Path 12-3: 04/20/96 193302-193522 GMT
Cloud Type: Cirrus

Path Height: 8223 m
Average Speed: 231 m/s

Cloud Base: 7035 m
Cloud Top: 8550 m

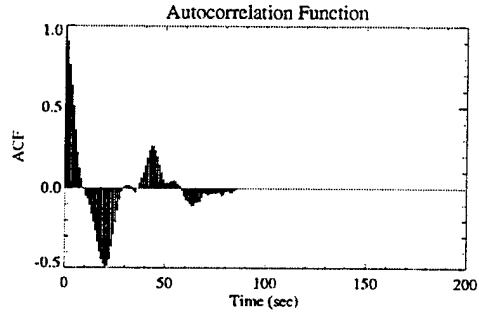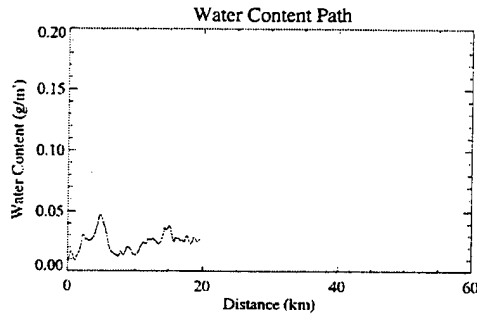Mean Water Content: 0.010 g/m³
Standard Deviation: 0.007 g/m³

Water Content Path

Autocorrelation Function

Log-log plot of Higuchi fractal code

Intercept = -1.008
Slope = -1.129
Hurst parameter = 0.871
Least squares fit weighted all points evenly.

Histogram of Water Content Along Path

144
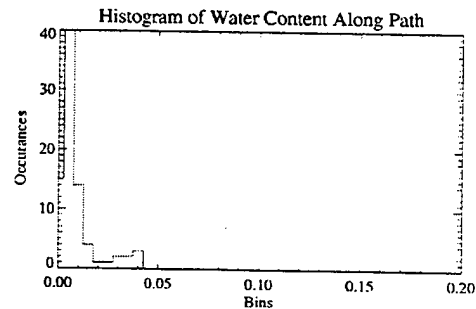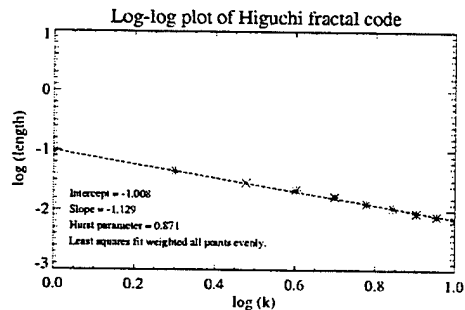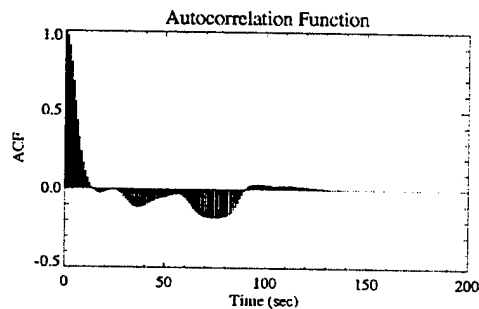
Aircraft Path 1: 04/21/96 182113-182439 GMT
Cloud Type: Cirrus

Path Height: 7318 m
Average Speed: 168 m/s

Cloud Base: 5850 m
Cloud Top: 8820 m

Mean Water Content: 0.037 g/m³
Standard Deviation: 0.031 g/m³

Water Content Path

Autocorrelation Function

Log-log plot of Higuchi fractal code

Intercept = -0.368
Slope = -1.146
Hurst parameter = 0.854
Least squares fit weighted all points evenly.

Histogram of Water Content Along Path

Aircraft Path 1-1: 05/08/96 182915-183141 GMT
Cloud Type: Cirrus

Path Height: 11886 m
Average Speed: 228 m/s

Cloud Base: 10575 m
Cloud Top: 12090 m

Mean Water Content: 0.008 g/m³
Standard Deviation: 0.002 g/m³

Water Content Path

Autocorrelation Function

Log-log plot of Higuchi fractal code

Intercept = -1.041
Slope = -1.318
Hurst parameter = 0.682
Least squares fit weighted all points evenly.

Histogram of Water Content Along Path

145

Aircraft Path 1-2: 05/08/96 183142-183503 GMT
Cloud Type: Cirrus

Path Height: 11887 m
Average Speed: 228 m/s

Cloud Base: 11790 m
Cloud Top: 12090 m

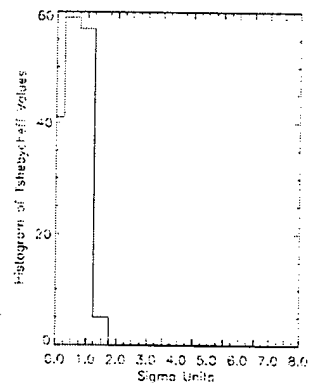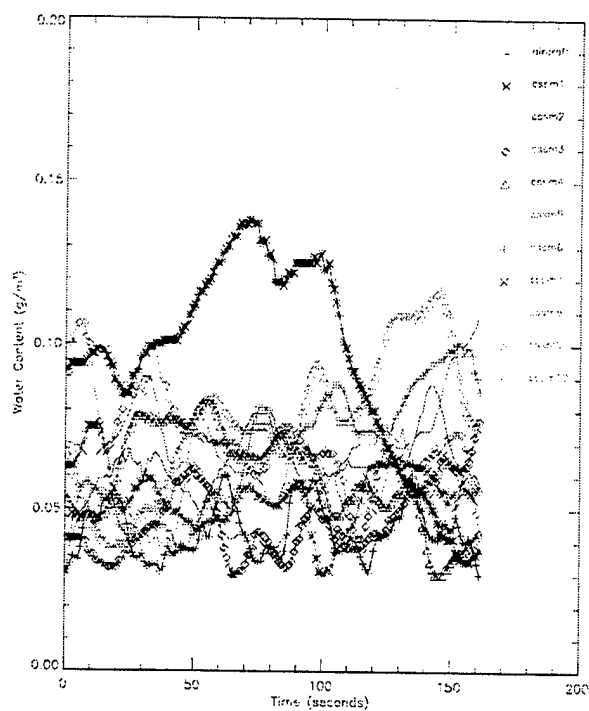Mean Water Content: 0.006 g/m³
Standard Deviation: 0.003 g/m³

Water Content Path

Autocorrelation Function

Log-log plot of Higuchi fractal code

Intercept = -0.999
Slope = -1.284
Hurst parameter = 0.716
Least squares fit weighted all points evenly.

Histogram of Water Content Along Path

Aircraft Path 1-3: 05/08/96 183504-183643 GMT
Cloud Type: Cirrus

Path Height: 11890 m
Average Speed: 233 m/s

Cloud Base: 10485 m
Cloud Top: 12030 m

Mean Water Content: 0.009 g/m³
Standard Deviation: 0.003 g/m³

Water Content Path

Autocorrelation Function

Log-log plot of Higuchi fractal code

Intercept = -1.146
Slope = -1.397
Hurst parameter = 0.603
Least squares fit weighted all points evenly.

Histogram of Water Content Along Path

146

Aircraft Path 1-4: 05/08/96 183644-184058 GMT
Cloud Type: Cirrus

Path Height: 11888 m
Average Speed: 234 m/s

Cloud Base: 9900 m
Cloud Top: 12030 m

Mean Water Content: 0.005 g/m³
Standard Deviation: 0.002 g/m³

Water Content Path

Autocorrelation Function

Log-log plot of Higuchi fractal code

Intercept = -1.089
Slope = -1.343
Hurst parameter = 0.657
Least squares fit weighted all points evenly.

Histogram of Water Content Along Path

Aircraft Path 2-1: 05/08/96 184437-184915 GMT
Cloud Type: Cirrus

Path Height: 11890 m
Average Speed: 233 m/s

Cloud Base: 10440 m
Cloud Top: 12090 m

Mean Water Content: 0.006 g/m³
Standard Deviation: 0.003 g/m³

Water Content Path

Autocorrelation Function

Log-log plot of Higuchi fractal code

Intercept = -1.051
Slope = -1.200
Hurst parameter = 0.800
Least squares fit weighted all points evenly.

Histogram of Water Content Along Path

147

Aircraft Path 2-2: 05/08/96 184916-185325 GMT
Cloud Type: Cirrus

Path Height: 11887 m
Average Speed: 234 m/s

Cloud Base: 10935 m
Cloud Top: 12000 m

Mean Water Content: 0.007 g/m³
Standard Deviation: 0.003 g/m³

Aircraft Path 2-3: 05/08/96 185326-185732 GMT
Cloud Type: Cirrus

Path Height: 11887 m
Average Speed: 233 m/s

Cloud Base: 10440 m
Cloud Top: 12090 m

Mean Water Content: 0.006 g/m³
Standard Deviation: 0.003 g/m³

148

Aircraft Path 1-1: 05/15/96 224817-224944 GMT
Cloud Type: Cirrus

Path Height: 6993 m
Average Speed: 224 m/s

Cloud Base: 6225 m
Cloud Top: 7215 m

Mean Water Content: 0.024 g/m³
Standard Deviation: 0.008 g/m³

Aircraft Path 3-1: 05/15/96 230656-230945 GMT
Cloud Type: Cirrus

Path Height: 6421 m
Average Speed: 212 m/s

Cloud Base: 5010 m
Cloud Top: 6885 m

Mean Water Content: 0.005 g/m³
Standard Deviation: 0.004 g/m³

149
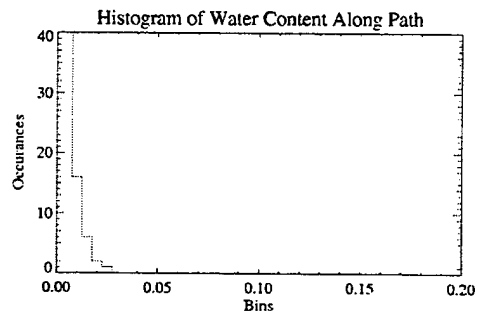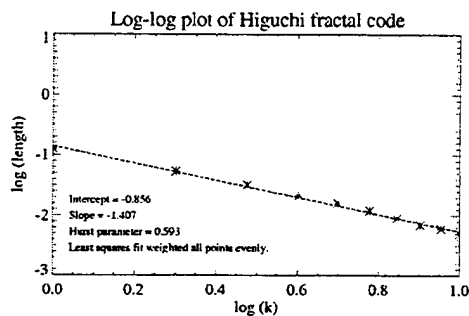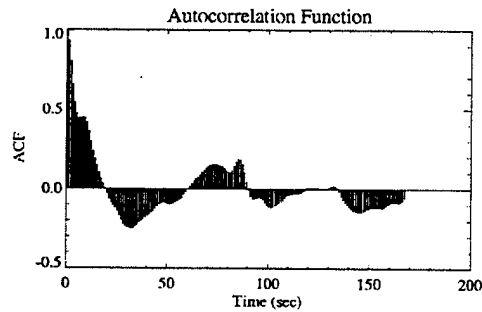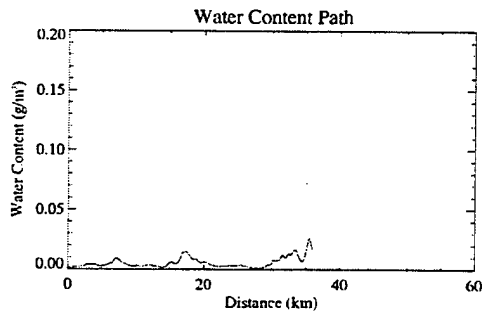
APPENDIX C
TSHEBYCHEFF ANALYSIS

Data and results from the Tshebycheff analysis. IWC data paths for aircraft and ten CSSM runs are presented on the left. Histogram of Tshebycheff inequality values (in units of sigma) are presented in the middle. Tshebycheff summary statistics are printed on the right.

04-21-96 Path 2-1 Cirrostratus
Tsnebycheff Values
(with means)

Sigma Level	Predicted (%)	Actual (%)	Pass? (Y/N)
2	0.250	0.000	✓
3	0.111	0.000	✓
4	0.062	0.000	✓
5	0.040	0.000	✓

Tshebycheff Values
(without means)

Sigma Level	Predicted (%)	Actual (%)	Pass? (Y/N)
2	0.250	0.000	✓
3	0.111	0.000	✓
4	0.062	0.000	✓
5	0.040	0.000	✓

04-21-96 Path 2-2 Cirrostratus

Tshebycheff Values
(with means)

Sigma Level	Predicted (%)	Actual (%)	Pass? (Y/N)
2	0.250	0.000	Y
3	0.111	0.000	Y
4	0.062	0.000	Y
5	0.040	0.000	Y

Tshebycheff Values
(without means)

Sigma Level	Predicted (%)	Actual (%)	Pass? (Y/N)
2	0.250	0.000	Y
3	0.111	0.000	Y
4	0.062	0.000	Y
5	0.040	0.000	Y

04-21-96 Path 3 Cirrostratus

Tshebycheff Values
(with means)

Sigma Level	Predicted (%)	Actual (%)	Pass? (Y/N)
2	0.250	0.025	Y
3	0.111	0.000	Y
4	0.062	0.000	Y
5	0.040	0.000	Y

Tshebycheff Values
(without means)

Sigma Level	Predicted (%)	Actual (%)	Pass? (Y/N)
2	0.250	0.000	Y
3	0.111	0.000	Y
4	0.062	0.000	Y
5	0.040	0.000	Y

152
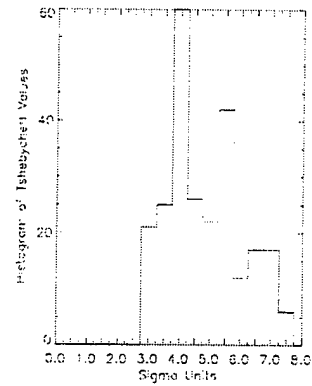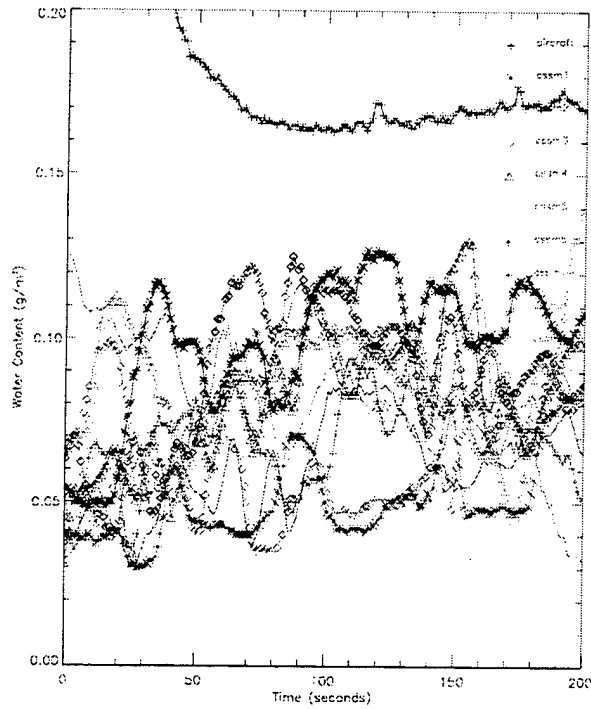
04-27-96 Path 1 Cirrostratus
Tshebycheff Values
(with means)

Sigma Level	Predicted (%)	Actual (%)	Pass? (Y/N)
2	0.250	1.000	N
3	0.111	0.988	N
4	0.062	0.951	N
5	0.040	0.220	N

Tshebycheff Values
(without means)

Sigma Level	Predicted (%)	Actual (%)	Pass? (Y/N)
2	0.250	0.035	Y
3	0.111	0.000	Y
4	0.062	0.000	Y
5	0.040	0.000	Y

04-20-96 Path 4-1 Cirrus
Tshebycheff Values
(with means)

Sigma Level	Predicted (%)	Actual (%)	Pass? (Y/N)
2	0.250	0.000	Y
3	0.111	0.000	Y
4	0.062	0.000	Y
5	0.040	0.000	Y

Tshebycheff Values
(without means)

Sigma Level	Predicted (%)	Actual (%)	Pass? (Y/N)
2	0.250	0.000	Y
3	0.111	0.000	Y
4	0.062	0.000	Y
5	0.040	0.000	Y

04-20-96 Path 4-2 Cirrus
Tshebycheff Values
(with means)

Sigma Level	Predicted (%)	Actual (%)	Pass? (Y/N)
2	0.250	0.000	✓
3	0.111	0.000	✓
4	0.062	0.000	✓
5	0.040	0.000	✓

Tshebycheff Values
(without means)

Sigma Level	Predicted (%)	Actual (%)	Pass? (Y/N)
2	0.250	0.000	✓
3	0.111	0.000	✓
4	0.062	0.000	✓
5	0.040	0.000	✓

04-20-96 Path 5-1 Cirrus
Tshebycheff Values
(with means)

Sigma Level	Predicted (%)	Actual (%)	Pass? (Y/N)
2	0.250	0.000	✓
3	0.111	0.000	✓
4	0.062	0.000	✓
5	0.040	0.000	✓

Tshebycheff Values
(without means)

Sigma Level	Predicted (%)	Actual (%)	Pass? (Y/N)
2	0.250	0.000	✓
3	0.111	0.000	✓
4	0.062	0.000	✓
5	0.040	0.000	✓

154

04-20-96 Path 5-2 Cirrus

Tshebycheff Values
(with means)

Sigma Level	Predicted (%)	Actual (%)	Pass? (Y/N)
2	0.250	0.000	Y
3	0.111	0.000	Y
4	0.062	0.000	Y
5	0.040	0.000	Y

Tshebycheff Values
(without means)

Sigma Level	Predicted (%)	Actual (%)	Pass? (Y/N)
2	0.250	0.000	Y
3	0.111	0.000	Y
4	0.062	0.000	Y
5	0.040	0.000	Y

04-20-96 Path 5-3 Cirrus

Tshebycheff Values
(with means)

Sigma Level	Predicted (%)	Actual (%)	Pass? (Y/N)
2	0.250	0.000	Y
3	0.111	0.000	Y
4	0.062	0.000	Y
5	0.040	0.000	Y

Tshebycheff Values
(without means)

Sigma Level	Predicted (%)	Actual (%)	Pass? (Y/N)
2	0.250	0.000	Y
3	0.111	0.000	Y
4	0.062	0.000	Y
5	0.040	0.000	Y

155

04-20-96 Path 5-4 Cirrus
Tshebycheff Values
(with means)

Sigma Level	Predicted (%)	Actual (%)	Pass? (Y/N)
2	0.250	0.000	Y
3	0.111	0.000	Y
4	0.062	0.000	Y
5	0.040	0.000	Y

Tshebycheff Values
(without means)

Sigma Level	Predicted (%)	Actual (%)	Pass? (Y/N)
2	0.250	0.000	Y
3	0.111	0.000	Y
4	0.062	0.000	Y
5	0.040	0.000	Y

04-20-96 Path 5-5 Cirrus
Tshebycheff Values
(with means)

Sigma Level	Predicted (%)	Actual (%)	Pass? (Y/N)
2	0.250	0.000	Y
3	0.111	0.000	Y
4	0.062	0.000	Y
5	0.040	0.000	Y

Tshebycheff Values
(without means)

Sigma Level	Predicted (%)	Actual (%)	Pass? (Y/N)
2	0.250	0.000	Y
3	0.111	0.000	Y
4	0.062	0.000	Y
5	0.040	0.000	Y

156

04-20-96 Path 7 Cirrus
Tshebycheff Values
(with means)

Sigma Level	Predicted (%)	Actual (%)	Pass? (Y/N)
2	0.250	0.000	Y
3	0.111	0.000	Y
4	0.062	0.000	Y
5	0.040	0.000	Y

Tshebycheff Values
(without means)

Sigma Level	Predicted (%)	Actual (%)	Pass? (Y/N)
2	0.250	0.000	Y
3	0.111	0.000	Y
4	0.062	0.000	Y
5	0.040	0.000	Y

04-20-96 Path 8 Cirrus
Tshebycheff Values
(with means)

Sigma Level	Predicted (%)	Actual (%)	Pass? (Y/N)
2	0.250	0.000	Y
3	0.111	0.000	Y
4	0.062	0.000	Y
5	0.040	0.000	Y

Tshebycheff Values
(without means)

Sigma Level	Predicted (%)	Actual (%)	Pass? (Y/N)
2	0.250	0.000	Y
3	0.111	0.000	Y
4	0.062	0.000	Y
5	0.040	0.000	Y

157

04-20-96 Path 9 Cirrus

Tshebycheff Values
(with means)

Sigma Level	Predicted (%)	Actual (%)	Pass? (Y/N)
2	0.250	0.000	Y
3	0.111	0.000	Y
4	0.062	0.000	Y
5	0.040	0.000	Y

Tshebycheff Values
(without means)

Sigma Level	Predicted (%)	Actual (%)	Pass? (Y/N)
2	0.250	0.000	Y
3	0.111	0.000	Y
4	0.062	0.000	Y
5	0.040	0.000	Y

04-20-96 Path 10 Cirrus

Tshebycheff Values
(with means)

Sigma Level	Predicted (%)	Actual (%)	Pass? (Y/N)
2	0.250	0.000	Y
3	0.111	0.000	Y
4	0.062	0.000	Y
5	0.040	0.000	Y

Tshebycheff Values
(without means)

Sigma Level	Predicted (%)	Actual (%)	Pass? (Y/N)
2	0.250	0.000	Y
3	0.111	0.000	Y
4	0.062	0.000	Y
5	0.040	0.000	Y

04-20-96 Path 11 Cirrus
Tshebycheff Values
(with means)

Sigma Level	Predicted (%)	Actual (%)	Pass? (Y/N)
2	0.250	0.638	N
3	0.111	0.589	N
4	0.062	0.511	N
5	0.040	0.482	N

Tshebycheff Values
(without means)

Sigma Level	Predicted (%)	Actual (%)	Pass? (Y/N)
2	0.250	0.68	N
3	0.111	0.397	N
4	0.062	0.135	N
5	0.040	0.000	Y
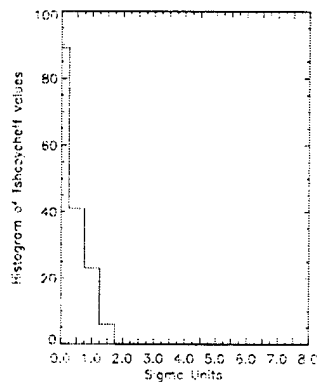
04-20-96 Path 12-1 Cirrus
Tshebycheff Values
(with means)

Sigma Level	Predicted (%)	Actual (%)	Pass? (Y/N)
2	0.250	0.000	Y
3	0.111	0.000	Y
4	0.062	0.000	Y
5	0.040	0.000	Y

Tshebycheff Values
(without means)

Sigma Level	Predicted (%)	Actual (%)	Pass? (Y/N)
2	0.250	0.000	Y
3	0.111	0.000	Y
4	0.062	0.000	Y
5	0.040	0.000	Y

04-20-96 Path 12-2 Cirrus
Tshebycheff Values
(with means)

Sigma Level	Predicted (%)	Actual (%)	Pass? (Y/N)
2	0.250	0.041	Y
3	0.111	0.000	Y
4	0.062	0.000	Y
5	0.040	0.000	Y

Tshebycheff Values
(without means)

Sigma Level	Predicted (%)	Actual (%)	Pass? (Y/N)
2	0.250	0.010	Y
3	0.111	0.000	Y
4	0.062	0.000	Y
5	0.040	0.000	Y

04-20-96 Path 12-3 Cirrus
Tshebycheff Values
(with means)

Sigma Level	Predicted (%)	Actual (%)	Pass? (Y/N)
2	0.250	0.000	Y
3	0.111	0.000	Y
4	0.062	0.000	Y
5	0.040	0.000	Y

Tshebycheff Values
(without means)

Sigma Level	Predicted (%)	Actual (%)	Pass? (Y/N)
2	0.250	0.000	Y
3	0.111	0.000	Y
4	0.062	0.000	Y
5	0.040	0.000	Y

160

04-21-96 Path 1 Cirrus
Tshebycheff Values
(with means)

Sigma Level	Predicted (%)	Actual (%)	Pass? (Y/N)
2	0.250	0.039	Y
3	0.111	0.019	Y
4	0.062	0.000	Y
5	0.040	0.000	Y

Tshebycheff Values
(without means)

Sigma Level	Predicted (%)	Actual (%)	Pass? (Y/N)
2	0.250	0.039	Y
3	0.111	0.019	Y
4	0.062	0.000	Y
5	0.040	0.000	Y

05-02-96 Path 1-1 Cirrus
Tshebycheff Values
(with means)

Sigma Level	Predicted (%)	Actual (%)	Pass? (Y/N)
2	0.250	0.000	Y
3	0.111	0.000	Y
4	0.062	0.000	Y
5	0.040	0.000	Y

Tshebycheff Values
(without means)

Sigma Level	Predicted (%)	Actual (%)	Pass? (Y/N)
2	0.250	0.000	Y
3	0.111	0.000	Y
4	0.062	0.000	Y
5	0.040	0.000	Y

161

Water Content (g/m³) vs **Time (seconds)**

Legend: aircraft, doom1, doom2, doom3

Histogram of Tshebycheff Values vs Sigma Units

05-06-96 Path 1-2 Cirrus
Tshebycheff Values
(with means)

Sigma Level	Predicted (%)	Actual (%)	Pass? (Y/N)
2	0.250	0.000	Y
3	0.111	0.000	Y
4	0.062	0.000	Y
5	0.040	0.000	Y

Tshebycheff Values
(without means)

Sigma Level	Predicted (%)	Actual (%)	Pass? (Y/N)
2	0.250	0.000	Y
3	0.111	0.000	Y
4	0.062	0.000	Y
5	0.040	0.000	Y

Water Content (g/m³) vs **Time (seconds)**

Legend: aircraft, doom1, doom2, doom3, doom4, doom5, doom6, doom7, doom8, ...

Histogram of Tshebycheff Values vs Sigma Units

05-06-96 Path 1-3 Cirrus
Tshebycheff Values
(with means)

Sigma Level	Predicted (%)	Actual (%)	Pass? (Y/N)
2	0.250	0.000	Y
3	0.111	0.000	Y
4	0.062	0.000	Y
5	0.040	0.000	Y

Tshebycheff Values
(without means)

Sigma Level	Predicted (%)	Actual (%)	Pass? (Y/N)
2	0.250	0.000	Y
3	0.111	0.000	Y
4	0.062	0.000	Y
5	0.040	0.000	Y

05-08-96 Path 1-4 Cirrus
Tshebycheff Values
(with means)

Sigma Level	Predicted (%)	Actual (%)	Pass? (Y/N)
2	0.250	0.000	Y
3	0.111	0.000	Y
4	0.062	0.000	Y
5	0.040	0.000	Y

Tshebycheff Values
(without means)

Sigma Level	Predicted (%)	Actual (%)	Pass? (Y/N)
2	0.250	0.000	Y
3	0.111	0.000	Y
4	0.062	0.000	Y
5	0.040	0.000	Y

05-08-96 Path 2-1 Cirrus
Tshebycheff Values
(with means)

Sigma Level	Predicted (%)	Actual (%)	Pass? (Y/N)
2	0.250	0.000	Y
3	0.111	0.000	Y
4	0.062	0.000	Y
5	0.040	0.000	Y

Tshebycheff Values
(without means)

Sigma Level	Predicted (%)	Actual (%)	Pass? (Y/N)
2	0.250	0.000	Y
3	0.111	0.000	Y
4	0.062	0.000	Y
5	0.040	0.000	Y

163

05-06-96 Path 2-2 Cirrus

Tshebycheff Values
(with means)

Sigma Level	Predicted (%)	Actual (%)	Pass? (Y/N)
2	0.250	0.000	Y
3	0.111	0.000	Y
4	0.062	0.000	Y
5	0.040	0.000	Y

Tshebycheff Values
(without means)

Sigma Level	Predicted (%)	Actual (%)	Pass? (Y/N)
2	0.250	0.000	Y
3	0.111	0.000	Y
4	0.062	0.000	Y
5	0.040	0.000	Y

05-06-96 Path 2-3 Cirrus

Tshebycheff Values
(with means)

Sigma Level	Predicted (%)	Actual (%)	Pass? (Y/N)
2	0.250	0.000	Y
3	0.111	0.000	Y
4	0.062	0.000	Y
5	0.040	0.000	Y

Tshebycheff Values
(without means)

Sigma Level	Predicted (%)	Actual (%)	Pass? (Y/N)
2	0.250	0.000	Y
3	0.111	0.000	Y
4	0.062	0.000	Y
5	0.040	0.000	Y

164

05-15-96 Path 1-1 Cirrus
Tshebycheff Values
(with means)

Sigma Level	Predicted (%)	Actual (%)	Pass? (Y/N)
2	0.250	0.000	Y
3	0.111	0.000	Y
4	0.062	0.000	Y
5	0.040	0.000	Y

Tshebycheff Values
(without means)

Sigma Level	Predicted (%)	Actual (%)	Pass? (Y/N)
2	0.250	0.000	Y
3	0.111	0.000	Y
4	0.062	0.000	Y
5	0.040	0.000	Y

05-15-96 Path 5-1 Cirrus
Tshebycheff values
(with means)

Sigma Level	Predicted (%)	Actual (%)	Pass? (Y/N)
2	0.250	0.000	Y
3	0.111	0.000	Y
4	0.062	0.000	Y
5	0.040	0.000	Y

Tshebycheff Values
(without means)

Sigma Level	Predicted (%)	Actual (%)	Pass? (Y/N)
2	0.250	0.000	Y
3	0.111	0.000	Y
4	0.062	0.000	Y
5	0.040	0.000	Y

REFERENCES

1. Arabey, E.N., 1975: Radiosonde data as means for revealing cloud layers, Meteor. Gidrol., 6, 32-37.

2. Aha, D.W., and R.L. Bankert, 1994: Feature selection for case-based classification of cloud types: An empirical comparison. In D. W. Aha (Ed.) Case-Based Reasoning: Papers from the 1994 Workshop (Technical Report WS-94-01). Menlo Park, CA: AAAI Press. (NCARAI TR:AIC-94-011). [Atmospheric and Environmental Research, Inc.], 1998: Automated Cloud Analysis Algorithms, Cambridge, Massachusetts, electronic version, http://www.aer.com/groups/sm/satmet_cloud_analysis.html.

3. Bankert, R.L., 1994: Cloud Classification of AVHRR Imagery in Maritime Regions Using a Probabilistic Neural Network, J. Appl. Meteor. 33, 909-918.

4. Bankert, R.L. and D.W. Aha, 1996: Improvement to a Neural Network Cloud Classifier. J. Appl. Meteor. 35, 2036-2039.

5. Chernykh, I.V. and R.E. Eskridge, 1996: Determination of Cloud Amount and Level from Radiosonde Soundings. J. Appl. Meteor. 35, 1362-1369.

6. Cianciolo, M. E., M. E. Raffensberger, E. O. Schmidt, and J. R. Stearns, Atmospheric scene simulation modeling and visualization, PL-TR-96-2079, April 1996. [NTIS AD-A312 179].

7. Cianciolo, M. E., and R.G. Rasmussen, Cloud Scene Simulation Modeling - the Enhanced Model, PL-TR-92-2106, April 1992. [NTIS AD-A265 958].

8. Cianciolo, M. E., Hersh, J. S., and M. P. Ramos-Johnson, Cloud Scene Simulation Modeling — interim technical report, PL-TR-91-2295, November 1991. [NTIS AD-A256 689].

9. Cohen I. D., and A. A. Barnes, Cirrus particle distribution study — Part 6, Air Force Surveys in Geophysics 430, AFGL-TR-80-0261, AD-A096772, 106 pp., September 1980.

10. Cohen I. D., Cirrus particle distribution study - Part 8, Air Force Surveys in Geophysics 437, AFGL-TR-81-0316, AD-A 118715, 110 pp., October 1981.

11. Danne, O., G. G. Mace, E. E. Clothiaux, X. Dong, and T. P. Ackerman, Observing structures and vertical motions within stratiform clouds using a vertical pointing 94-GHz cloud radar, Beitr. Phys. Atmosph., vol. 69, no. 1, pp. 229-237, February 1996.

12. Development of an Atmospheric Scene Simulation Model, January 1996, TASC Proposal TP-02485.

13. Ebert, E. E., and J. A. Curry, A parameterization of ice cloud optical properties for climate models, J. of Geophys. Res., vol. 97, no. D4, pp. 3831-3836, March 20, 1992.

14. Eskridge, R.E., Polansky, A.C., Doty, S.R., and H.V. Frederick, 1996: A Comprehensive Aerological Reference Data Set (CARDS): The Database. NCDC Rep., 35 pp.

15. Feddes, R. G., A synoptic-scale model for simulating condensed atmospheric moisture, USAFETAC-TN-74-4, 1974.

16. Forsythe, J.M., Reinke, D.L., Randel, D.L., Eis, K.E., and C.L. Combs, 1996: CLVL — A Global High-Resolution Layered-Cloud Database. Proceedings of the 1996 Battlespace Atmospherics Conference, Naval Command, Control and Surveillance Center, RTD & E Division, San Diego, California. ADA 323 038

17. Gibson, J.K., Kallberg, P., Nomura, A., and Uppala, S., 1994: The ECMWF Re-Analysis (ERA) Project — Plans and Current Status. Tenth International Conference on Interactive Information and Processing Systems For Meteorology, Oceanography, and Hydrology, Nashville, Tennessee, 23-28 January, 164-167.

18. Harnett, E.J., 1996: GEOS-1 Multi-Year Assimilation, NASA Goddard Space Flight Center Data Assimilation Office, Greenbelt, Maryland, electronic version, http://dao.gsfc.nasa.gov/experiments/assim54A.html.

19. Heymsfield, A.J., 1972: Ice crystal terminal velocities, J. Atmos. Sci., vol. 29, pp. 1348-1357.

20. Higuchi, T., 1988: Approach to an irregular time series on the basis of the fractal theory, Physical D Nonlinear Phenomena, vol. 31, pp. 277-283.

21. Heymsfield, A.J., 1972: Ice crystal terminal velocities, J. Atmos. Sci., vol. 29, pp. 1348-1357.

22. Heymsfield, A. J., 1974: Ice crystal growth in deep cirrus systems, in Proc. of the Conference on Cloud Physics of the Am. Met. Society, Tucson, AZ, pp. 311-316.

23. Heymsfield, A. J., 1974: Precipitation development in stratiform ice clouds: a microphysical and dynamical study, J. of Atmos. Sciences, vol. 34, pp. 367-381.

24. Heymsfield, A. J., 1975a: Cirrus uncinus generating cells and the evolution of cirriform clouds. Part I: Aircraft Observations of the growth of the ice phase, J. of Atmos. Sciences, vol. 32, pp. 799-808.

25. Heymsfield, A. J., 1975b: Cirrus uncinus generating cells and the evolution of cirriform clouds. Part II: The structure and circulations of the cirrus uncinus generating head, J. of Atmos. Sciences, vol. 32, pp. 809-819.

26. Heymsfield, A. J., 1975c: Cirrus uncinus generating cells and the evolution of cirriform clouds. Part III: Numerical computations of the growth of the ice phase, J. of Atmos. Sciences, vol. 32, pp. 820-830.

27. Heymsfield, A. J., and J. L. Coen, 1996: Parameterization of cirrus microphysical and radiative properties in larger-scale models, downloaded from the ARM Web page.

28. Heymsfield, A. J., and L. J. Donner, 1990: A scheme for parameterizing ice-cloud water content in general circulation models, J. of the Atmos. Sciences, vol. 47, no. 15, pp. 1865-1877.

29. Heymsfield, A. J., R. G. Knollenberg, 1972: Properties of Cirrus Generating Cells, J. of Atmos. Sciences, vol. 29, pp. 1358-1366.

30. Heymsfield, A. J., K. M. Miller, and J. D. Spinhirne, 1990: The 27-28 October 1986 FIRE IFO cirrus case study: cloud microstructure, Monthly Weather Review, vol. 118, pp. 2313-2328.

31. Heymsfield, A. J., and L. M. Miloshevich, 1996: Relative humidity and temperature influences on cirrus formation and evolution: observations from wave clouds and FIRE II, J. of Atmos. Sciences, vol. 52: pp. 4302-4326.

32. Heymsfield, A. J., and C. M. R. Platt, 1991: An empirical model of the physical structure of upper-layer clouds, Atmos. Research, vol. 26, pp. 213-228.

33. Isaccs, R.G., 1994: Remote Sensing of Cloud for Defense and Climate Studies: An Overview. Atmospheric and Environmental Research, Inc. (AER), Cambridge, MA. In: Lynch, David K. (ed.), Passive infrared remote sensing of clouds and the atmosphere., Bellingham, WA, SPIE (Society of Photo-Optical Instrumentation Engineers), 1993. p. 2-35. Refs., figs., tables. (SPIE-The International Society for Optical Engineering. SPIE Proceedings Series, Volume 1934). M.G.A. (1994), 45:2-436

34. Kalnay, E., Kanamitsu, M., Kistler, R., Collins, W., Deaven, D., Gandin, L., Iredell, M., Saha, S., White, G., Woollen, J., Zhu, Y., Chelliah, M., Ebisuzaki, W., Higgins, W., Janowiak, J., Mo, K.C., Ropelewski, C., Wang, J., Leetmaa, A., Reynolds, R., Jenne, R., and D. Joseph, 1996: The NCEP/NCAR 40-Year Reanalysis Project. Bull. Amer. Meteor. Soc. 77, 437-471.

35. Keller, J. M., Chen, S., and R. M. Crownover, 1989: Texture description and segmentation through fractal geometry, Computer Vision, Graphics and Image Processing, vol. 45, pp. 150-166.

36. Kosarev, A. L., and I. P. Mazin, 1991: An empirical model of the physical structure of upper-layer clouds, Atmos. Research, vol. 26, pp. 213-228.

37. Kosarev, A. L., I. P. Mazin, and A. N. Nevzorov, 1988: The empirical model of the structure of cirrus clouds in middle latitudes, Annalen der Meteorologie, A.M. Offenbach, vol. 2, no. 25, pp. 482-484.

38. Laha, R.G., and V.K. Rohatgi, *Probability Theory*, Wylie, New York, 1979, pg. 33.

39. Marshak, A. , W. Wiscombe, and A. Davis, 1992: On the analysis of the multifractal properties of cloud liquid water data, Proceedings of IRS '92, Keevailik and Karner (Eds.), pp. 116-119.

40. Matrosov, S. Y., B. W. Orr, R. A. Kropfli, and J. B. Snider, 1994: Retrieval of vertical profiles of cirrus cloud microphysical parameters from Doppler radar and infrared radiometer measurements, J. of Applied Meteorology, vol. 33, pp. 617-626.

41. Minnis, P., D. F. Young, K. Sassen, J. M. Alvarez, and C. J. Grund, 1990: The 27-28 October 1986 FIRE IFO cirrus case study: cirrus parameter relationships derived from satellite and lidar data, Monthly Weather Review, vol. 118, pp. 2402-2425.

42. Mitchell, D. L., S. K. Chai, Y. Liu, A. J. Heymsfield, and Y. Dong, 1996: Modeling cirrus clouds. Part I: treatment of bimodal size spectra and case study analysis, J. of Atmos. Science, vol. 53, no. 20, pp. 2952-2966.

43. Mitchell, D. L., A. Macke, and Y. Liu, 1996: Modeling cirrus clouds. Part II: treatment of radiative properties, JAS, vol. 53, no. 20, pp. 2967-2988.

44. [National Center for Atmospheric Research], 1998: ECMWF Re-Analyses, Boulder, Colorado, electronic version, http://www.scd.ucar.edu/dss/pub/ec-reanalysis.html.

45. [National Climatic Data Center], 1998: Products and Services Guide: Digital Datasets: AWS's HIRAS, Asheville, North Carolina, p. 77.

46. [National Climatic Data Center], 1998: Products and Services Guide: Digital Datasets: TD9950 — Air Weather Service's (AWS) DATSAV2 Surface-Worldwide Stations, Asheville, North Carolina, p. 77. [National Geophysical Data Center], 1994: TerrainBase Global Terrain Model Summary Documentation, Boulder, Colorado, electronic version, ftp://ftp.ngdc.noaa.gov/Solid_Earth/CD_ROMS/TerrainBase_94/data/global/tbase/tbase.txt.

47. Orr, B. W., and R. A. Kropfli, 1993: Estimation of cirrus cloud particle fallspeeds from vertically pointing Doppler radar, Proc. of 26th Annual Conference on Radar Meteorology, Norman, OK, May 24-28, pp. 588-590.

48. Piironen, A. K., E. W. Eloranta, 1995: Convective boundary layer mean depths and cloud geometrical properties obtained from Volume Imaging Lidar data, J. of Geophys. Res., vol. 100, D12, pp: 25569-25576.

49. Platt, C. M. R., 1997: A parameterization of the visible extinction coefficient of ice clouds in terms of the ice/water content, J. of Atmos. Sciences, vol. 54, pp. 2083-2098.

50. Platt, C. M. R., and A. C. Dilley, 1981: Remote sounding of high clouds. IV: Observed temperature variations in cirrus optical properties, J. of Atmos. Sciences, vol. 38, pp. 1069-1082.

51. Platt, C. M. R., and Harshvardhan, 1988: Temperature dependence of cirrus extinction: implications for climate feedback, J. of Geophys. Res., vol. 93, no. D9, pp. 11051-11058.

52. Poix, C., G. Febvre, A. Fouilloux, H. Larsen, and J. F. Gayet, 1996: The retrieval of cloud microphysical properties using satellite measurements and an in situ database, Annales Geophysicae, vol. 14, pp. 98-106.

53. Quante, M., E. Raschke, F. Albers, A. Grattzki, P. Scheidgen, and Y. Zhang, 1990: The international cirrus experiment (ICE) - results from the pilot experiment 1987, Conference on Atmos. Radiation, 7th, San Francisco, CA, July 1990, Preprints (A92-13901 03-47), Boston, MA, American Society, pp. 30-37.

54. Randall, D. A., and K. M. Xu, 1995: Use of ARM data to test an improved parameterization of upper tropospheric clouds for use in climate models, Final Report to the U.S. DOE.

55. Rienke, D.L., Forsythe, J.M., and T.H. Vonder Haar, 1997: Global High-Resolution Layered Cloud Database — Research and Development at the Cooperative Institute for Research in the Atmosphere, Colorado State University. Proceedings of the Cloud Impacts on DoD Operations and Systems 1997 Conference, U.S Naval War College, Newport, Rhode Island, 23-25 September, 159-161.

56. Rossow, W.B., A.W., Beuschel, D.E., and M.D. Roiter, 1996: International Satellite Cloud Climatology Project (ISCCP) Documentation of New Cloud Datasets. WMO/TD-No. 737, World Meteorological Organization, 115 pp.

57. Sassen, K., 1987: Ice cloud content from radar reflectivity, Applied Meteorology, vol. 26, pp. 1050-1053.

58. Sassen, K., D. O'C Starr, T. Uttal, 1989: Mesoscale and microscale structure of cirrus clouds: three case studies, J. of the Atmos. Sciences, vol. 46, no. 3, pp. 371-396.

59. Saupe, D., Point evaluation of multi-variable random fractals, *Visualisierung in Mathematik und*

60. *Naturwissenschaft*, H. Jurgens and D. Saupe, Eds., Springer-Verlag, Heidelberg, 1989, pp. 117-129.

61. Schubert, S.D., Rood, R.B. and J. Pfaendtner, 1993: An Assimilated Data Set for Earth Science Applications, Bull. Amer. Meteor. Soc. 74, 2331-2342.

62. Soden, B. J., and L. J. Donner, 1994: Evaluation of a GCM cirrus parameterization using satellite observations, J. of Geophys. Res., vol. 99, no. d7, pp. 14401-14413.

63. Starr, D. O'C., S. K. Cox, 1985: Cirrus clouds. Part I: a cirrus cloud model, J. of Atmos. Sciences, vol. 42, no. 23, pp. 2663-2681.

64. Starr, D. O'C., S. K. Cox, 1985: Cirrus clouds. Part II: numerical experiments on the formation and maintenance of cirrus, JAS, vol. 42, no. 23, pp. 2682-2694.

65. Starr, D. O'C., D. P. Wylie, 1990: The 27-28 October 1986 FIRE cirrus case study: meteorology and clouds, Monthly Weather Review, vol. 118, pp. 2259-2287.

66. Sundqvist, H., 1978: A parameterization scheme for non-convective condensation including prediction of cloud water content, Quarterly J. R. Met. Soc., vol. 104, pp. 677-690.

67. Uddstrom, M.J. and W.R. Gray, 1996: Satellite Cloud Classification and Rain-Rate Estimation Using Multispectral Radiances and Measures of Spatial Texture. J. Appl. Meteor. 35, 839-858.

68. [U.S. Geological Survey], 1997: GTOPO30 Documentation, [readme], Sioux Falls, South Dakota, U.S. Geological Survey, EROS Data Center, electronic version, http://edcwww.cr.usgs.gov/landdaac/gtopo30/README.html.

69. [U.S. Geological Survey], 1997: 5 Minute Gridded Earth Topography Data, Sioux Falls, South Dakota, U.S. Geological Survey, EROS Data Center, electronic version, http://edcwww.cr.usgs.gov/glis/hyper/guide/etopo5.

70. Varley, D. J., 1978: Cirrus particle distribution study — Part 1, Air Force Surveys in Geophysics 394, AFGL-TR-78-0192, AD-A061485, 71 pp.

71. Varley, D. J., and D. M. Brooks, 1978: Cirrus particle distribution study — Part 2, Air Force Surveys in Geophysics 399, AFGL-TR-78-0248, AD-A063807, 108 pp.

72. Varley, D. J., 1978: Cirrus particle distribution study — Part 3, Air Force Surveys in Geophysics 404, AFGL-TR-78-0305, AD-A066975, 67 pp.

73. Varley, D. J., and A. A. Barnes, 1979: Cirrus particle distribution study — Part 4, Air Force Surveys in Geophysics 413, AFGL-TR-79-0134, AD-A074763, 91 pp.

74. Varley, D. J., I. D. Cohen, and A. A. Barnes, 1980: Cirrus particle distribution study — Part 7, Air Force Surveys in Geophysics 433, AFGL-TR-80-0324, AD-A100269, 82 pp.

75. Wang, J. and W.B. Rossow, 1995: Determination of Cloud Vertical Structure from Upper-Air Observations. J. Appl. Meteor. 34, 2243-2258.

76. Wiscombe, W., A. Davis, and A. Marshak, 1996: Two complementary multifractal analysis techniques for non-stationary atmospheric processes with an application to cloud liquid water content, downloaded from the ARM Web page.

77. Wylie, D.P., Menzel, W.P., Woolf, H.M., and K.I. Strabala, 1994: Four Years of Global Cirrus Cloud Statistics Using HIRS, J. Climate 7, 1972-1986.

78. Wylie, D.P. and W.P. Menzel, 1997: Global Cloud Data for System Design and Simulation. Proceedings of the Cloud Impacts on DoD Operations and Systems 1997 Conference, U.S Naval War College, Newport, Rhode Island, 23-25 September, 155-158.

79. Zinn, J., 1996: A model of the microphysical evolution of a cloud, downloaded from the ARM Web page.